Received: 31 December 2022 | Revised: 8 April 2023 | Accepted: 17 May 2023

DOI: 10.1002/cey2.425

REVIEW

CARBON ENERGY WILEY

Charting the course to solid-state dual-ion batteries

Habtom D. Asfaw[1] | **Antonia Kotronia**[2] | **Nuria Garcia-Araez**[2] | **Kristina Edström**[1] | **Daniel Brandell**[1]

[1]Department of Chemistry, Ångström Laboratory, Uppsala University, Uppsala, Sweden

[2]Department of Chemistry, University of Southampton, Southampton, UK

Correspondence
Habtom D. Asfaw and Daniel Brandell, Department of Chemistry, Ångström Laboratory, Uppsala University, Lägerhyddsvägen 1, PO Box 538, 75121 Uppsala, Sweden.
Email: habtom.desta.asfaw@kemi.uu.se and daniel.brandell@kemi.uu.se

Funding information
H2020 European Research Council, Grant/Award Number: 771777; VINNOVA, Grant/Award Number: 2019-00064; StandUp for Energy consortium; Faraday Institution, Grant/Award Numbers: EP/S003053/1, FIRG024

Abstract

An electrolyte destined for use in a dual-ion battery (DIB) must be stable at the inherently high potential required for anion intercalation in the graphite electrode, while also protecting the Al current collector from anodic dissolution. A higher salt concentration is needed in the electrolyte, in comparison to typical battery electrolytes, to maximize energy density, while ensuring acceptable ionic conductivity and operational safety. In recent years, studies have demonstrated that highly concentrated organic electrolytes, ionic liquids, gel polymer electrolytes (GPEs), ionogels, and water-in-salt electrolytes can potentially be used in DIBs. GPEs can help reduce the use of solvents and thus lead to a substantial change in the Coulombic efficiency, energy density, and long-term cycle life of DIBs. Furthermore, GPEs are suited to manufacture compact DIB designs without separators by virtue of their mechanical strength and electrical performance. In this review, we highlight the latest advances in the application of different electrolytes in DIBs, with particular emphasis on GPEs.

KEYWORDS

anion intercalation, concentrated electrolytes, dual-ion battery, graphite, ionic liquids, polymer electrolyte

1 | INTRODUCTION

Rising demands for scarce and high-cost transition metal minerals containing, for example, Co or Ni, will make lithium-ion batteries less appealing for applications requiring inexpensive and large-scale energy storage deployment. For instance, batteries meant for stationary energy storage must use safe, abundant, and cost-effective resources suited for utility-scale applications. To date, state-of-the-art stationary batteries are based on active materials consisting of elements that are expensive (e.g., nickel–metal hydride batteries and vanadium redox flow batteries) and toxic (e.g., nickel–cadmium and lead–acid batteries), or those that operate at exceedingly high temperatures (e.g., sodium–sulfur batteries). A viable alternative to current stationary batteries is the dual-ion battery (DIB), which has emerged as a promising chemistry for future energy storage applications.[1] In a DIB, the electrolyte provides charge carriers while acting as part of the active materials needed for energy storage. As opposed to the classical "rocking chair" model of lithium-ion batteries, the charge storage mechanism in a DIB involves intercalation of both cations (Li^+, Na^+, K^+, Ca^{2+}, or Al^{3+}), anions (halides, $AlCl_4^-$, ClO_4^-, BF_4^-, PF_6^-, bis(trifluoromethanesulfony) imide [TFSI], and bis(fluorosulfonyl)imide [FSI]) in two graphite electrodes.[2–6] Such a

versatile working principle provides the possibility to design stationary energy storage systems that can not only avoid costly transition metals but also can use a wide selection of inexpensive electrolytes. This review is intended to cover some of the latest achievements in the formulation and application of electrolytes in DIBs. It highlights the salient features of various types of electrolytes currently in use and pinpoints their important limitations, as well as explores research efforts leading toward solid-state DIB designs. First, let us explore the roles of electrolytes and graphite intercalation compounds (GICs) in developing the DIBs.

1.1 | The development of acceptor-type GICs: A historical timeline

A typical DIB makes use of donor- and acceptor-type GICs as its negative and positive electrodes, respectively. Acceptor-type GICs are prepared by oxidative intercalation of anions from electrolytic solutions. The earliest report about anion-intercalated graphite can be traced back to 1841 when Schafhäutl[7] treated graphite and carbon-containing iron with a mixture of concentrated sulfuric acid and concentrated nitric acid. As a result of the oxidizing nature of the reagent, bisulfate anions, along with some sulfuric acid molecules, were intercalated in the graphitic carbon, causing considerable interlayer expansion. Similar studies were also reported by Brodie in 1859.[8] In 1918, Kohlschütter and Haenni[9] presented a detailed study of what they termed "graphitic acid" prepared by treating graphite with concentrated sulfuric acid, concentrated nitric acid, and potassium chlorate. Following the definitive description of the crystal structure of graphite using X-ray diffraction (XRD) by Hassel and Mark,[10] and Bernal[11] in 1924, more studies of anion-intercalated GICs ensued. In particular, Hofmann and Frenzel[12] in 1930 used XRD to provide a detailed account of the structure of H_2SO_4-GICs, and the stage formation mechanism of HSO_4^- intercalation in graphite in the presence of various types of oxidizing agents. The accompanying crystal structure changes were extensively studied by Rüdorff and Hofmann[13] in 1938. In essence, a similar approach was employed by Hummers and Offeman[14] to prepare graphitic oxide in a mixture of concentrated sulfuric acid, sodium nitrate, and potassium permanganate. This approach, now commonly known as the "Hummers method," formed the basis for the production of state-of-the-art graphene oxide. Following a report by Thiele[15] on $FeCl_3$-intercalated graphite in 1932, considerable interest in the synthesis of complex GICs of halogens, interhalogens, and metal halides emerged.[15–19] Classic examples of GICs based on metal chlorides include C_xCuCl_2 (where $x = 4.9$ for Stage I, and $x = 13.4$ for Stage II),[17,20] C_xFeCl_3 (where $x = 5$–9 for Stage I and $x = 20$ for Stage II),[18,19] C_xAlCl_{3+y} (where $x = 9$–10 for Stage I and $x = 18$ for Stage II),[21,22] and C_xSbCl_5 (where $x = 12$ for Stage I and $x = 24$ for Stage II).[18] They are usually prepared at elevated temperatures by reacting graphite with the molten or vapor phases of the respective salts in the presence of Cl_2 gas that is needed to oxidize the graphite hosts.[17,21,22] In contrast, most halide and interhalide GICs such as C_8Cl,[16] C_8Br,[16] and C_8ICl[23,24] were found to be relatively unstable but could instead be prepared at lower temperatures under the saturation vapor pressure of the respective halogen gases. Other examples of GICs with fluorinated anions which were obtained via chemical routes included C_xAsF_6 ($x \geq 8$–16 for Stage I), as shown in Equation (1). Those were first synthesized by Bartlett et al.[25–28] in 1978 and extensively studied by others, using quantitative amounts of dioxygenyl hexafluoroarsenate ($O_2[AsF_6]$) under reduced pressures.

$$xC + O_2^+AsF_6^- \rightarrow (C_x)^+AsF_6^- + O_2. \quad (1)$$

1.2 | From acceptor-type GICs to DIBs

In addition to the conventional chemical approaches, acceptor-type GICs can be prepared via the electrochemical oxidation of graphite in electrolytic solutions. In 1963, Bottomley et al.[29] concluded, using a chronopotentiometric method, that anodic oxidation of highly oriented pyrolytic graphite in concentrated acids such as H_2SO_4, $HClO_4$, and $ClSO_3H$ resulted in $C_{24}^+HSO_4^-(2H_2SO_4)$, $C_{24}^+ClO_4^-$, and $C_{24}^+ClSO_3^-(n ClSO_3H)$ compounds. Further studies by Beck et al.[30] in 1981 verified that electrochemical intercalation of anions (A) like HSO_4^-, BF_4^-, and ClO_4^- in 4 M electrolytic solutions of HA (HA) = H_2SO_4, HBF_4, and $HClO_4$ formed GICs with a maximum $C_{24}A(HA)_x$ stoichiometry in which varied amounts of undissociated molecules of the acids were cointercalated. They also studied the dependence of the Coulombic efficiency (CE) and intercalation potential on the electrolyte concentration. The higher the concentration, the better the CE, and the lower the onset intercalation potential. Similarly, electrochemical anodic intercalation in graphite has been studied in nonaqueous electrolytes as well. A study from 1972 by Besenhard and Fritz[31] detailed the electrochemical formation of $C_{24}A$ GICs in solutions of $LiClO_4$, $NaBF_4$, KPF_6, and $KAsF_6$ in propylene carbonate (PC), nitromethane, and acetonitrile (AN) solvents. They further concluded that solvent cointercalation caused self-discharge upon storage in the electrolyte for 24 h.

Solvent cointercalation, along with dramatic swelling of the graphite electrode, was also observed in 1978 by Deshapande and Bennion[32] who investigated ClO_4^- and BF_4^- intercalation in Li–graphite half-cells using electrolytic solutions of $LiClO_4$ and $LiBF_4$ salts in dimethyl sulfite (DMS) and PC solvents. Reportedly, 1 M $LiClO_4$ in DMS resulted in higher CE (~95%) as compared to 0.9 M $LiClO_4$-PC (~42%), 1 M $LiBF_4$-DMS (~72%), and 1.55 M $LiBF_4$-PC (~50%). Further electrochemical and XRD studies on ClO_4-GIC prepared in 2 M $LiClO_4$-PC were reported in 1978 by Ohzuku et al.[33] who suggested a $C_{96}ClO_4$ composition for the GIC. In addition, they indicated that a specific capacity of 24 mAh g^{-1} with 80%–90% CE could be achieved and that the graphite electrode disintegrated when overcharged. In 1983, a comparative study conducted by Matsuda et al.[34] established that the CE increased in the order $ClO_4^- < BF_4^- < PF_6^-$ for intercalation in graphite foil and graphite felt in 1 M solutions of the respective salts in PC. They also observed that intercalation capacity increased upon repetitive cycling. In short, it can be assumed that these works were particularly important in the development of the nonaqueous DIB concept. In a work that marked the beginning of aluminum DIBs (Al-DIBs), Fouletier and Armand[35] successfully demonstrated in 1979 the electrochemical synthesis of $AlCl_3$-GICs in a eutectic melt of $AlCl_3$ and LiCl. They proposed the compositions $C_{62}^+(Al_nCl_{3n+1})^-$ and $C_{37}^+(Al_nCl_{3n+1})^-$ for compounds obtained, respectively, at 1.8 and 1.95 V versus Al^{3+}/Al. The next significant development came in the form of a series of works on the development of room temperature melts of $AlCl_3$-alkylpyridinium chlorides.[36,37] A seminal report in 1982 by Wilkes et al.[38] on the synthesis of dialkylimidazolium chloroaluminate electrolytes paved the way for the advent of more efficient electrolytes for DIBs. Later in 1988, Gifford and Palmisano[39] demonstrated a rechargeable Al-DIB in which Al plating and stripping, and $AlCl_4^-$ intercalation in graphite were conducted in a room-temperature ionic liquid (IL) composed of $AlCl_3$ and 1,2-dimethyl-3-propylimidazolium chloride (DMPICl).

Patents filed in 1989 by McCullough et al.[40,41] described DIB prototypes consisting of graphitized carbon cloths as positive and negative electrodes, both immersed in an electrolyte composed of 15 wt% $LiClO_4$ in PC. It was reported that some cells could deliver up to 69 mAh g^{-1} and sustain thousands of cycles with >90% CE.[41] In 1989 and 1990, Maeda[42] employed in situ thermal energy measurement to show that intercalation of cations and anions in graphite involved exothermic changes, while deintercalation displayed the reverse, using electrolytic solutions of 2 M $LiClO_4$, 2 M $KClO_4$, and 1 M $NaBF_4$ in AN, dimethyl sulfoxide (DMSO)[43] and PC[43] solvents. Afterward, Carlin et al.[44,45] in 1994 and 1996 explored the electrochemical intercalation of anions from IL electrolytes based on room or low-temperature molten salts of substituted imidazolium cations (1-ethyl-3-methylimidazolium [EMI^+] or 1,2-dimethyl-3-propylimidazolium [$DMPI^+$]) and anions ($AlCl_4^-$, BF_4^-, PF_6^-, $CF_3SOF_3^-$, and $C_6H_5CO_2^-$). At the same time, a prototype of a graphite-graphite full-cell was reported by Santhanam and Noel[46] in 1995 using 0.65 M tetrabutylammonium perchlorate (TBA-ClO_4) in PC as the electrolyte, and making use of TBA cation and ClO_4^- anion intercalation. Although this was a demonstration that dual-graphite cells can be operated, the CEs were typically low, ranging from 14% to 57%.

Another significant contribution to the development of the DIB concept could be credited to Seel and Dahn[47,48] who in 2000 verified using in situ XRD that electrochemical PF_6^- intercalation in Li–graphite and graphite–graphite cells is dependent on the salt concentration and type of solvent used in the electrolyte (2 M $LiPF_6$ in ethyl methyl sulfone [EMS] and 1–3 M in ethylene carbonate [EC] and diethyl carbonate [DEC]). They concluded that the electrolyte based on EMS solvent had higher oxidative potential and gave rise to discharge capacities of 95–98 mAh g^{-1} (with an initial CE [iCE] of 83%). Accordingly, the design of better DIBs requires selecting solvents with high oxidative stability and optimizing salt concentrations. Increasing salt concentration beyond a critical limit leads to lower ionic conductivity as a result of increasing electrolyte viscosity and the formation of salt aggregates. In this regard, the so-called sulfonylimide salts such as $LiN(SO_2F)_2$ (LiFSI) and $LiN(SO_2CF_3)_2$ (LiTFSI) have generated particular interest as they are highly soluble in most organic solvents, allowing for the preparation of >3 M concentrations. Chemical preparation of TFSI-intercalated GIC was demonstrated for the first time by Zhang et al.[49] in 1999 by oxidizing graphite flakes using K_2MnF_6 dissolved in a mixture of HF and LiTFSI. A series of TFSI-GICs with compositions varying between C_{101}TFSI to C_{32}TFSI were obtained and studied using XRD. Later in 2001, Yan and Lerner[50] from the same research group prepared Stage I GICs containing TFSI anions via electrochemical oxidation in a 0.33 and 0.66 M solution of LiTFSI in nitromethane and in EMS, respectively. In the former electrolyte, a discharge capacity of up to 97 mAh g^{-1} was achieved at 5.25 V, corresponding to the C_{22}TFSI composition, but with very poor CE (only 22%). Higher intercalation overpotentials were observed in the EMS-based electrolyte, which also showed slightly better anodic stability.

Concurrent studies on the synthesis of room-temperature ILs and a better understanding of their properties have directly contributed to the progress in

DIB research. Especially, substituted imidazolium-based ILs with fluorinated anions were found to have ionic conductivities ranging from 5 to 14 mS cm^{-1} and were found attractive as electrolytes for batteries.[51,52] However, imidazolium ILs such as EMI-FSI and BMI-BF_4 have limited cathodic stability,[53,54] with the potential window being typically between 1 and 5 V versus Li^+/Li.[52] The introduction of LiTFSI in EMI-FSI increased compatibility with graphite-negative electrodes.[55] However, the most important milestone was achieved by replacing imidazolium cations with substituted pyrrolidinium cations, which resulted in increased reduction stability and better performance in batteries.[56,57] Following this, Placke et al.[58,59] reported in 2012 a Li–graphite half-cell and a $Li_4Ti_5O_{12}$ (LTO)–graphite full-cell DIB making use of 1 M LiTFSI and 1 M LiFSI in *N*-butyl-*N*-methylpyrrolidinium bis (trifluoromethanesulfonyl)imide as the main electrolyte. The results were very promising and clearly established that discharge intercalation capacity (96–100 mAh g^{-1}) increased for cut-off potentials above 5 V but at the expense of the CE. The study provided clear evidence that the intercalation capacity in a DIB could be limited by the stability of the electrolytes. Further studies using similar ILs focused on the role of some additives to enhance the performance of dual-graphite DIBs.[60,61] Structural investigations using XRD also indicated that a maximum of 115 mAh g^{-1} could be achieved with the corresponding GIC composition being between C_{19}TFSI and C_{20}TFSI.[62,63]

In 2015, Lin et al.[64] introduced an Al-DIB with a stable discharge capacity of 66 mAh g^{-1} obtained at 0.1–5 A g^{-1} using $AlCl_4^-$ intercalation in pyrolytic graphite and $Al_2Cl_7^-$ reduction to Al metal in an IL electrolyte formed by mixing $AlCl_3$ with 1-ethyl-3-methylimidazolium chloride (EMICl) (see Figure 2B). That inspired intense research efforts to develop electrolytes with comparable performance, but more efficient, cheaper and less corrosive.[65]

Needless to say, aqueous electrolytes are particularly interesting as they are safe and cheaper compared to those based on organic solvents or ILs. Recent studies have shown that a considerable increase in capacity can be achieved when halides, interhalides, or metal–chloride complexes are intercalated in graphite from concentrated aqueous electrolytes, commonly known as water-in-salt electrolytes (WISE). In 2019, Stage I C_7[BrCl] GIC was prepared in hydrated salt electrolytes composed of LiBr·xH_2O and LiClx·H_2O, where $x = 0.34$.[66] The GIC cathode exhibited a reversible capacity >240 mAh g^{-1} at 80 mA g^{-1} obtained within 3.2–4.9 V versus Li^+/Li range. In addition, intercalation of ICl^- in graphite was investigated in an aqueous mixture of a deep eutectic solvent (DES) choline chloride (ChCl) and zinc chloride in the presence of KI (typically 120 m (mol kg^{-1}) ChCl + 30 m $ZnCl_2$ + 5 m KI). Based on the intercalation of ICl^-, a Zn–graphite DIB could deliver reversible capacities of 290 mAh g^{-1} at 30 mA g^{-1}.[67] Evidently, the halogen-containing GICs were able to provide much higher capacities than what could be obtained in ILs and organic electrolytes (typically <100 mAh g^{-1})[47,61,65,68-71] or with other types of aqueous electrolytes (typically 20–42 mAh g^{-1}).[72,73] Similarly, intercalation of magnesium chloro complexes, such as $[MgCl_4]^{2-}$ and $[MgCl_3(H_2O)]^-$ have been exploited to design aqueous DIBs. An electrolyte containing a mixture of 9 m $MgCl_2$ and 30 m ChCl in water resulted in 150 mAh g^{-1} at 100 mA g^{-1}.[74] A Zn–graphite DIB using 30 m $ZnCl_2$ reported by Guo et al.[75] exhibited a discharge capacity of >134 mAh g^{-1} attributed to intercalation of $[ZnCl_x]^{2-x}$ occurring >1.9 V versus Zn^{2+}/Zn. A summary of the historical development and milestones in the preparation of n-type GICs and their application in DIBs is presented in Figure 1. Based on this historical survey, it can be concluded that progress in the synthesis, stability, and application of anion-intercalated graphite compounds was clearly influenced by the development of efficient electrolytes. It should also be noted that other materials such as conducting polymers and metal-organic frameworks have been proposed as hosts for anions. Interested readers are referred to recent reviews on electrode materials for DIBs.[78,79]

2 | DESIGN PRINCIPLES OF EFFICIENT ELECTROLYTES

The schematic diagrams in Figure 2A,B illustrate the mechanism of charge storage in two variants of DIB prototypes. The graphite–graphite cell involves intercalation and extraction of cations and anions in graphite electrodes. The Al–graphite cell illustrated in Figure 2B operates by aluminum plating and stripping at the negative electrode, which is paralleled by intercalation and extraction of $AlCl_4^-$ in the positive graphite electrode. Ideally, Stage I GICs are required to maximize the capacity of DIBs, but achieving this electrochemically usually requires stable electrolytes which can resist degradation at high operating potentials. As can be seen in Figure 2C,D, the process of anion intercalation in graphite occurs at high potentials (4–5.2 V vs. Li^+/Li) where most electrolytes are prone to oxidative decomposition. Fine-tuning the salt concentration, oxidative and reductive stability, viscosity, ion conductivity, and wettability of electrolytes is key to ensuring the optimum performance of DIBs. The electrochemical stability

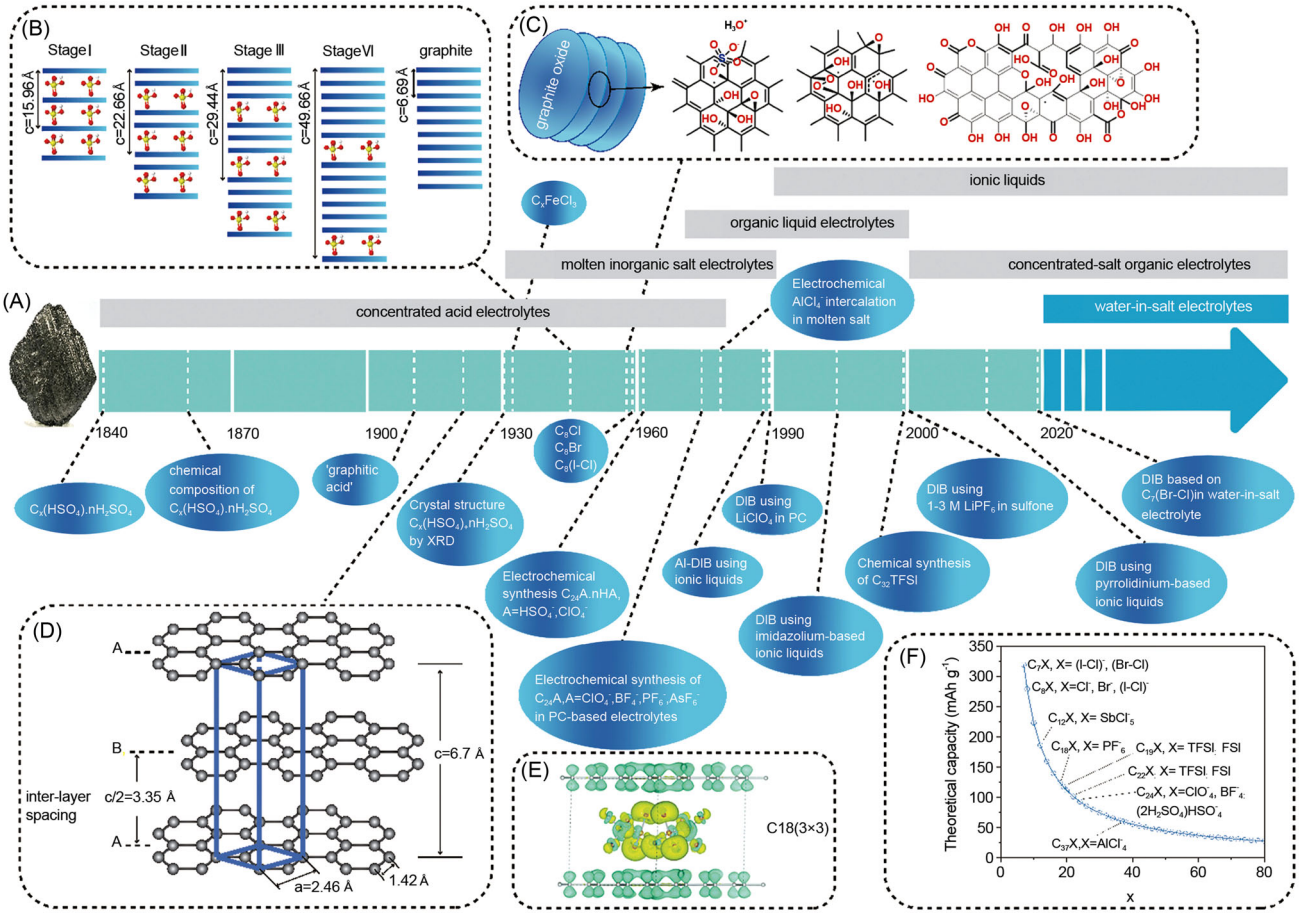

FIGURE 1 Historical milestones in the development of anion-intercalated graphite compounds and their applications: (A) synthesis of various anion-intercalated graphites in different types of electrolytes since 1840, (B) formation of lamellar anion-intercalated GICs in concentrated H_2SO_4 acid and elucidation of the associated crystal structures determined by Rüdorff and Hofmann,[13] (C) simplified structures of graphene oxide obtained from oxidation and anion intercalation of graphite (Reproduced under the terms of the Creative Commons Attribution 4.0 International license: Copyright 2020, IOP Publishing[76]), (D) representation of the crystal structures and unit cell parameters of graphite with Bernal stacking, (E) isosurface plot of the electron density difference for the C_{18}TFSI compound showing electron gain in yellow and electron loss in cyan (Reproduced with permission: Copyright 2018, Royal Society of Chemistry[77]), and (F) expected theoretical capacities for various types of anion-intercalated graphite compounds.

window (ESW) of electrolytes (see Figure 3) is determined by the oxidative and reductive stability of solvents and salts used. The open-circuit voltage (V_{OC}) of a cell is in turn related to the difference between the electrochemical potentials (a measure of the Fermi energy of electrons) of the negative electrode (μ_-) and the positive electrode (μ_+) as expressed below:

$$V_{OC} = -\frac{(\mu_+ - \mu_-)}{ne}, \quad (2)$$

where e is the electronic charge and n is the number of electrons being transferred. An ideal electrolyte must be stable within these limits of electrode chemical potentials. However, this is usually not the case in DIBs, and most electrolytes undergo reduction on the negative electrode and/or oxidation on the positive electrode. In the presence of some additives (salts and solvents), the electrolytes are able to form interfacial layers (the solid electrolyte interphase [SEI] and the cathode–electrolyte interface [CEI]) that passivate the electrodes by limiting direct contact with the electrolytes, analogous to Li-ion batteries. The long-term stability of these layers determines the efficiency, safety, and longevity of DIBs.

Apart from interfacial stability, the salt and solvent combination can also dictate the reversibility and kinetics of the anion intercalation in the positive electrode. It has previously been shown that the salt concentration and the interplay between anions and solvent molecules can influence the onset potential for anion intercalation, as well as the maximum discharge capacity and CE. Figure 2C shows the intercalation and

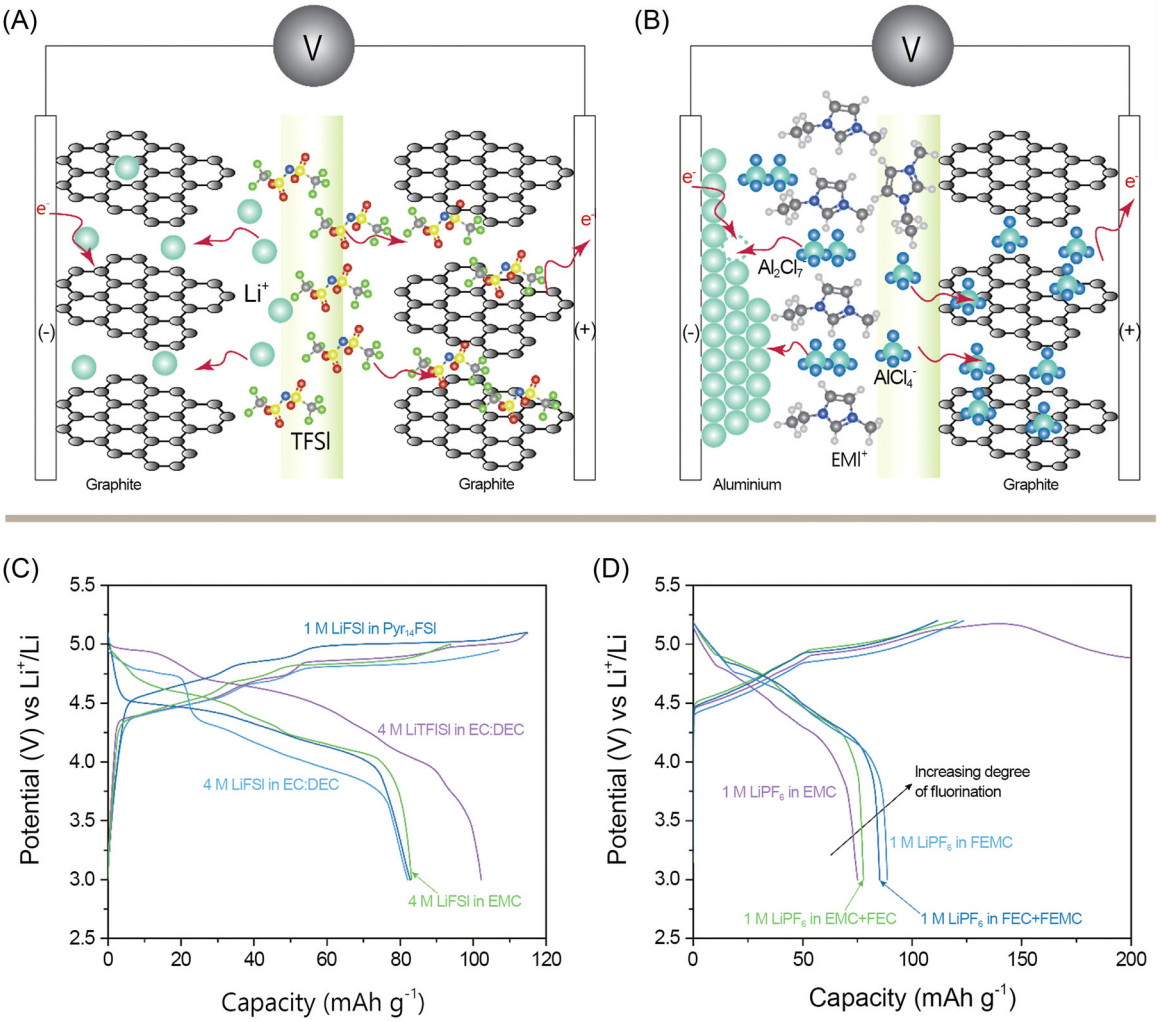

FIGURE 2 Schematic illustration of (A) a graphite–graphite dual-ion battery using lithium-based electrolyte, (B) an Al–graphite dual-ion battery involving aluminum metal plating and stripping at the negative electrode and intercalation of aluminum tetrachloro anion complexes in the graphite-positive electrode, and (C) examples of galvanostatic curves showing the characteristic features of anion intercalation in graphite and its dependence on electrolyte solvents. Reproduced under the terms of the Creative Commons Attribution (CC-BY): Copyrigt 2021, American Chemical Society.[80] All galvanostatic curves except that for 4 M LiFSI-EMC (unpublished data) are based on data reported in the cited reference. (D) Galvanostatic curves measured at 10 mA g^{-1} for PF_6^- intercalation from electrolytes based on carbonate solvents with varying degrees of fluorination (fluoroethylene carbonate and 2-fluoroethyl methyl carbonate). Reproduced with permission: Copyright 2022, Wiley-VCH GmbH.[81]

extraction processes of FSI and TFSI anions and the different features in the galvanostatic curves.[80] The intercalation potential is also affected by the nature of the solvents present in the electrolytes. In this respect, the magnitude of anion charge density, rather than anion size, and the prospect of inducing ion-pairing and solvent cointercalation play important roles in deciding the amount and reversibility of anion uptake. As regards the nature of the solvent, both capacity and CE have been observed to increase as the degree of fluorination in the solvents increased, as shown in Figure 2D in which examples of galvanostatic charge–discharge curves are given for different electrolytes based on 1 M $LiPF_6$ in ethyl methyl carbonate (EMC) and fluorinated carbonate solvents.[81] In brief, in dual-ion cells, both intercalation potential and capacity depend on the type and concentration of salt anions and solvent molecules in the electrolyte under consideration. Host–guest interactions in the GIC electrodes and ion–solvent interactions in the electrolyte also determine the cell potential and the ESW expressed in Equation (2). For instance, Dahn and Seel[48] demonstrated that energy density increased with increasing concentration of $LiPF_6$ salt in the electrolyte until 2 M, at which a maximum was achieved. In a typical

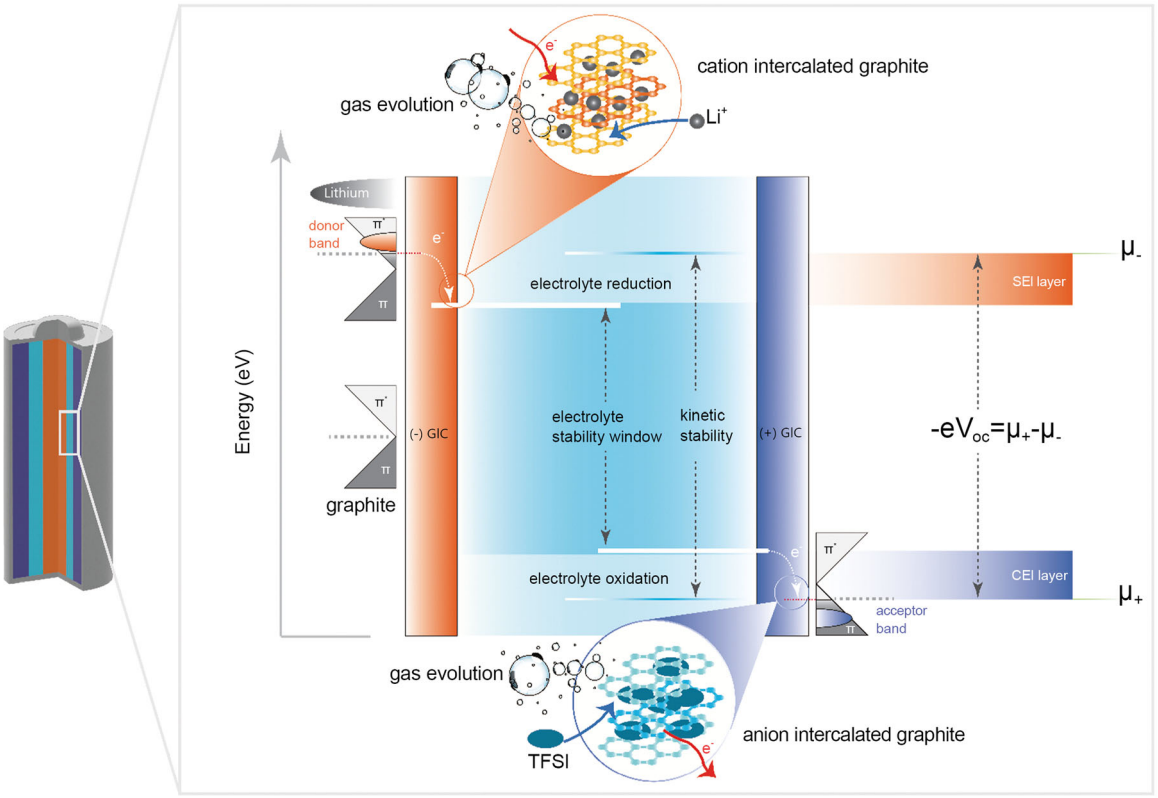

FIGURE 3 Schematic illustration showing electrolyte–electrode interfaces and electrochemical stability window of an electrolyte vis-á-vis the chemical potentials of graphite intercalation compounds used in a graphite–graphite dual-ion battery using LiTFSI salt in the electrolyte. A graphite–graphite DIB must employ an electrolyte that is stable toward cation- and anion-intercalated graphite compounds.

graphite-graphite DIB based on LiA (A stands for anion) electrolyte salt, the following reactions take place at the two graphite electrodes:

$$xC + Li^+ + e^- \rightleftarrows LiC_x \quad \text{negative electrode.} \tag{3}$$

$$yC + A^- - e^- \rightleftarrows AC_y \quad \text{positive electrode.} \tag{4}$$

$$Li^+ + A^- + (x+y)C \rightleftarrows LiC_x + AC_y \quad \text{cell reaction.} \tag{5}$$

Assuming infinite dilution limit for a binary LiA salt electrolyte and combining with Equation (2), these reactions lead to a cell potential given as[47]

$$V = \frac{1}{e}\left(\mu^{o}_{Li^+} - \mu_{Li} + \mu^{o}_{A^-} - \mu_{A} + kT\ln[Li^+][A^-]\right), \tag{6}$$

where $\mu_{Li+}°$ and $\mu_{A-}°$ represent the chemical potentials of the cation and anion, respectively, in 1 M solution, μ_{Li} is the chemical potential of Li intercalated in the graphite-negative electrode, and μ_A is the chemical potential of the anion within the graphite-positive electrode. A direct corollary of this simplified Equation (6) is that the cell potential can be affected by salt concentration in the electrolyte. However, it should be noted that increasing salt concentration increases viscosity and can, beyond a certain critical limit, adversely impact the ionic conductivity[82] as well as wetting and percolation of the electrolyte into the porous structure of the electrodes. Some properties of the solvent such as melting point, dielectric constant, and viscosity play critical roles in deciding the maximum salt concentration that can be attained without compromising ionic conductivity. Since ionic conductivity depends upon the mobility of ions in the electrolyte and is affected not only by ion–ion but also ion–solvent interactions, it is essential to take the properties of the solvent into account when formulating electrolytes for DIBs. The electrolyte must possess sufficiently high ionic conductivity over a broad temperature range to ensure optimum power performance, and it must also contain as much salt as possible to reach the maximum energy density of DIBs. Last but not least, safety aspects of the electrolyte including health and fire hazards must be considered, especially in DIBs in which high operating potentials can aggravate decomposition reactions as well as increase the risk of gassing (pressure build-up) in the cell.

2.1 | A comparative look at electrolytes for DIBs

As pointed out in the previous section, typical examples of DIB electrolytes are concentrated protic acids, molten inorganic salts, organic electrolytes, room-temperature ILs, highly concentrated organic electrolytes (HCEs) deep-eutectic solvent electrolytes, WISE, and gel polymer electrolytes (GPEs). This section presents an overview of the characteristic properties of common electrolytes along with the pros and cons of their use in DIBs.

2.1.1 | Molten inorganic salt electrolytes

Early on, it was realized that molten salt electrolytes could play a crucial role in the synthesis and study of various acceptor-type GICs. In particular, eutectic mixtures of inorganic salts have been proved valuable to prepare GICs in the absence of solvents which usually complicate structure determination and worsen the stability of the GICs. For instance, a NaCl–$AlCl_3$ molten salt electrolyte (eutectic at ~110°C) was used in an Al–graphite DIB which maintained a reversible capacity of 60 mAh g^{-1} after 5000 cycles.[83] Furthermore, a quaternary mixture of $AlCl_3$, NaCl, LiCl, and KCl salts was prepared at 75°C. At 90°C, an Al-DIB using this electrolyte offered a discharge capacity of ~115 mAh g^{-1} at 200 mA g^{-1} with stable performance for over 1500 cycles.[84] More recent studies have shown that molten salt electrolytes based on sodium bis(fluorosulfonyl) imide (NaFSI) and KFSI salts can offer novel characteristics which are appealing in DIBs.[85] For instance, a eutectic mixture of 56% NaFSI and 44% KFSI salts was observed to melt at ~60°C.[85] The molten salt electrolyte was found to be stable up to 5.2 V and exhibited an ionic conductivity of 3.3 mS cm^{-1} at 90°C.[85] Operating at 90–120°C and at a current density of 20 mA g^{-1}, a typical DIB cell using these electrolytes delivered a reversible capacity of 108 mAh g^{-1} with an average potential of ~4.2 V (vs. Na^+/Na) and a CE of 97%– 98%.[86] The absence of solvent molecules in the electrolyte could help prevent Al dissolution,[87-89] which is commonly encountered in organic electrolytes based on FSI and TFSI salts, in which the formation of $[Al(FSI)_x]^{3-x}$ complexes has been detected.[1] The main drawback of molten salt electrolytes is the comparatively high operating temperature required for cell operation, making them less attractive for most practical applications.[84,90,91]

2.1.2 | Ionic liquids

Room temperature ionic liquids (RTILs) possess physicochemical properties suited for use as electrolytes and solvents in DIBs.[92,93] As opposed to electrolytes containing organic solvents, these are nonvolatile, nonflammable, and more stable at higher potentials and higher temperatures.[59,93,94] It should be pointed out, however, that pure IL electrolytes have high melting points and suffer from poor rate performance at freezing temperatures as a result of a drastic decrease in ionic conductivity.[95,96] Nevertheless, improvements have been made using eutectic mixtures of different ILs[97,98] and also by adding organic solvents.[99-102] Common cations in ILs are imidazolium, pyridinium, pyrrolidinium, ammonium, and phosphonium. The counterpart anions are selected from TFSI, FSI, chloroaluminate ($AlCl_4^-$), BF_4^-, PF_6^- and halides such as Cl^-.

The introduction of ILs has contributed toward considerable advances in the development of especially Al-DIBs. An Al–graphite DIB consists typically of an aluminum metal anode, an IL electrolyte, and a graphite cathode.[64,103–105] For instance, room temperature melts of $AlCl_3$ and alkylimidazolium chlorides such as 1-butyl-3-methylimidazolium chloride, EMICl,[106–114] 1-methyl-3-propylimidazolium chloride,[115] benzyltriethylammonium chloride,[116] and DMPICl[117] are commonly used in Al-DIBs. In such devices, $AlCl_4^-$ intercalates in graphite along with concurrent reactions involving the reduction of $Al_2Cl_7^-$ to Al metal at the negative electrode. An Al-DIB employing a metallic Al anode and synthetic graphite as the cathode in 1-ethyl-methylimidazolium IL electrolyte ($AlCl_3$:EMICl) could operate for over thousands of cycles with a reversible capacity of 67 mAh g^{-1}.[64] However, the ILs listed above are expensive, corrosive, and sensitive to moisture, which severely limits their large-scale application in Al-DIBs.[118–121]

Studies have shown that pyrrolidinium- and piperidinium-based ILs possess higher reductive stability than imidazolium-based RTILs and are thus more suitable for application in DIBs.[56,60,122,123] The majority of RTILs currently used in DIBs are composed of 1-butyl-1-methylpyrrolidinium (Pyr_{14}^+) or 1-butyl-1-methylpiperidinium (PP_{14}^+) cations, and anions such as bis(pentafluoroethanesulfonyl) imide (BETI), fluorosulfonyl (trifluoromethanesulfonyl) imide (FTFSI), TFSI, and FSI.[59,61,94,124–128] In pure TFSI- and FSI-based IL electrolytes, aggravated dissolution of the Al current collector produces $[Al(FSI)_x]^{3-x}$ and $[Al(TFSI)_x]^{3-x}$ complexes which destroy the native oxide passivation layer,[80,129,130] resulting in poor CE, fast discharge, and disruption of electrical contact to the active materials. A neat PP_{14}TFSI IL used in a graphite–graphite DIB offered a specific capacity ranging from 40 to 80 mAh g^{-1} but with only ~66%–80% CE.[131,132] Adding a small amount of salts such as $LiBF_4$, and $LiPF_6$ [80,129,133] can promote Al passivation and improve cyclic performance, as well as ensuring higher specific capacities.[134,135] For

instance, in a pure $Pyr_{14}TFSI$ electrolyte, a graphite–graphite DIB achieved a reversible specific capacity of 49 mAh g^{-1} at a current density of 50 mA g^{-1}.[122] However, in the same IL, the capacity increased to 98 mAh g^{-1} at 0.1 A g^{-1} in the presence of 1 M LiTFSI[60] and to ~70 mAh g^{-1} upon addition of 0.7 M NaTFSI.[123] In addition, salt or solvent additives can boost the interfacial compatibility of common RTILs with negative graphite electrodes.[56,96,136] Applying a certain amount of FEC and ethylene sulfite (ES) in $Pyr_{14}TFSI$ and piperidinium-based RTILs (such as $PP_{13}FSI$ and $PP_{14}TFSI$) stabilized the SEI layer, leading to better performance in graphite DIBs, which otherwise would suffer from sharp capacity fading.[60,123,137]

2.1.3 | Electrolytes based on DES

DES have been suggested as a cheaper and more sustainable alternative electrolytes to ILs in Al-DIBs (among other applications).[138-145] Studies have shown that DES such as $AlCl_3$-urea, which are less expensive than $AlCl_3$-EMICl ILs, can provide comparable performance.[138,139,143,146,147] Typically, an $AlCl_3$-Et_3NHCl electrolyte can be obtained by mixing $AlCl_3$ with triethylammonium chloride (Et_3NHCl). In an Al-graphite DIB, the electrolyte resulted in a capacity of 112 mAh g^{-1} at 5 A g^{-1} for over 30,000 cycles with 97.3% retention,[145] while performing better than the $AlCl_3$-urea electrolyte.[138,139,143,146,147] However, $AlCl_3$-Et_3NHCl is corrosive and moisture-sensitive, similar to the conventional IL electrolytes employed in Al-DIB. Replacing the Et_3NHCl with ethylpyridine produced an IL that was less corrosive and more tolerant toward moisture. Even though the capacity at 25 mA g^{-1} was comparably good (95 mAh g^{-1}), the DIB had a lower rate capability.[119]

2.1.4 | Water-in-salt electrolytes

Replacing organic solvents with water is an attractive approach to make DIBs safer and more cost-effective.[148,149] However, aqueous electrolytes are prone to oxygen evolution reaction (OER) at potentials lower than that required for anion intercalation into graphite. The reduction of water to H_2 (called hydrogen evolution reaction) also occurs before cation insertion,[73,150,151] and its corresponding potential is typically <1.5 V. Increasing salt concentration has been found to extend the stability window.[152] Such electrolytes, widely termed as "WISE," can reportedly resist oxidative degradation up to 5 V versus Li^+/Li.[153-156] The enhanced electrochemical stability of WISE can be ascribed to the significant reduction in the number of uncoordinated water molecules. Some studies have demonstrated that anion intercalation in graphite and layered polyaromatic compounds like coronene can be achieved in WISE.[66,73,157,158] For instance, it was observed that FSI anion intercalation in 1 m NaFSI was extremely irreversible with negligible discharge capacity. The capacity, however, increased to 20 mAh g^{-1} only when the salt concentration increased to 19 m[73]; even so, the associated CE only rose to a meager ~40%, making such an electrolyte of limited importance. To improve the performance of WISE, it will be necessary to further minimize reductive or oxidative degradation of water molecules as well as the anions. A more straightforward approach is to increase the salt concentration as much as possible so that fewer free water molecules are available, and also to use salts with anions that are more stable than FSI.[159-161] For instance, mixing LiTFSI and LiFSI salts raised the potential for OER from 4.8 V in 22 m LiTFSI to 5 V in 37 m LiFSI + LiTFSI electrolyte.[159] The electrolyte was used in a graphite-activated carbon DIB for which a discharge capacity of >50 mAh g^{-1} was obtained at 500 mA g^{-1} during the first cycle, which later stabilized at ~70 mAh g^{-1} after 50 cycles. In comparison, the 22 m LiTFSI and 30 m LiFSI electrolytes exhibited shorter cycle life, with the respective discharge capacities reaching 20 mAh g^{-1} after 50 cycles. Despite this improvement, one should bear in mind that the CE remained <80%, which was indicative of the need to further curb oxidative destruction of the electrolytes. Similarly, the ESW could be extended to 2.5–2.6 V in aqueous electrolytes consisting of 21 m LiTFSI + 3 m $Zn(OTf)_2$, and 20 m NaFSI + 0.5 m $Zn(TFSI)_2$ which proved valuable for use in Zn–graphite DIBs.[160,161] Lastly, recent reports indicate that alkali metal halides can be employed to realize aqueous DIBs with higher capacities. As indicated in the preceding section, intercalation of halides (Cl^- and Br^-) and interhalides ($BrCl^-$ and ICl^-) can produce high capacity due to the formation of GICs in which the carbon to anion ratio can be as high as 7:1. For instance, intercalation of $BrCl^-$ from a $LiBr{\cdot}xH_2O + LiCl{\cdot}xH_2O$ (for $x \sim 0.34$) electrolyte resulted in a discharge capacity of 243 mAh g^{-1} at 80 mA g^{-1} along with ~82% capacity retention after 230 cycles.[66,162] Similar studies also demonstrated that ICl^- intercalation in graphite from 120 m ChCl + 30 m $ZnCl_2$ + 5 m KI electrolyte allowed a reversible capacity of 291 mAh g^{-1} at 30 mA g^{-1}.[67] These results demonstrate that the DIB concept holds more potential in store for the diversification of the energy storage landscape. Major challenges to the practical application of the chloride-based DIB concept are linked to Al dissolution aggravated by the presence of chloride ions, the generation of Cl_2 gas in the cell, and its high

reactivity toward electrode materials and electrolytes.[80,109,163,164] The evolution of Cl_2 can be suppressed by chemisorption on iodine or ammonium methyl iodide, by reacting with bromine and iodine to form interhalide (BrCl and ICl) intercalants in graphite,[66] or by conducting the intercalation process at low temperature to induce liquefaction of the halide intercalant.[165]

2.1.5 | Highly concentrated organic electrolytes

A high salt concentration is essential to maximizing volumetric and gravimetric energy density, and suppressing parasitic reactions (i.e., Al corrosion, graphite exfoliation), as well as reducing the flammability of DIB electrolytes. How much salt can be dissolved in a given solvent is determined by the strength of the cation–anion interactions, the ion–solvent interactions, and solvent properties such as permittivity and viscosity. In this section, a review of the salts and solvents commonly encountered in highly concentrated organic electrolyte (HCEs) is provided along with the impacts on the performance of DIBs.

2.2 | Salts

Similar to lithium-ion batteries, salts for DIBs must ideally possess a range of properties including

- high ionic conductivity,
- high degree of solubility in common solvents,
- electrochemical stability,
- thermal stability,
- stability against hydrolysis,
- ability to help generate stable SEI and CEI layers, and
- compatibility with the Al current collector or the ability to passivate it in the course of electrochemical cycling.

Various salts containing the anions shown in Figure 4 have so far been studied for DIB applications. Anions such as chloride (Cl^-),[66,162] bromide (Br^-),[67] tetrachloroaluminate ($AlCl_4^-$),[64,166] perchlorate (ClO_4^-),[63,167-169] tetrafluoroborate (BF_4^-),[63,167-171] hexafluorophosphate (PF_6^-),[47] difluoro(oxalato)borate (DFOB),[172,173] FSI,[94] TFSI,[80,82,94] and FTFSI[94] have been demonstrated to reversibly intercalate in graphite. The electrochemical stability, the charge density of the anion in the salt, and the strength of its interaction with the solvent molecules

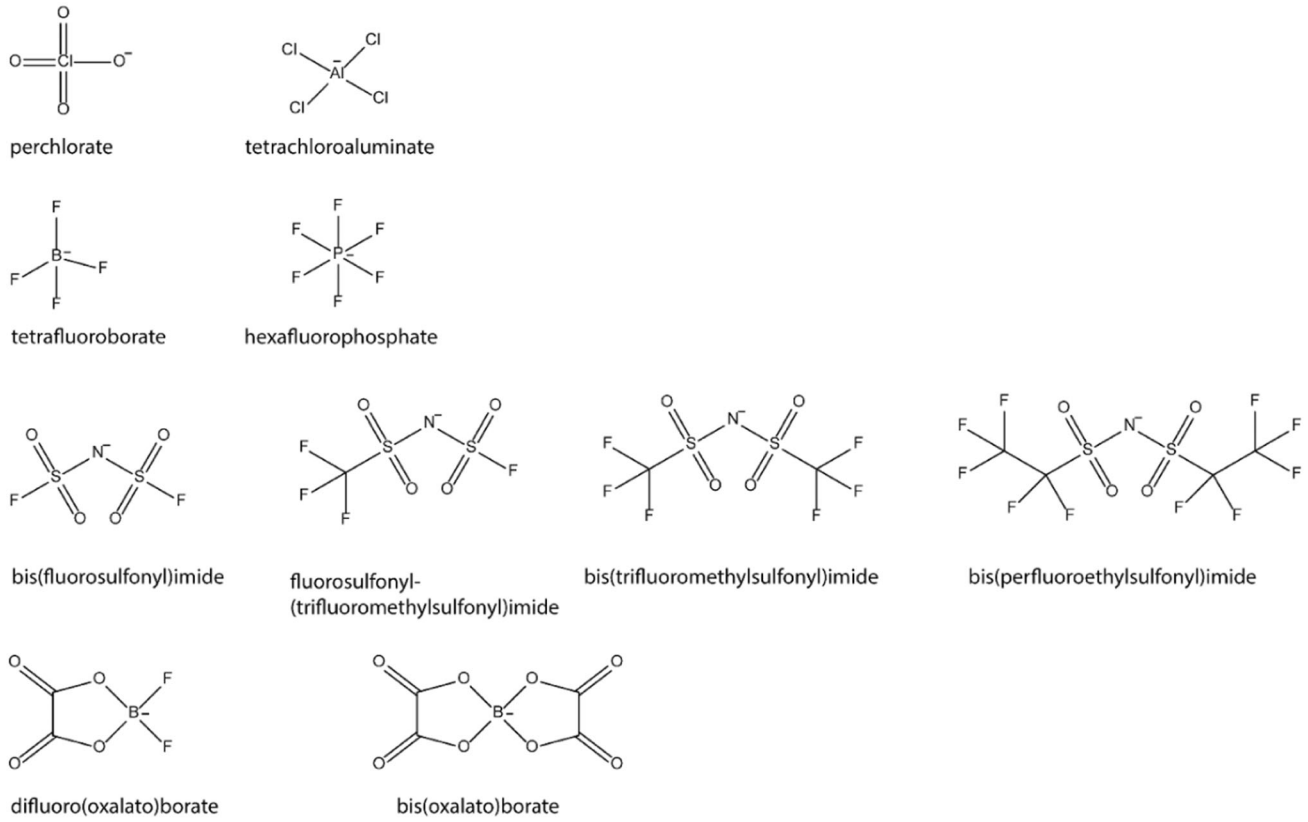

FIGURE 4 Examples of anions that are of interest in dual-ion battery chemistry.

can affect the intercalation capacity and kinetics.[80,124,174,175] Speaking of electrochemical stability, perchlorate (ClO_4^-), for instance, undergoes less efficient intercalation as compared to BF_4^- and PF_6^- due to its poor reductive stability, inevitably causing excessive electrolyte decomposition.[123,176] On the other hand, salts containing BF_4^- anions have limited solubility in organic solvents while PF_6^--containing salts are sensitive to the presence of water, which restricts their applicability in DIBs. Salts with weakly coordinating anions such as FSI and TFSI are highly soluble in most solvents encountered in batteries and thus are more suited to prepare concentrated electrolytes with optimum ionic conductivities.[177] High salt concentration substantially improves stability at high potentials and makes such electrolytes of particular importance in DIBs.[80,178] Another important question concerns how the size of a given anion influences intercalation capacity and kinetics. Intuitively, smaller anions could be expected to intercalate more readily, thereby allowing for high discharge capacity. Experimental data, however, indicate no clear relation between anion size and intercalation capacity, but rather that the type of solvent used in the electrolyte has a remarkable influence on the extent of anion intercalation.[60,61,63,94,124] For instance, BF_4^-, which is smaller than most anions mentioned above, has lower intercalation capacity in carbonate solvents as compared to PF_6^-, ClO_4^-, FSI, and TFSI.[176,179]

Despite the more facile intercalation, electrolytes containing LiTFSI and LiFSI salts dissolved in organic or IL solvents cause incessant dissolution of the Al current collector during anodic polarization (>4.0 V vs. Li^+/Li), leading to the formation of soluble $[Al(FSI)_x]^{3-x}$ complexes.[133,180] As a consequence, such reactions result in extensive pitting on the Al surface. These shortcomings can be remedied using salt additives like $LiPF_6$, $LiBF_4$, and LiDFOB, which can generate reactive fluoride ions needed for efficient passivation of the Al current collectors even above 5.2 V.[133] Naturally, combining salts can be a viable strategy to prepare electrolytes with high ionic conductivity and ability to passivate Al, while also enhancing anion uptake.[94,181,182] For instance, a 0.8 M KFSI electrolyte has higher conductivity but suffers from severe degradation even at potentials <4.5 V, as opposed to electrolytes containing a mixture of KFSI and KPF_6 salts (1:3 molar ratio). The electrolytes with mixed salts exhibit electrochemical stability ranging from 4.8 to 5.2 V, suggesting that KPF_6 salt mitigates electrolyte decomposition and Al corrosion, which in turn increases the reversible intercalation capacity to 103 mAh g^{-1}.[181] Another example shows that mixing $LiPF_6$ salt with $NaPF_6$ and $Ca(PF6)_2$ salts enables the design of Na- and Ca-based DIBs with enhanced rate performance, longer cycle life, and more stable interfacial layers.[182,183] A summary of the advantages and disadvantages of salts commonly used in DIBs is given in Table S2.

2.3 | Solvents

Different types of solvents including water, carbonates, carboxylate esters, phosphates, sulfones, ethers, ILs, and DES have been considered in the preparation of electrolytes for DIBs. Examples of these solvents and their relevant properties are provided in Tables 1 and S1. In addition, some pros and cons of various solvent classes are presented in Table S3. Structures of representative examples are shown in Figure 5. When choosing a solvent, the primary focus must be on its ability to

- withstand reduction and oxidation within the electrochemical window required for DIB operation,
- dissolve sufficiently high amount of salt needed to prepare concentrated electrolytes, and
- maintain safety to ensure a low risk of health and fire hazards.

Even though ethers are good solvents in electrolytes desired for high-rate applications, they have limited stability at potentials beyond 4 V versus Li^+/Li, and hence, they are not commonly used in DIBs. However, a few examples exist in which they are used as diluents in ILs,[184] or as solvents in the presence of high salt concentration or additives which can help minimize oxidative decomposition to some extent.[185]

2.3.1 | Carbonates

Carbonates are by far the most common solvents used in DIB electrolytes (see Figure 5B). They exhibit a range of dielectric constants, dynamic viscosity, density, and electrochemical stability depending on chemical structure and composition. Classic examples are cyclic carbonates such as EC and PC, and linear carbonates like EMC, DMC, and DEC.[186–192] Generally, cyclic carbonates possess a high dielectric constant and are favorable for dissolving electrolytes salts,[193] while linear carbonates lower the viscosity and enhance ion conduction as a consequence.[194] To prepare concentrated electrolytes, a high dielectric constant carbonate such as EC and low-viscosity carbonates such as DMC and EMC are mixed in specific proportions to achieve a trade-off between ionic conductivity and salt concentration required for high power and high energy performance (see Figure 7A–D).[2,86,183,186–188,194–201] For example, the

TABLE 1 Some solvents commonly used in electrolytes for dual-ion batteries.

Solvent	Molar mass (M) (g mol^{-1})	Dynamic viscosity (cP) at 25°C	Density (g cm^{-1}) at 25°C	Permittivity (ε)	Boiling point (°C)	Melting point (°C)	Flash point (°C)	Autoignition temperature (°C)
MA	74	0.36	0.93	6.7	57–58	−98	−13	454
MDFA	110.06	–	1.26	–	85–87	–	19–24	–
EA	88.11	0.43	0.89	6	76.5–77.5	−84	−4	426–427
MP	88.11	0.43	0.91	6.2	79.8	−88	−2	469
GBL	86.09	1.73	1.12	41.7	208	−44	98	435
DMC	90.08	0.59	1.06	3.2	90	4.6	18	458
EMC	104.10	0.65	1	2.4	109	−53	23	446
DEC	118.13	0.75	0.97	2.82	127	−43	33	445
FEMC	122	1.4	1.2	7.3	–	–	–	–
MTFEC	158	0.74[a]	1.33	7.1	90	–	38	–
EC	88.6	1.9[a]	1.32[a]	90[a]	248	38	160	465
VC	86.05	–	1.36	126	162–178	15–22	72–80	355
PC	102.9	2.51	1.2	65	242	−49	132	455
BC	116.12	3.2	1.14	56.1	241	−53	135	–
FEC	106.05	–	–	–	212	18–23	>100	–
EMS	108.16	4[b]	1.16[c]	57.5[d]	239–247	32–37	>110	–
SL	120.17	10.4[d]	1.26	43.4[d]	285	20–26	177	528
MSL	134.2	11	1.2	29	276	0.5	154	–
TMP	140.07	1.3	1.2	21.26	197	−46	148	391
TEP	182.15	1.6	1.07	13	216	−56.4	117	454
TPP	224.23	1.01	–	–	120–122	252	113	–

Abbreviations: BC, 1,2-butylene carbonate; DEC, diethyl carbonate; DMC, dimethyl carbonate; EA, ethyl acetate; EC, ethylene carbonate; EMC, ethyl methyl carbonate; EMS, ethyl methyl sulfone; FEC, fluoroethylene carbonate; FEMC, 2-fluoroethyl methyl carbonate; GBL, γ-butyrolactone; MA, methyl acetate; MDFA, methyl difluoroacetate; MP, methyl propionate; MSL, 3-methyl sulfolane; MTFEC, methyl-2,2,2-trifluoroethyl carbonate; PC, propylene carbonate; SL, sulfolane; TEP, triethyl phosphate; TMP, trimethyl phosphate; TPP, tripropyl phosphite; VC, vinylene carbonate.

[a]Data at 40°C.

[b]Data at 35°C.

[c]Data at 50°C.

[d]Data at 30°C.

first discharge capacity for a Li-graphite DIB was observed to reach a maximum as the $LiPF_6$ concentration in PC increased to about 2 M, and then dropped to a minimum at 3 M. In contrast, in the case of concentrated $LiPF_6$ salt in DMC, EMC, and MP, it increased continuously with increasing concentration of the salt.[202] In a related study, a 5 M KFSI in EC + DMC electrolyte was used in a K-graphite DIB in which the specific energy increased substantially to ~207 Wh kg^{-1}.[178]

Despite its ability to dissolve salts and create SEI layers on graphite-negative electrodes, EC has a strong tendency to coordinate to anions like BF_4^- and PF_6^-, thereby limiting their intercalation in graphite, as verified using XRD, electrochemical quartz crystal microbalance (EQCM) and Raman spectroscopy.[80,170,171,174,175,186,203-208] In situ XRD has been used to assess the extent of PF_6^- intercalation in graphite from electrolytes containing PC and EC solvents.[207,208] The XRD patterns showed that the characteristic (002) peak of graphite experienced a noticeable shift as the cells containing PC-based electrolytes were charged to 3.7 V, indicating the onset of PF_6^- intercalation. In contrast, hardly any shift was observed in the (002) peak position for the EC-based electrolyte even after charging to 4.7 V, which verified that EC hampered the electrochemical intercalation process. However, it is worth noting that EC-based electrolytes can have low ionic conductivity and high

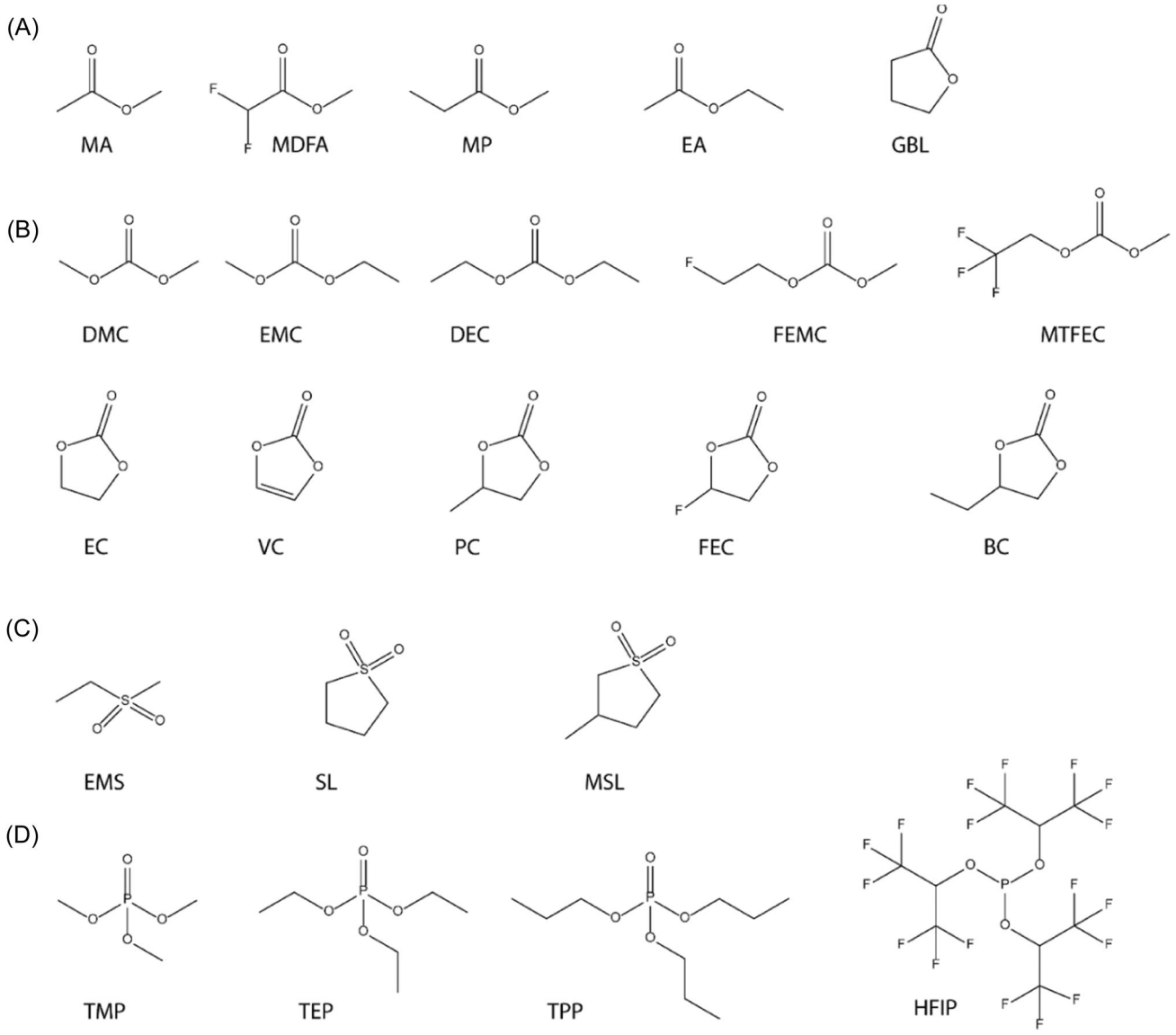

FIGURE 5 Solvents and additives for the dual-ion battery chemistry: (A) carboxylate esters such as methyl acetate (MA), methyl difluoroacetate (MDFA), ethyl acetate (EA), methyl propionate (MP), and γ-butyrolactone (GBL), (B) linear and cyclic carbonates including dimethyl carbonate (DMC), ethyl methyl carbonate (EMC), diethyl carbonate (DEC), 2-fluoroethyl methyl carbonate (FEMC), methyl-2,2,2-trifluoroethyl carbonate (MTFEC), ethylene carbonate (EC), vinylene carbonate (VC), propylene carbonate (PC), fluoroethylene carbonate (FEC), and 1,2-butylene carbonate (BC), (C) sulfones like ethyl methyl sulfone (EMS), sulfolane (SL), and 3-methyl sulfolane (MSL), and (D) phosphates including trimethyl phosphate (TMP), triethyl phosphate (TEP), tripropyl phosphate (TPP), and tris(1,1,1,3,3,3-hexafluoro-2-propyl) phosphite (HFIP).

resistive loss which causes a shift in the intercalation potential. A similar tendency to impede anion intercalation was also observed in electrolytes containing $LiPF_6$ dissolved in SL, γ-butyrolactone (GBL), and trimethyl phosphate (TMP) solvents, as shown in Figure 6.[175,189,204,210] The addition of low-viscosity solvents such as DMC and EMC is expected to weaken the interactions between EC and PF_6^-, thereby increasing the intercalation capacity.[4,186,203,204] For example, a DIB using 1 M $LiPF_6$ in EC + DMC electrolyte delivered a discharge capacity of ~48 mAh g^{-1}.[69] In the electrolytes containing 1 M $LiPF_6$ in EC + PC, an increase in the amount of EC caused a sharp decrease in the discharge capacity. In contrast, adding 1,2-butylene carbonate (BC) to a 1 M $LiPF_6$ PC + BC electrolyte caused the discharge capacity to decrease from 64 to 52 mAh g^{-1} where it stabilized. The discharge capacity of the graphite electrode in the $LiPF_6$ dissolved in EC is much lower than that in electrolytes containing PC and BC, conclusively showing that PF_6^- intercalation is severely hampered by the presence of EC.[211] Studies have additionally shown that electrolytes containing PC and BC solvents allow for a higher amount of BF_4^- storage in the graphite electrode in the absence of EC.

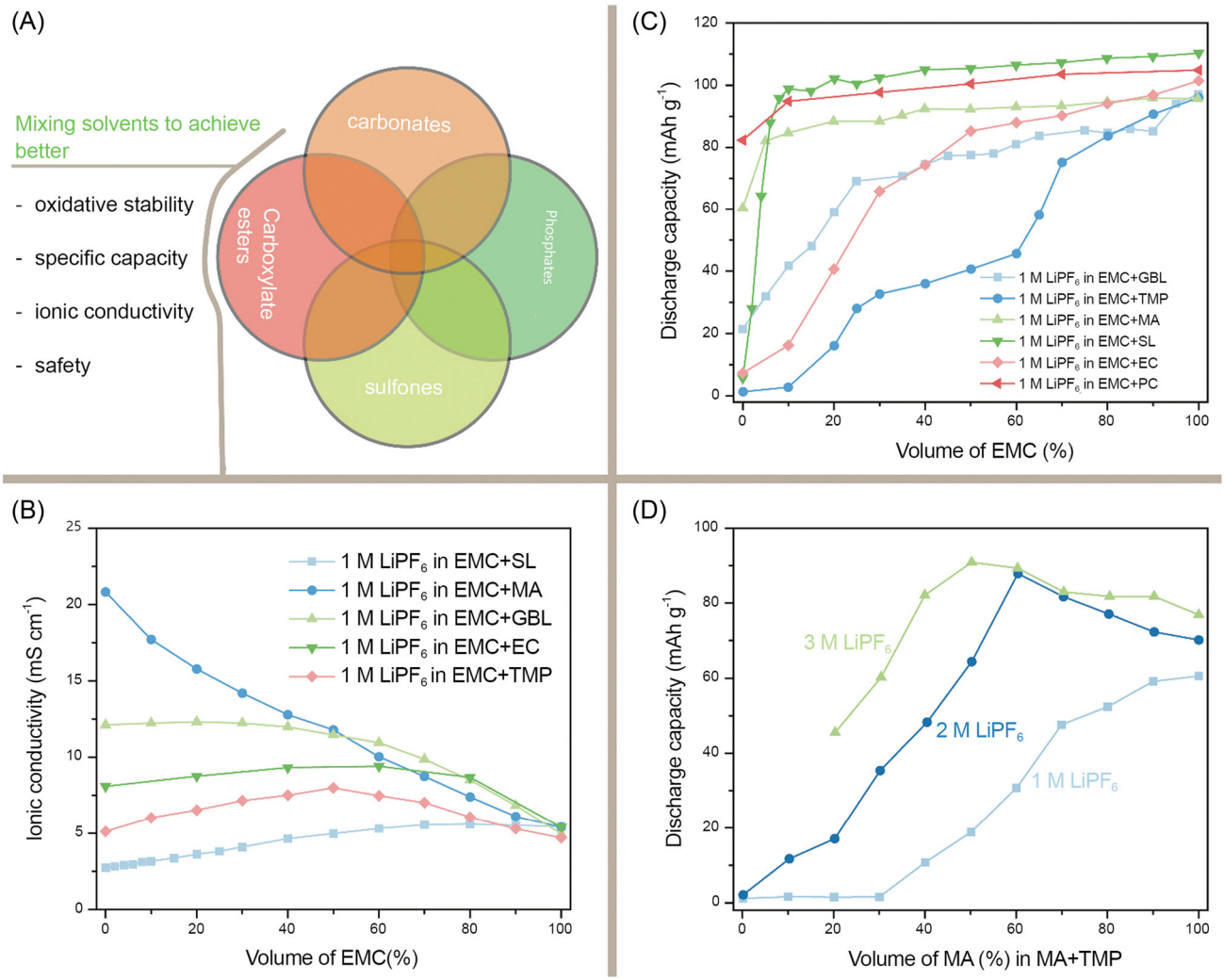

FIGURE 6 Mixing solvents to enhance reversible capacity without affecting ionic conductivity: (A) the benefits of mixed solvents with different functions, (B) impact of adding EMC to different types of solvents on the ionic conductivity of 1 M $LiPF_6$, (C) trend in discharge capacity with increasing volume of EMC as a function of solvent mixtures, and (D) the dependence of discharge capacity on salt concentration and the volume proportion of MA in TMP. Data for these plots were extracted from the different publications cited in this paper using WebplotDigitizer version 4.4.[209]

In both EC + PC and EC + GBL mixtures, the initial discharge capacity for BF_4^- intercalation decreased significantly as the EC content rose.[171] Similar to EC, pure GBL appeared to suppress PF_6^- intercalation, as evidenced by XRD, Raman, and EQCM studies.[212] Interestingly, adding EMC increased the intercalation capacity. The capacities of PF_6^- intercalation for the electrolytes 1 M $LiPF_6$ in EMC and 1 M $LIPF_6$ in GBL, the capacities associated with PF_6 intercalation were, respectively, 97 and 21 mAh g^{-1}. These observations also confirm that EMC is more suitable than other carbonates for PF_6^- intercalation, as shown in Figure 6C.[213,214] In line with this conclusion, a higher PF_6^- intercalation capacity, namely ~110 mA h g^{-1} at 200 mA g^{-1}, was also reported for an Al–graphite DIB using an electrolyte based on neat EMC solvent.[65] Apart from differences in intercalation capacity, solvents affect the onset overpotentials required for anion intercalation. Amongst DEC, DMC, and EMC, for which discharge capacities of 80–95 mAh g^{-1} were demonstrated, EMC showed less intercalation overpotential (~0.26 V) as compared to both DMC and DEC (0.34–0.38 V).[215] Furthermore, a recent study by Wang et al.[81] demonstrated the benefits of substituting EC and EMC with their fluorinated counterparts FEC and FEMC. Even though a low salt concentration was employed (1 M $LiPF_6$), the highly fluorinated electrolytes exhibited remarkably high oxidative stability (vis-à-vis 1 M $LiPF_6$ in EMC) in Li–graphite DIBs cycled between 3.0 and 5.2 V versus Li^+/Li. Optimal performance was achieved in 1 M $LiPF_6$ in FEC + FEMC (3:7), which increased the capacity retention to ~95% after 5000 cycles. Essential performance metrics of DIBs in different electrolytes are summarized in Table S4 and Figure 7A–D.

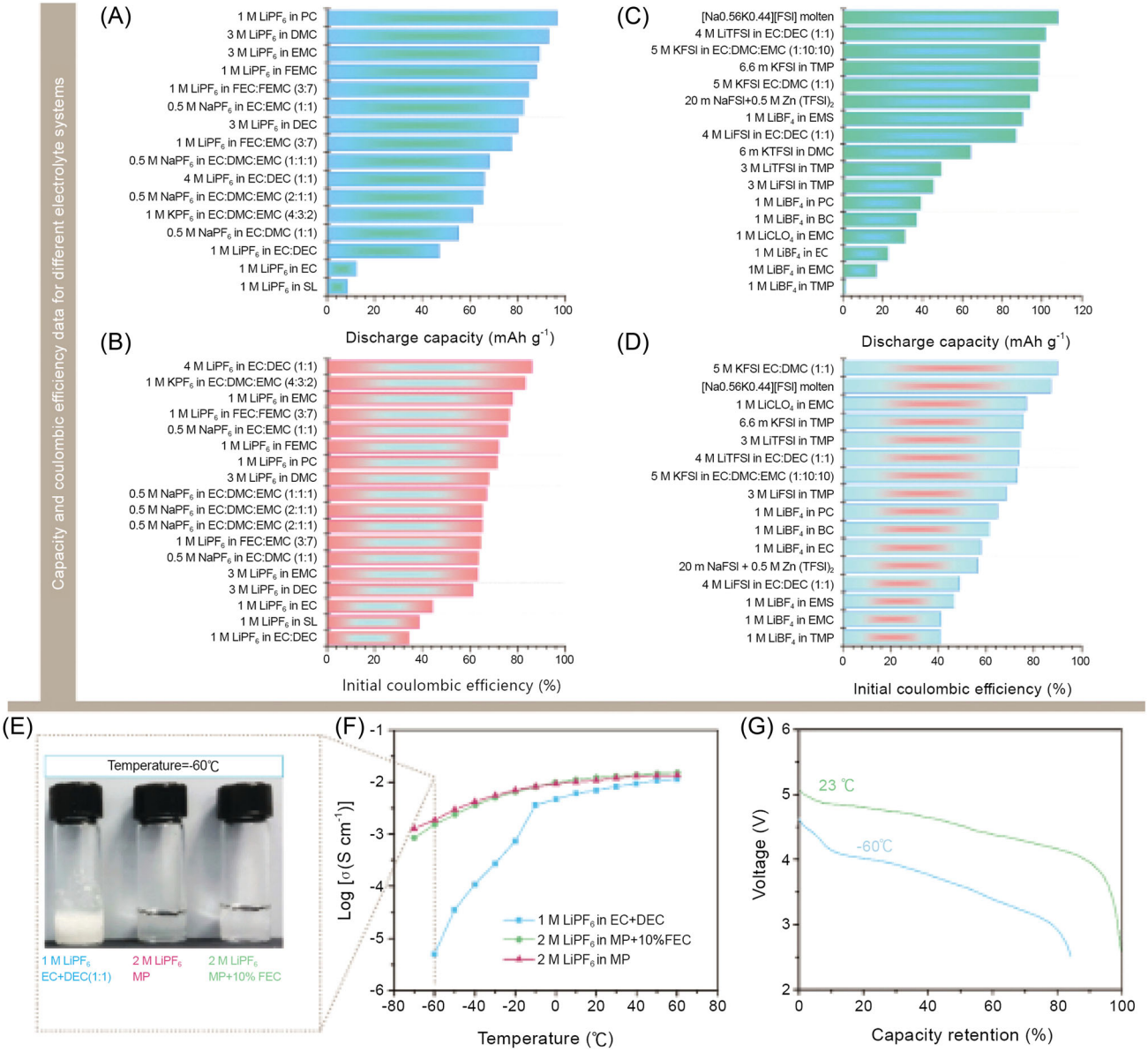

FIGURE 7 Electrochemical performance for selected electrolytes used in dual-ion cells: (A) specific capacity values for PF_6^- intercalation in graphite from electrolytes containing different concentrations of APF_6 (A = Li^+, Na^+, and K^+) in organic solvents, (B) initial Coulombic efficiency values corresponding to the data in (A), (C) a summary of the discharge capacities from graphite electrodes intercalated with anions other than PF_6^-, that is, ClO_4^-, BF_4^-, TFSI and FSI, (D) the Coulombic efficiencies for the electrolytes shown in (C, E), three electrolytes containing different amounts of $LiPF_6$ in carbonate and carboxylate esters at −60°C, (F) plots display how temperature influences the ionic conductivities of the three electrolytes shown in (E), and (G) discharge curves measured at 80 mA g^{-1} and two different temperatures (23°C and −60°C) for a graphite–graphite dual-ion cells using 2 M $LiPF_6$ in MP + 10% FEC electrolyte. The bar charts shown in (A–D) are based on the data tabulated in Table S2 in which the related references are included. The picture in (E) and the data plotted in (F) and (G) were Reproduced with permission: Copyright 2019, Wiley-VCH Verlag GmbH & Co. KGaA[216] The data shown in the plots in (F) and (G) were data extracted from the published graphs using WebplotDigitizer version 4.4.[209]

2.3.2 | Sulfones

Solvents bearing the sulfone functional group such as EMS and sulfolane (SL) have notable anodic stability and possess high dielectric constant allowing for high salt concentrations, which is desirable for DIB applications.[217-220] The electrochemical PF_6^- intercalation from an electrolyte based on EMS (stable up to 5.6 V) was reported to be more efficient than that containing EC and DEC (stable up to 5.2 V).[47] Charging to 5.45 V, a Li–graphite DIB containing a 2 M $LiPF_6$ in EMS electrolyte allowed for a discharge capacity of 95 mAh g^{-1} with 83% CE for the initial cycle. Apart from $LiPF_6$, salts composed of the sulfonylimide anions have also

been employed together with sulfones. At low salt concentrations like in 1 M LiTFSI and LiBETI in EMS, the electrolytes were more prone to degradation when charged to 5.0–5.6 V, resulting in 20%–74% CE in addition to lower discharge capacity. For example, only a maximum of 63 mAh g^{-1} was achieved for 1 M LiTFSI.[61] The favorable stability of sulfones is manifest in a 0.8 m LiFSI in SL electrolyte which allowed for more reversible intercalation (discharge capacity of ~48 mAh g^{-1} with 64% CE) in the range 3.0–5.2 V as compared to a 0.8 m LiFSI in EC + DMC (1:1 vol/vol) electrolyte.[221] As expected, increasing the salt concentration from 0.8 to 4 m in SL further enhanced oxidative stability with the capacity and CE at 200 mA g^{-1} increasing to nearly 113 mAh g^{-1} and 93%, respectively. This clearly demonstrates the benefit of using sulfones and the positive impact of higher salt concentrations on DIB performance.

SL can extend electrolyte stability to about 6 V versus Li^+/Li allowing for increased capacity. For instance, intercalation of BF_4^- in graphite cycled between 4.5 and 5.5 V versus Li^+/Li in an electrolyte containing 1 M $LiBF_4$ dissolved in a neat SL was characterized by a reversible capacity of 80 mAh g^{-1}. This is dramatically higher than what has been observed for BF_4^- in carbonate solvents.[222,223] Nevertheless, SL has a high viscosity and high melting point (see Table 1),[175,224] which may limit the rate capability of DIBs, particularly at low temperatures. Therefore, SL is usually mixed with low-viscosity carbonates like EMC to prepare electrolytes with a good balance between ionic conductivity and oxidative stability. Introducing EMC or PC into a 1 M $LiPF_6$ in SL electrolyte has been shown to increase both PF_6^- intercalation and ionic conductivity by reducing the viscosity of SL (see Figure 6B,C).[175,225,226] In a Li–graphite DIB cycled between 3.0 and 5.4 V, adding even 10% EMC increased the cell capacity from ~5 to ~100 mAh g^{-1}, which is comparable to that for pure EMC.[175] The same DIB cell cycled at 200 mAg^{-1} using an electrolyte based on 1 M $LiPF_6$ dissolved in a mixture of SL and EMC (1:4) showed a reversible capacity of 105 mAh g^{-1} along with 93% capacity retention over 1000 cycles. Similar behavior has been observed for BF_4^- intercalation. In a 1 M $LiBF_4$ solution, mixing EMC with SL and MSL appeared to increase the capacity, with the effect being more dramatic in the case of MSL.[223] As compared to the neat MSL for which negligible capacity was obtained (~2 mAh g^{-1}), a graphite DIB delivered a discharge capacity >30 mAh g^{-1} upon adding 50% EMC. It is worth noting that the discharge capacity from BF_4^- intercalation in a neat EMC solvent was likewise negligible.[168,170]

2.3.3 | Phosphates

Phosphate solvents such as TMP are beneficial to reducing or eliminating the flammability of electrolytes, hence ensuring operational safety.[227,228] However, most phosphates possess lower oxidative stability as compared to carbonates and sulfones. No significant intercalation capacity can be attained in electrolytes composed of 1 M $LiPF_6$, $LiBF_4$, LiTFSI, or LiFSI salts dissolved in pure TMP. Increasing salt concentration has been shown to alleviate this shortcoming.[229] For 3 M salt concentrations in these electrolytes, the discharge capacity increased to 40–50 mAh g^{-1} (for a potential cut-off ranging from 5.2 to 5.8 V). However, the potential hysteresis (polarization) was very high, particularly in the case of $LiPF_6$ and $LiBF_4$. Another comparative study dealing with 3 M LiTFSI in alkyl phosphate solvents including TMP, TEP, TPP, and TBP further indicated that TMP performed better in terms of reversible capacity and rate capability in a Li–graphite DIB charged to 5.2 V.[230] The study underlined that the structure and molecular mass of the phosphates impacted anion intercalation. Moreover, a hard carbon–graphite DIB using an electrolyte based on NaTFSI salt in TMP (1:2 molar ratio) exhibited a reversible capacity reaching ~47 mAh g^{-1} at 500 mA g^{-1} within the 2.0–4.6 V range, but the capacity faded to 71% over 200 cycles.[231] Adding EMC improves the capacity and oxidation stability of phosphates, leading to better results in DIBs. Notably, only limited BF_4^- intercalation (1–3 mAh g^{-1}) was observed from a solution of 1 M $LiBF_4$ dissolved in either EMC or TMP, while mixing the two solvents in a 4:1 ratio increased the capacity to ~27 mAh g^{-1}.[170] In contrast, more efficient and considerable intercalation behavior has been observed in the range of 3.0–5.2 V for electrolytes such as 1 M $LiPF_6$ in EMC electrolyte, and 1–3 M $LiPF_6$ in a mixture of EMC and TMP.[189] In a 3 M $LiPF_6$ in a mixture of TMP and EMC solvents (3:7), a discharge capacity of ~100 mAh g^{-1} and iCE ~85% were observed, which were higher than those for 1 M $LiPF_6$ in EMC and 1 M $LiPF_6$ in 3:7 of TMP and EMC (<80 mAh g^{-1}).

2.3.4 | Carboxylate esters

Carboxylate esters have a relatively low melting point and viscosity, which promotes ionic conductivity and electrochemical performance, even at freezing temperatures (see Table 1).[232] Common examples of esters include MA, MP, and GBL, the structures of which are shown in Figure 5A. For example, an electrolyte with 2 M $LiPF_6$ dissolved in methyl propionate (MP) could stay

liquid even at −60°C while the ionic conductivity was 1.89 mS cm^{-1} (see Figure 7E,F).[216] For this reason, MP can be chosen as a solvent or cosolvent in battery electrolytes due to its low melting point of ~−88°C. Important limitations of MP are related to its poor reductive stability below 0.5 V versus Li^+/Li, which leads to irreversible Li plating as observed in a 2 M $LiPF_6$-MP electrolyte.[232] Adding 10% (vol/vol) FEC improved the anodic stability and reversibility of Li plating as it likely results in a more stable SEI layer,[232] without compromising its conductivity at low temperatures, as shown in Figure 7F. A graphite–graphite DIB cycled at −40 and −60°C was able to retain, respectively, 93% and 84% of its room temperature capacity (see Figure 7G).[216] PF_6^- intercalation in pure MP solvent gave rise to a maximum reversible capacity of ~118 mA h g^{-1} and performed well as compared to electrolytes based on EMC solvent.[171] Increasing salt concentration was observed to improve both intercalation capacity, CE, and long-term capacity retention, although the ionic conductivity decreased. For instance, in a 3.5 M $LiPF_6$ in MP electrolyte a discharge capacity of 110 mA h g^{-1} was obtained with a 90% retention after 300 cycles for a Li–graphite DIB cycled in the range 3.0–5.2 V.[233] In essence, mixing carbonates and carboxylate esters can help achieve electrolytes with sufficient oxidative stability and enhanced performance at low temperatures. A mixed electrolyte based on 1 M $LiPF_6$ in EMC + MA (1:1, vol/vol) exhibited an ionic conductivity of ~12 mS cm^{-1} (Figure 6B). The electrolyte performed well at −25°C in a Li–graphite DIB which delivered a discharge capacity of ~40 mAh g^{-1} with 70% capacity retention after 200 cycles, which was much higher than that for 1 M $LiPF_6$ in EMC (~9 mAh g^{-1}) at the same temperature.[234]

In addition to poor reductive stability, carboxylate esters possess low flash points and are highly flammable, and thus they present a serious fire hazard (see Table 1). In general, adding flame-retardant solvents such as TMP can be an effective remedy to boost safety. As shown in Figure 6C, pure MA resulted in a reversible capacity of 60 mAh g^{-1} for PF_6^- intercalation, unlike the negligible capacity in pure TMP.[235] A DIB using 3 M $LiPF_6$–MA electrolyte could maintain about 77 mAh g^{-1} with <80% CE for only 100 cycles, which may be related to the lower oxidative stability of MA. When 50% TMP was added into this electrolyte, however, the initial discharge capacity increased to roughly 90 mAh g^{-1} with the CE improving to over 97%. Nevertheless, an optimum amount of TMP should be used to avoid performance degradation. The discharge capacity varied between 47 and 77 mAh g^{-1} as the volume of TMP decreased from 50% to 20% in the 3 M $LiPF_6$ in MA + TMP electrolyte (see Figure 6D).

2.4 | Interfacial reactions on anion-intercalated graphite electrodes

Indisputably, the DIB technology can be an attractive alternative energy storage system from the perspective of materials sustainability and availability. Besides, high cell voltages of DIBs will ultimately offer the benefit of fairly high energy density. This advantage, however, comes at the expense of increased chances of parasitic reactions at both the negative and positive electrodes, since the electrode reactions lie outside the ESW of most electrolytes (see Figure 3). As discussed in the previous sections, the majority of electrolyte salts and solvents are not stable at both potential extremes. In particular, the relatively high potential (>4.3 V) needed for anion intercalation subjects the DIB concept to severe electrolyte degradation and corrosion which result in limited cycle life and rapid self-discharge. Such side reactions most often entail the reductive/oxidative decomposition of salt anions and solvents in the electrolyte, while other seemingly inactive cell components such as the binders and current collectors can degrade in the course of cell operation. Apart from the deterioration of cell performance, parasitic reactions eventually lead to electrolyte dry-up and gas pressure build-up causing swelling of the cell[236] as well as loss of mechanical integrity and electronic contact within the electrodes. Hence, suppressing side reactions at both electrode–electrolyte interfaces is a research topic of paramount importance as far as improving the performance, lifetime, and safety of dual-ion cells are concerned. In this section, highlights of studies dealing with interfaces in DIBs are presented.

2.4.1 | The CEI layer

Reactions at the interface of the positive electrode and the electrolyte can entail anion intercalation, solvent cointercalation, oxidation of solvent molecules and anions, anodic dissolution of the Al current collector, and binder degradation. To combat undesired reactions at the interface, strategies focusing on the modification of the electrode–electrolyte interfaces have become common. As illustrated in Figure 8A, the principal aim is to create

- a thin, uniform protective layer on the positive graphite electrode that is electronically insulating to prevent side reactions but permeable to anions, and
- a passivation layer on the Al current collector that renders it inaccessible to solvent molecules.

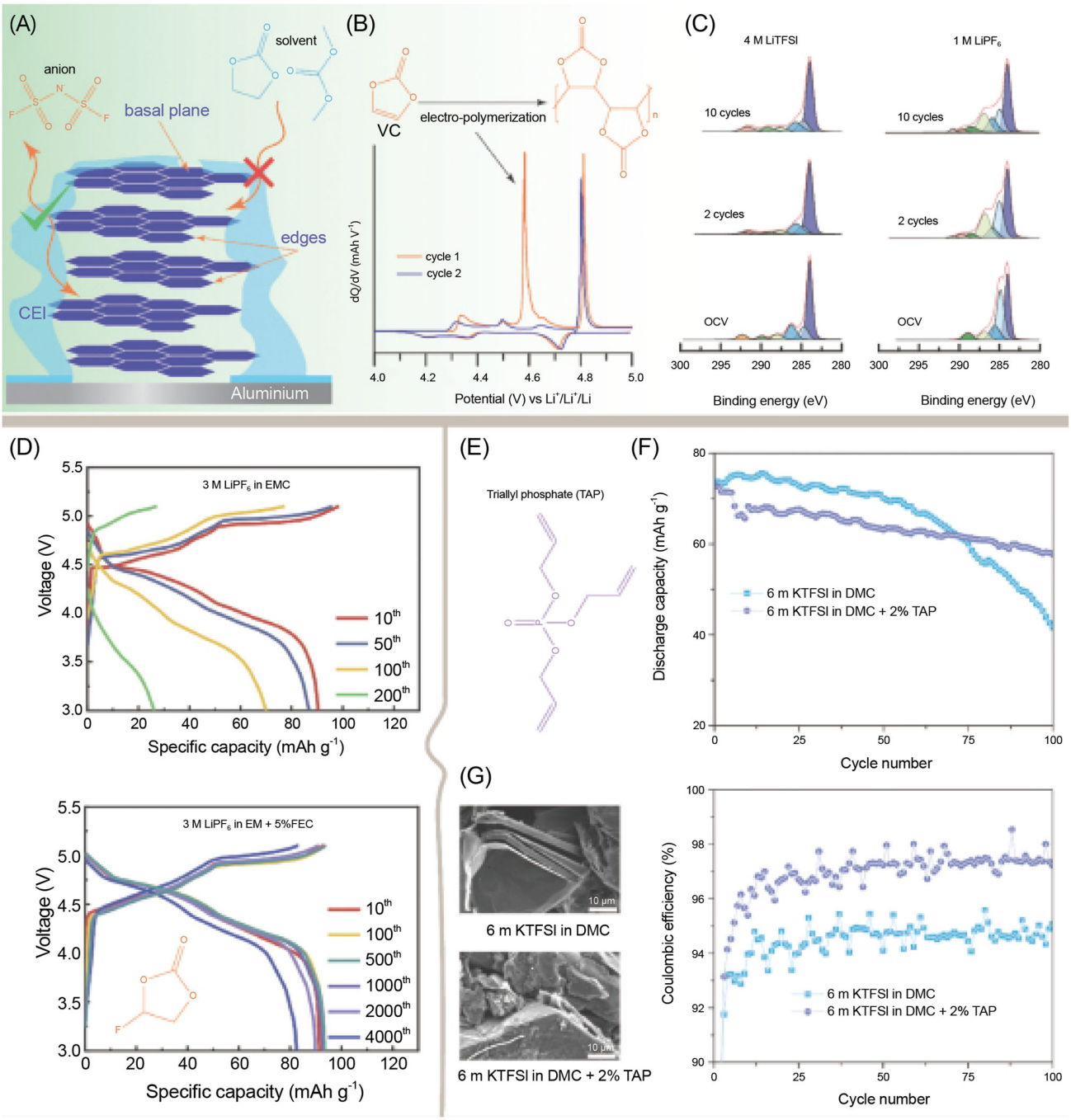

FIGURE 8 Understanding the nature of interfacial reactions in a DIB and mitigating their impact on cell performance: (A) schematic illustration showing the structure of graphite and the cathode-interface layer on the surface, and (B) oxidative polymerization of the VC additive indicated in the differential capacity plots for two cycles. Reproduced with permission: Copyright 2023, Elsevier Ltd.[237] (C) Comparisons of the C 1s XPS for graphite electrodes before and after cycling in 4 M LiTFSI and 1 M $LiPF_6$ in EC-DEC electrolytes. Reproduced under a Creative Commons Attribution (CC-BY): Copyrigt 2021, American Chemical Society.[80] (D) Galvanostatic curves at 500 mA g^{-1} for a selected number of cycles in 3 M $LiPF_6$ in EMC electrolyte with and without FEC additive. Reproduced with permission: Copyright 2020, Elsevier B.V.[238] (E) The chemical structure of triallyl phosphate. (F) SEM images of graphite electrodes after 100 cycles in 6 m KTFSI in DMC electrolytes with and without TAP additive, and (G) extended cycling at 50 mA g^{-1} and associated Coulombic efficiency of MoS_2-graphite KDIBs employing an electrolyte consisting of 6 m KTFSI in DMC with and without TAP additives.[82] Reproduced under the Creative Commons License (CC-BY): Copyright 2021, Cell Press.[82]

Unlike in a lithium-ion battery,[239] the CEI layer in a DIB is supposed to conduct only anions while keeping solvent molecules at bay. In fact, inorganic decomposition products that form in the presence of EC and $LiPF_6$, for instance, are highly undesirable as they hamper the intercalation of anions in graphite.[80] It is also important to note that other cell components like binders can impact or even modify the electrode–electrolyte interface as they are in intimate contact with the active materials and current collectors.[240] The formation of a stable CEI can be carried out in situ or ex situ in the dual-ion cells. These approaches adopted in the design of the CEI layer include

- coating the pristine graphite electrodes before cell assembly[82] or precycling the electrodes in the presence of interface modifying additives, and
- adding critical amounts of cosolvents and/or salt additives[133,238,241–243] which can induce the formation of stable interfacial layers.

Examples of the first instance are thin layers of titanium and aluminum oxides coated onto graphite electrodes to mimic stable CEI layers. A thin coating of LTO on graphite electrode has been reported to improve capacity retention (~85% after 2000 cycles)[244] attributed to its structural stability,[245] although it has a suspected ability to catalyze electrolyte decomposition[246] and polymerization of some solvents like SL. Likewise, an Al_2O_3 (ALO) thin film has been proposed to alleviate side reactions occurring during anion intercalation.[198] Performance enhancements related to the ALO-coated graphite (capacity retention of 82.3% after 1000 cycles) were attributed to ALO leading to the generation of a CEI rich in organic species in a 4 M $LiPF_6$ in EMC electrolyte. This was different from the electrode cycled without modification, in which case the CEI contained predominantly LiF and $Li_xPF_yO_z$ species. The increased contribution from polymerized CEI species with the ALO coating was suggested to enhance the flexibility of the CEI, and subsequently, its ability to withstand volumetric changes experienced in the course of anion intercalation and extraction cycles.

In the second instance, some additives in the electrolyte can help create an efficient CEI layer during cycling. In particular, critical proportions of monomers with vinyl or allyl moieties can be included in the electrolyte formulation and later allowed to polymerize in situ on the electrode surface either electrochemically or chemically using radical initiators.[82,241,242,247] In this regard, there are a few examples of additives such as EC, fluoroethylene carbonate (FEC), vinylene carbonate (VC), and triallyl phosphate (TAP) (structures shown in Figures 5 and 8B) used to enhance the CEI layer on graphite electrodes.

Incorporating only a critical amount of salt and solvent additives can improve the electrochemical performance of DIBs.[208,248,249] The additives preferentially decompose to generate stable SEI and CEI layers that can inhibit further electrolyte decomposition. The addition of 0.03 M $LiNO_3$ to a 4 M $LiPF_6$ EMC (with 3 vol% VC) electrolyte is able to enhance the cycling life of Li–graphite DIB, leading to ~80% capacity retention over 1000 cycles in the range of 3.4–5.0 V.[247] Salts with reactive fluorinated anions can produce hydrofluoric acid (HF) which further reacts with the ALO layer on the Al surface, giving rise to a passivation layer composed of AlF_3.[133] In Al–graphite DIB, adding 2 wt% AlF_3 to the 3 M $LiPF_6$ EMC + DMC electrolyte with 3 wt% VC enabled intercalation of PF_6^- and AlF_4^- anions, resulting in a specific capacity of ~100 mAh g^{-1} at 0.2 A g^{-1} while preventing Al dissolution.[250]

Solvent additives or cosolvents can also improve oxidative stability and reduce the corrosive tendency of electrolytes, leading to longer cycle life of DIB prototypes. Adding 1–5 wt% VC was observed to effectively enhance the cycling stability of the Al–graphite DIB. A VC additive in 4 M $LiPF_6$ in EMC decomposed at ~4.37 V, forming a protective layer on the Al anode[251] as well as undergoing oxidative polymerization at ~4.6 V versus Li^+/Li (as shown in Figure 8B)[252] to generate a poly(VC) film that suppressed electrolyte decomposition.[241,242,253] Another type of additive, ES, improved the SEI layer on the graphite anode, increasing the discharge capacity of graphite–graphite DIB from 50 to 97 mAh g^{-1}. This is of vital importance in DIBs, given that concentrated electrolytes with sulfonylimide anions often fail to generate stable CEI layers, while those based on PF_6^- are prone to excessive decomposition resulting in thick coverage on the surface as X-ray photoelectron spectroscopy (XPS) studies have verified (see Figure 8C). In particular, fluorinated solvents and ethers such as FEC, FEMC, methyl difluoroacetate (MDFA), and tris (1,1,1,3,3,3-hexafluoro-2-propyl) phosphite (HFIP) (see Figure 5) are considered suitable cosolvents or additives in DIB electrolytes. For instance, improved passivation of Al can be achieved in an electrolyte containing 1 M LiTFSI dissolved in MDFA.[180] In a 1.7 M $LiPF_6$ in FEC + EMC (4:6 wt/wt) electrolyte, adding 5 mM HFIP was reported to improve cycle life and delivered a specific capacity of 85 mAh g^{-1} in the potential range 4.0–5.2 V versus Li^+/Li.[71] In addition, fluorinated carbonates can enhance the stability of the SEI layer on negative electrodes as well as impart oxidative stability. It was, for example, reported that adding 1–10 wt% FEC in IL electrolytes can improve the capacity from ~29 to

$80\ mA\ h\ g^{-1}$ and the cycle life of an Al–graphite DIB, with the CE rising from ~83% to 90%. Incorporating 2 vol% FEC in 1 M $LiPF_6$ in a mixture of EC, DEC, and EMC (1:1:1, vol/vol/vol) was reported to improve DIB performance as a more stable SEI layer formed.[254] There are also some reports which claim that FEC can help create thinner CEI layers on the positive graphite electrode, leading to more reversible PF_6^- cycling.[238] For instance, a Li–graphite DIB using 3 M $LiPF_6$ in EMC containing 5% FEC as the electrolyte could cycle with ~99% CE and ~85% capacity retention over 5000 cycles with a cut-off voltage of ~5 V (see galvanostatic curves in Figure 8D). However, it is important to note that there is no consensus on whether FEC helps in the CEI layer formation on positive electrodes. Possibly, fluorinated monomers can impart further stability to the CEI layer; otherwise, the monomers can be used together with salt additives that can supply labile fluorine species formed during cycling. Another class of additives that will likely enhance the cyclability of DIBs are monomers which can polymerize before or in the course of anion intercalation. Examples include TAP and diethyl vinyl phosphonate which can be polymerized electrochemically or chemically using 2,2-azobisisobutyronitrile (AIBN) as an initiator.[82,255] An interfacial layer formed from such polymers is anticipated not only to improve charge efficiency and cycle life but also to prevent excessive solvent cointercalation and graphite exfoliation, which is a common problem in DIBs (see Figure 8E–G).

2.4.2 | Detection and mitigation of gaseous decomposition products

Gas release can be a good indication of electrolyte decomposition. Identifying the evolved gases and their respective sources is necessary to gaining an in-depth understanding of degradation mechanisms.[256] Quantitative measurements of gases given off during cycling have, for instance, been achieved both in commercial pouch cell setups, by measuring either the cell thickness or making use of Archimedes principle, as well as in lab-scale prototype cells such as modified Swagelok cells equipped with pressure transducers.[257] To identify the gases, additional techniques such as gas chromatography combined with time-of-flight mass spectrometry (GC-MS) and electrospray ionization-high resolution mass spectrometry (ESI-HRMS) are necessary. While GC-MS is suitable for the identification of highly volatile species, ESI-HRMS extends the analysis regime down to moderately volatile compounds, including oligomers of polymerized solvent molecules. Ultimately, it is most useful to perform an operando gas analysis, which is feasible via the use of differential electrochemical mass spectrometry (DEMS) or online electrochemical mass spectrometry (OEMS) measurements.[256] Few studies have dealt with gas evolution in DIBs thus far. Using pouch cells (and based on Archimedes principle), the evolved gas volumes were compared for LTO-graphite cells containing the following electrolytes: (1) a mixture of 1.8 M $LiPF_6$ and 0.2 M $LiBF_4$ in DMC, EMC, and PC (1:1:1, wt/wt/wt), (2) 2 M $LiBF_4$ in PC, and (3) 2.0 M $LiBF_4$ in DMC. While volume changes were negligible in the cells containing $LiBF_4$ in PC and $LiBF_4$ in DMC, the cells containing $LiPF_6$/$LiBF_4$ in DMC/EMC/PC exhibited a dramatic volume increase in the first 1035 cycles, reaching $702\ cm^3\ g^{-1}$.[258] In a follow-up study combining gas volume estimation with gas chromatography, alternative electrolyte formulations helped suppress parasitic side-reactions to an even greater extent.[259] In this study, the mixture 1.8 M $LiPF_6$ and 0.2 M $LiBF_4$ in DMC:EMC:PC (1:1:1, wt/wt) electrolyte was compared to an electrolyte based on pure $LiPF_6$ salt and to an electrolyte composed of 1.6 M $LiPF_6$ and 0.3 M tetraethylammonium tetrafluoroborate ($TEABF_4$). After approximately 1020 cycles, the pure $LiPF_6$ electrolyte resulted in gas generation amounting to $276 \pm 53\ cm^3\ g^{-1}$, while the $LiPF_6$ electrolyte containing $LiBF_4$ and $TEABF_4$ led to 179 ± 19 and $54 \pm 18\ cm^3\ g^{-1}$, respectively. Gas chromatography revealed that H_2 was the dominant gas formed in the presence of the $LiBF_4$ and $TEABF_4$ additives (on the LTO negative electrode), along with trace amounts of CH_4 and C_2H_6 for the $LiPF_6 + LiBF_4$ composition. In addition, CO and CO_2 gases were detected in conjunction with the analysis of the graphite-positive electrode, although in a less amount from the cell using the $LiPF_6 + TEABF_4$ electrolyte.

A study using an OEMS setup was conducted on MnO–graphite DIBs containing 4 M $LiPF_6$-EMC electrolyte to verify the formation of volatile decomposition products.[241] In the mass spectra, the signals at m/z ratios of 47 and 48 were, respectively, tentatively assigned to PO radical species and CH_3CH_2F, which indicated the early decomposition of the electrolyte in the voltage ranging from 3.0 to 4.5 V range. Gas evolution intensified at voltages between 4.5 and 5.0 V, where a significant amount of CO_2 ($m/z = 44$) was also detected. In addition, VC was used to passivate the reactive cathode–electrolyte interfaces in the cell. The corresponding OEMS data indicated early decomposition of VC, shown by substantially enhanced CO_2 gas evolution around 3.5 V. The formation of poly(VC) suppressed the signals from PO and CH_3CH_2F during subsequent cycles; however, recurring CO_2 gas evolution around 3.5 V indicated the continuous reformation of the poly(VC) based SEI/CEI. Since these measurements were conducted in single-compartment full-cells, it is difficult to trace the causes of

gas evolution back to a specific electrode. Another study by Tong et al.[221] evaluated the electrochemical stability and gaseous decomposition products of electrolytes like 0.8 m LiFSI in EC + DMC (1:1 vol/vol), 0.8 m LiFSI in tetramethylene sulfone (TMS) and 4.0 m LiFSI in TMS employed in Li–graphite half-cells (at 0.1 mV s^{-1}, between 3.0 and 5.2 V). Interestingly, 0.8 m LiFSI in EC + DMC resulted in considerable amount of CO gas at potentials above 3.2 V versus Li^+/Li, while H_2 was the main gas formed in the cell containing LiFSI in TMS electrolyte. Furthermore, increasing the electrolyte concentration minimized the amount of H_2 detected; however, the impact of the high electrolyte viscosity on gas transport properties must be further studied to render these systems comparable. A study by Han et al.[244] indicated that the major gas formed when charging a Li-graphite cell with a 1.0 M $LiPF_6$ in EMC + SL electrolyte was CO_2 accompanied by trace amounts of SO_2 gas, and the latter was most likely released from SL· radicals.

Gel polymer electrolytes employed in the design of semi-solid-state DIBs can be expected to reduce gassing, as a result of the low or negligible amount of free solvent present. This was also observed in a study where the electrolyte contained microporous poly(vinylidene fluoride-*co*-hexafluoropropylene) (PVdF-HFP) membranes impregnated with $LiPF_6$ in EMC + 3 wt% VC.[260] Comparing the in situ gas partial pressures of cells subjected to a charging step at 5.0 V and employing either the gelled electrolyte or merely the liquid component ($LiPF_6$ in EMC + 3 wt% VC) showed that H_2 generation is more extensive in the latter case. Furthermore, lowering the potential to 4.8 V for the cell with a gelled electrolyte completely diminished the H_2 release. Further improvement in the interfacial properties of PVdF-HFP membranes can be achieved by introducing 40% polyvinyl acetate (PVAc).[217] In this case, the membranes were soaked in 1.0 M $LiPF_6$ in EMC + SL (1:4 vol:vol), which also served as the control liquid electrolyte. DEMS measurements during the first cycle suggested that less amount of CO_2 is evolved at elevated potentials (>5.0 V vs. Li^+/Li) in the case of the gelled electrolytes.

2.4.3 | Stability of current collectors

Although most studies focus exclusively on the interface between the active material and the electrolyte, interfacial contact between the electrolyte and the current collector, and the binder are just as important. In DIBs, an interface of particular interest is that between the Al-current collector and the electrolyte. The stability of the Al current collector suffers in the expanded electrochemical potential window of DIBs. Numerous studies have reported anodic dissolution of Al current collectors at potentials >4.0 V versus Li^+/Li, especially in electrolytes containing some of the most commonly used salts in DIBs, such as LiFSI[129] and LiTFSI.[261,262]

The use of HCEs[87,263-266] and ILs[88,102] has proved successful in alleviating Al dissolution. As few noncoordinated solvent molecules exist in HCEs, the solubility of Al^{3+}-anion complexes diminishes considerably, which in turn kinetically hinders Al corrosion. Some salts with labile fluoride ions such as $LiPF_6$, $LiBF_4$, and LiDFOB can be included to further enhance the stability of the Al current collector in HCEs and ILs. Anodic dissolution of Al in a LiTFSI in *N*-methyl-*N*-propyl-pyrrolidinium bis (fluorosulfonyl)imide (Pyr_{13}-FSI) electrolyte can, for example, be inhibited with the help of $LiPF_6$ additive.[129] In particular, the suggested 0.9 M LiTFSI + 0.1 M $LiPF_6$ in Pyr_{13}-FSI electrolyte formulation exhibited Al passivation as AlF_3 formed when the native oxide layer reacted with HF originating from PF_6^- hydrolysis. Similarly, the inclusion of 0.5 wt% of $LiPF_6$, $LiBF_4$, LiDFOB, or MDFA additives in a 0.3 M LiFSI in Pyr_{14}FSI electrolyte (baseline electrolyte) impacted the stability of Al current collectors to varying degrees.[133] Based on chronocoulometric measurements performed at 5.0 V versus Li^+/Li for 72 h, the stability of the Al current collector is enhanced in the increasing order of LiDFOB < baseline electrolyte < MDFA < $LiPF_6$ < $LiBF_4$. Depositing corrosion-resistant films on the Al current collector has provided an alternative strategy to improve cell performance. For example, magnetron sputtering has been employed to deposit chromium nitride (CrN and Cr_2N) coatings on the Al current collector.[267] The coated Al showed more enhanced stability as compared to the bare Al in coulometric experiments performed in 1 M LiTFSI in EC:DMC (1:1, wt/wt) and 1 M LiTFSI in EMS electrolytes. Other similar materials like TiN thin films have also been used for the same purpose.[268] A TiN coating sputtered on stainless steel and polyimide substrates demonstrated good oxidative stability in $AlCl_3$–EMICl, outperforming pristine stainless steel, aluminum, molybdenum, tungsten, and titanium substrates.

3 | GEL POLYMER ELECTROLYTES

3.1 | General characteristics

A solvent-free electrolyte that is capable of conducting both cations and anions to the same extent is desirable to ensure optimum performance in a DIB. So far, no such fully solid-state electrolyte has been developed and implemented in DIBs. Nevertheless, various types of

GPEs are considered promising for DIB applications. GPEs consisting of polymeric frameworks and liquid electrolytes usually show higher ionic conductivity than solid polymer electrolytes (SPEs), and can easily be fabricated into forms and sizes to fit the desired applications.[269] Simply put, a GPE is made up of a polymeric matrix plasticized with a specified amount of solvent sufficient for salt dissolution and ionic transport (see illustration in Figure 9).[270-272] The polymeric component imparts mechanical integrity as well as acting as a host for the liquid electrolyte, which is needed to enhance ionic conductivity.[270] The polymer host must satisfy some requirements. To operate with no or limited amounts of liquid electrolyte, it must (i) have high chain segmental motion, (ii) possess functional groups needed to coordinate salt ions, (iii) support high ionic conductivity, (iv) possess low glass transition temperature, (v) be stable within a wide electrochemical window, and (vi) possess high thermal stability.[273-276] If a liquid electrolyte phase is present, such as in GPEs, it is enough if the polymer can swell in it and retain the liquid, while still maintaining chemical and mechanical stability, but it is nevertheless desirable if it can also aid in the transport of ions. Most GPEs used in DIB prototypes are fabricated using commonly available polymer materials (see Figure 10A) such as poly(ethylene oxide) (PEO),[282] polyamide,[283] poly(vinyl alcohol) (PVA),[284] PVAc,[217] PVdF,[217] PVdF-HFP,[260,277,285] poly(acrylonitrile),[286] and polyacrylamide.[278] Most of these polymers contain both ion-coordinating and noncoordinating parts. Amongst all these, PVdF-HFP is commonly used in GPEs proposed for DIBs mainly as it

- withstands oxidative degradation at high potentials due to its highly fluorinated nature,
- soaks up and retains liquid electrolytes, and
- functions as a mechanically pliable separator.[270,272,285,287]

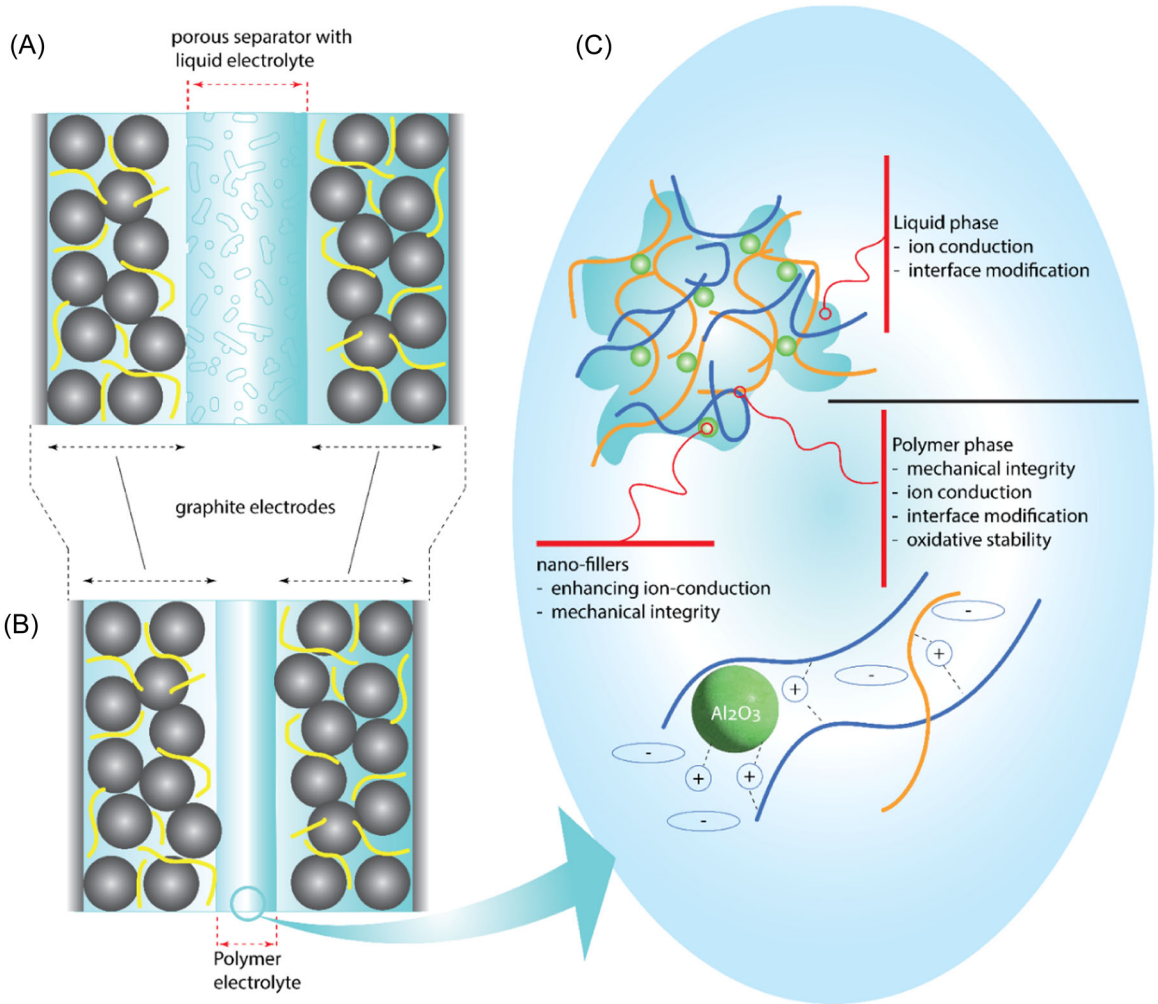

FIGURE 9 Schematic illustrations of (A) a typical DIB with a porous separator impregnated with a concentrated electrolyte, (B) a more compact DIB design based on gelled polymer electrolyte, and (C) a gelled-polymer electrolyte and description of its constituents.

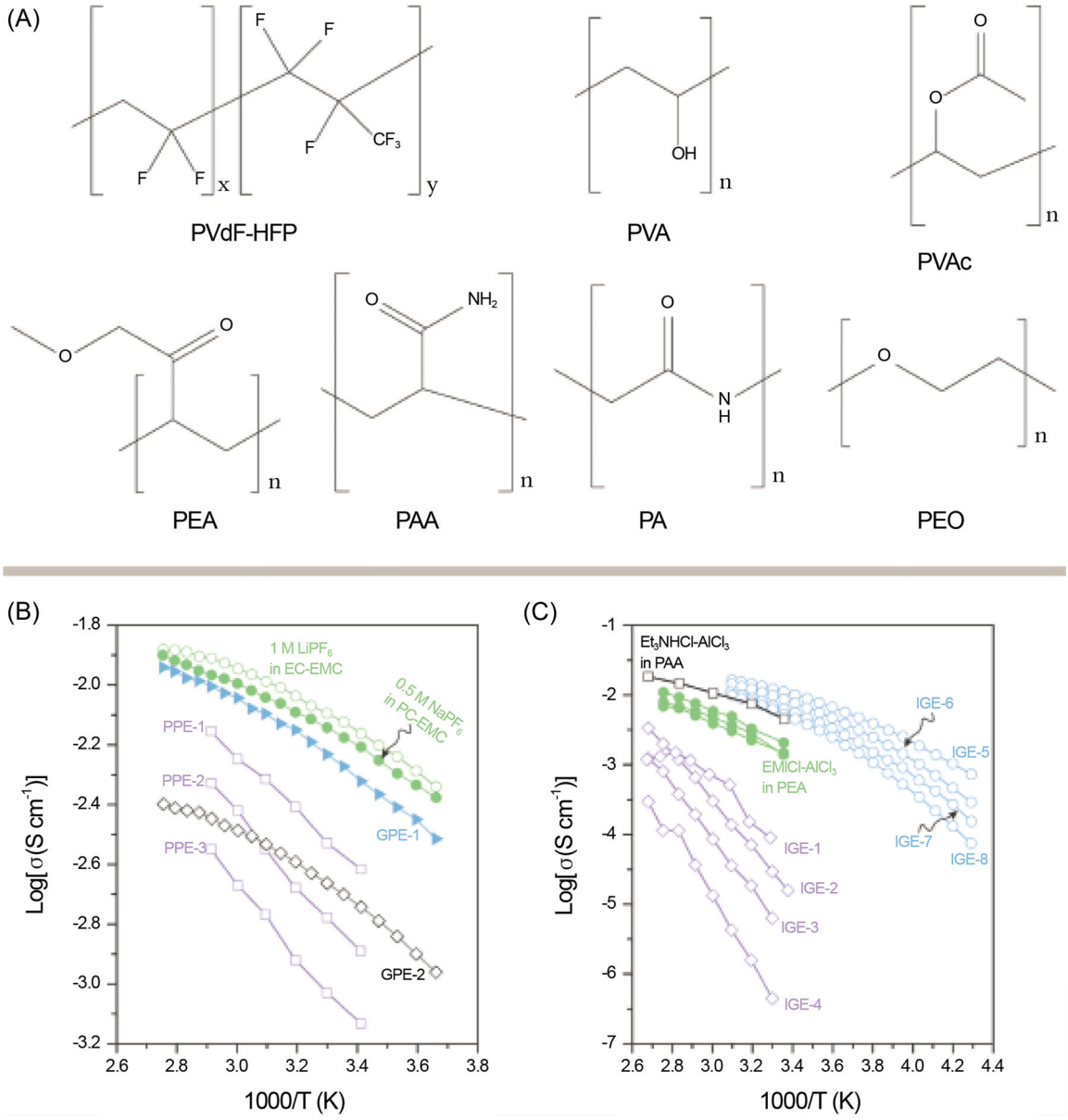

FIGURE 10 Gel polymer electrolytes in dual-ion batteries: (A) structures of polymers commonly used in the preparation of GPEs for dual-ion batteries: poly(ethylene oxide) (PEO), poly(acrylamide) (PAA), poly(ethyl acrylate) (PEA), poly(methyl methacrylate) (PMMA), poly(amide) (PA), poly(vinylidene difluoride-co-hexafluoropropylene) (PVdF-HFP), poly(vinyl alcohol) (PVA) and poly(vinyl acetate) (PVAc), (B) comparison of ionic conductivities at different temperatures for liquid electrolytes and different types of GPEs (GPE-1: poly (ethoxylated pentaerythritol tetraacrylate) gelled with a 0.5 M $NaPF_6$-PC:EMC:FEC (1:1:1 by volume) + 4 wt % PS, GPE-2: crosslinked poly (diethyl allyl phosphate) consisting of 1 M $LiPF_6$ dissolved in a 1:6:3 volume mixture of fluoroethylene carbonate (FEC), 2,2,2-trifluoroethylmethyl carbonate (FEMC), and 1,1,2,3,3,3-hexafluoropropyl-2,2,2-trifluoroethylether (HTE), and 1 M $LiPF_6$ EMC-VC electrolyte contained in porous polymer electrolytes (PPE) prepared from different compositions of PVdF-HFP, SiO_2, and dibutyl phthalate plasticizer), and (C) ionogel electrolytes used in AlDIBs (IGEs based on PAA and PEA polymers gelled, repspectively, with Et_3NHCl-$AlCl_3$ DES and EMICl-$AlCl_3$ ionic liquid), KDIBs (IGE-1 to IGE-4 consisted poly[diallyldimethylammonium bis (trifluoromethanesulfonyl)imide] (pDDA-TFSI), KFSI salt and $Pyr_{14}FSI$ ionic liquid in different proportions), and LiDIBs (IGE-5 to IGE-8, which consisted of different proportions of PVdF-HFP, 1-butyl-1-methylpyrrolidinium triflurometh anesulfonate (BMPyrrOTf), lithium triflurometh anesulfonate (LiOTf) and succinonitrile (SN)). Data shown in (B) and (C) were extracted using WebPlotDigitizer version 4.4[209] from plots in references.[255,260,277-281]

However, PVdF-HFP is not in itself a good ionic conductor and possesses very little ion dissolving properties. The liquid phase (plasticizer) in GPEs can be based on aqueous electrolytes,[284,288,289] organic liquid electrolytes conducting univalent or multivalent cations and anions,[217,260,279,282] ILs [272,280,281,290,291] with and without additional salts, and DES containing the desired concentration of salts.[278,283] Apart from salts and solvents, GPEs can incorporate fillers such as nanosized SiO_2[260] and Al_2O_3 particles,[292] which enhance mechanical and thermal performance as well as provide additional coordinating sites[293] for cations and anions. All in all, GPEs can potentially help develop semi-solid-state DIBs by reducing the amount of solvent used in the electrolytes while retaining ion transport properties.

As compared to liquid electrolytes, GPEs can often ensure a better combination of safety, ionic conductivity (both anions and cations), mechanical flexibility, and resilience toward stress caused by volume variations in the active materials. At the same time, they can suppress dendrites and lower the risk of electrolyte leakage.[269,294-297] Apart from these benefits, GPEs can effectively remove the necessity for thick separators normally required by liquid electrolytes employed in DIBs. This in turn is anticipated to allow for the reduction in electrolyte volume while eliminating the separator. Ideally, the polymeric component in a GPE should also function as a binder in the electrodes, as well as modify the interfacial contact depending on the functional groups that it is composed of. Such a multifunctional role of GPEs will result in considerable weight- and volume-saving, which in turn will enable the design of DIBs with better energy and power densities.[282] A range of electrolyte properties must be investigated to fully unlock the potential of so-called "quasi-solid-state DIBs." To start with, the ionic conductivities of the GPEs must be reasonably comparable to that of liquid electrolytes to ensure the desired rate performance. Also, a critical amount of salt concentration is required to support high ion conduction while supplying sufficient ions to be stored in the electrodes.[281] Figure 10B,C provides conductivity–temperature plots for selected liquid electrolytes and GPEs including ionogel electrolytes (IGEs). In IGEs, the ionic conductivity usually increases as the proportion of the IL is raised. For instance, the ionic conductivities at 20°C of the poly(acrylamide) hosts containing EMICl–$AlCl_3$ varied between 5.29×10^{-5} and 1.66×10^{-3} S cm^{-1} as the proportion of the IL increased from 50 to 80 wt%.[291] Although, such an increase in the IL content comes at the expense of the mechanical stiffness that the polymer component affords.[281] For instance, a system of ternary IGE prepared from KFSI (18%), poly[diallyldimethylammonium bis(trifluoromethanesulfonyl) imide] (pDDA-TFSI) (41%), and $Pyr_{14}FSI$ (41%) had the highest conductivity at 25°C as compared to other compositions with lower contents of IL, but it was mechanically feeble to be used in a DIB.[281] Thus, an optimum trade-off should be maintained between the conflicting electrical properties and mechanical rigidity of IGEs to ensure acceptable performance in DIBs.

Furthermore, it is important to note that the electrochemical/electrical behavior of GPEs can be dominated by ion mobility either in the liquid phase or along the polymer backbone, or both, which is usually revealed in the conductivity–temperature relations. In the former case, the polymer component in the GPE performs only mechanically and plays the same role as a separator, which is still a very essential role. Since the conduction of ions involves a vehicular mechanism of a liquid phase with low T_g, a linear relationship (similar to ionic hopping in a fixed lattice) is generally observed for $\log(\sigma)$ versus T^{-1} plot according to the Arrhenius relation:

$$\sigma = \sigma_o \exp\left(-\frac{E_a}{k_B T}\right), \tag{7}$$

where σ_o is the pre-exponential factor, E_a the activation energy, k_B is the Boltzmann constant, and T is the temperature of measurement.[298] In ILs, the ionic transport can also occur through a Grotthuss-type mechanism rather than in a vehicular mode, whereby the conductivity also follows an Arrhenius relationship as a function of temperature. In contrast, ionic conductivity dominated by the mobility of polymer chains gives rise to $\log \sigma_{dc}$ versus T^{-1} trend governed by the Vogel–Tammann–Fulcher (VTF) equation[299-301]:

$$\sigma_{dc}(T) = AT^{-1/2} \exp\left[-\frac{E_a}{k_B(T - T_o)}\right], \tag{8}$$

where A is the pre-exponential factor, E_a is the pseudoactivation energy linked to the free volume for ionic conduction, k_B is the Boltzmann constant, and T_0 is the equilibrium Vogel scaling temperature. In an Arrhenius plot, this gives rise to a bent curve. In this scenario, the polymer host plays a multifunctional role as it provides a conduction medium for ions as well as ensuring mechanical rigidity and physical separation of the two electrodes. Thus, it is important to study the dependence on temperature of the ionic conductivity to gain insight into the role of each component in the GPE (see Figure 10B,C). It is observed that the plots of $\log \sigma_{dc}$ versus T^{-1} for some ionogels obey a VTF-type behavior, indicating that ion transport can be strongly influenced by the dynamics of the polymer chains.[277,280]

3.2 | Synthesis of GPEs

Broadly speaking, a GPE for a DIB application can be prepared by

- extraction of a solvent from a polymeric membrane followed by liquid electrolyte infiltration,[260]
- a casting method in which the polymer host, the plasticizing solvent, and the electrolyte salt are mixed in a volatile solvent which is evaporated afterward,[281,285,302,303] and
- in situ polymerization of a monomer initially added to the liquid electrolyte.[255,278-280,291]

In the first instance, an example includes a microporous polymer electrolyte (PPE) that was prepared by extracting dibutyl phthalate (DBP) plasticizer from a composite of PVdF-HFP polymer and 30 nm SiO_2 particles, and subsequently infiltrated with $LiPF_6$-EMC liquid electrolyte with a 3 wt% VC.[260] The membrane consisting of 15 wt% PVdF-HFP, 25 wt% SiO_2, and 60 wt% DBP was able to retain up to 70% of the initial electrolyte volume, and its ionic conductivity was ~2.40 mS cm^{-1}.[260] Using this electrolyte, a DIB can be charged to 4.8 V, allowing for a reversible discharge capacity of ~80 mA h g^{-1} over 1000 cycles.[260] Similarly, a flexible and free-standing PVdF–PVAc (40 wt% PVAc) GPE membrane immersed in 1.0 M $LiPF_6$ in EMC + SL (1:4 vol/vol) provided an ionic conductivity of 4.8×10^{-4} S cm^{-1} at room temperature.[217] A DIB making use of the GPEs exhibited an encouraging performance in the voltage range from 3.00 to 5.35 V versus Li^+/Li with the initial discharge capacity being 93 mA h g^{-1} and a CE of 71% for the initial cycle and 92% after two cycles. In contrast, the first three CEs of the DIB using the liquid electrolyte were only 61%, 79%, and 80%, respectively. However, increasing the amount of PVAc resulted in lower iCEs due to its poor oxidative stability, although in the subsequent cycles, the CE gradually increased to 95%. Further studies have shown that improvements can be achieved when some additives such as VC are included in the electrolyte formulation. A flexible Al–graphite DIB operating in the potential range of 3.0–4.95 V can be fabricated employing a GPE consisting of composite membranes of PVdF-HFP, PEO, and GO soaked with 4 M $LiPF_6$-EMC with a 2% VC additive leading to ionic conductivity of 2.1 mS cm^{-1}.[282] The cell exhibited a discharge capacity of ~100 mAh g^{-1} at 500 mA g^{-1} with an average voltage of 4.0 V and capacity retention of 92% after 2000 cycles.[282] Apart from GO[282] and SiO_2,[260] other nanoparticles such as Al_2O_3[292] can also be added to PVdF–HFP polymer to form microporous GPEs. When nanosized Al_2O_3 particles (5 wt% of Al_2O_3 nanoparticles) were dispersed in the PVdF-HFP matrix, a three-dimensional (3D) framework with continuous porosity was generated, as a result of which enhanced ionic conductivity and mechanical stability were achieved. The membrane produced a semi-transparent gel after soaking up a liquid electrolyte (1 M $NaPF_6$ in EC-DMC-EMC 1:1:1 vol/vol/vol), with its ionic conductivity reaching up to 1.3×10^{-3} S cm^{-1}.[292] A tin–graphite DIB using this GPE could deliver nearly 100 mAh g^{-1} at 200 mA g^{-1} with about 98% capacity retention after 600 cycles at 500 mA g^{-1} over a wide temperature range (–20°C to 70°C).[292]

Polymerization of monomers dissolved in the liquid electrolytes to in situ prepare GPEs can be a neat strategy (Figure 11) to prepare GPEs within the electrode before electrochemical cycling. Monomers such as acrylamide, ethyl acrylate (EA), diethyl allylphosphonates, and pentaerythritol tetraacrylate (PETA; see Figure 11A,B) are polymerized thermally or using radical initiators. For instance, ethoxylated pentaerythritol tetraacrylate (EPETA) monomer was polymerized using radical initiators such as AIBN in the presence of 0.5 M $NaPF_6$ in PC + EMC + FEC (1:1:1, vol/vol/vol) electrolyte containing FEC cosolvent and 1,3-propanesultone (PS) additives.[279] The additives FEC and PS (4%) are expected to inhibit electrolyte degradation by enhancing the stability of the SEI and the CEI, respectively. The Na–graphite cell employing the electrolyte was able to deliver a specific discharge capacity of 115 mAh g^{-1} at 10 mA g^{-1} and better rate performance as compared to cells based on just the liquid electrolytes (0.5 M $NaPF_6$-PC + EMC, 0.5 M $NaPF_6$-PC + EMC + FEC, and 0.5 M $NaPF_6$-PC + EMC + FEC + PS). Similarly, another type of GPE was synthesized in situ by copolymerization of 3 wt% diethyl allyl phosphate monomer and 1.5 wt% PETA crosslinker in the presence of an electrolyte containing fluorinated solvents.[255] To prepare the liquid electrolyte, 1 M $LiPF_6$ salt was dissolved in a mixture of FEC, 2,2,2-trifluoroethylmethyl carbonate (FEMC), and 1,1,2,3,3,3-hexafluoropropyl-2,2,2-trifluoroethylether (HTE) in 1:6:3 volume proportion. The FEC was meant to increase compatibility with Li metal, while FEMC allows for reversible PF_6^- intercalation in the graphite-positive electrode. Likewise, the presence of fluorinated solvents was meant to reinforce the nonflammability of the GPE without compromising its ionic conductivity (1.99 mS cm^{-1} at 25°C), to extend the electrochemical window (up to 5.5 V versus Li^+/Li) and to boost interfacial compatibility against Li metal anode (manifest in 99.7% CE for lithium plating and stripping). In the Li–graphite DIB, the GPE demonstrated a discharge capacity of 89.8 mAh g^{-1} with a capacity retention of 93% after 1000 cycles, while the CE stabilized at ~99%. Hence, the GPE was instrumental in ensuring highly reversible intercalation of PF_6^-.

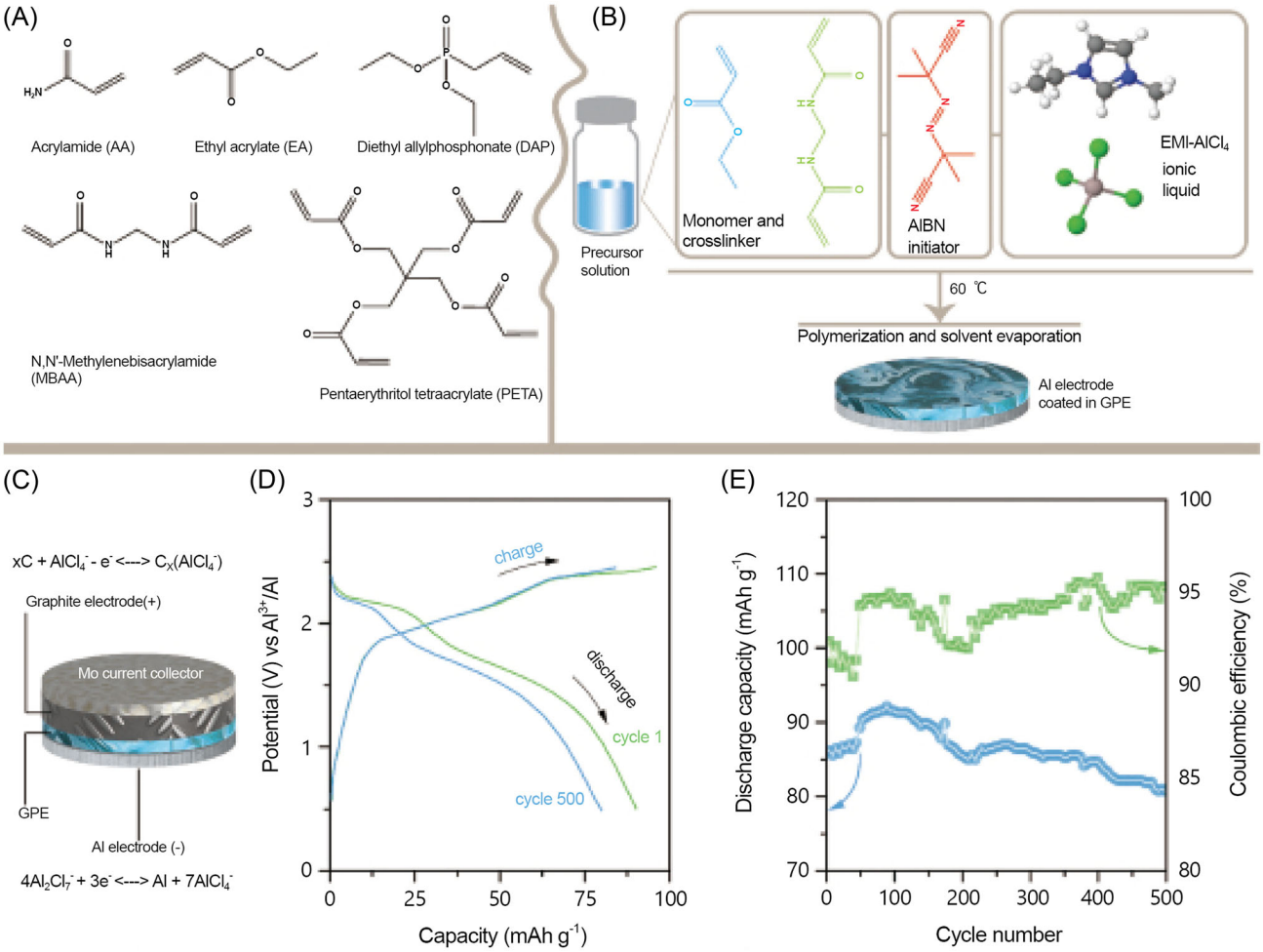

FIGURE 11 Preparation of GPEs via in situ polymerization and their use in a dual-ion battery: (A) common monomers and crosslinkers used in GPE preparation, (B) a description of the synthesis of a GPE based on highly crosslinked poly(ethyl acrylate) with EMI-$AlCl_4$ ionic liquid on polished Al electrode, and (C) schematic illustration of the components of Al-DIB and redox reactions at each electrode. (D) Galvanostatic curves recorded at 200 mA g^{-1} and showing the charge and discharge features of the Al-DIB reactions during the initial and the 500th cycles[280] and (E) extended cycling performance of the same cell cycled at 200 mA g^{-1}. Reproduced with permission: Copyright 2021, Elsevier B.V.[280]

3.3 | Ionogel electrolytes

Since ILs are able to dissolve polymers and salts, they offer a unique opportunity to design gelled electrolytes, commonly known as IGEs, with high ionic conductivity and the ability to transfer mechanical load. IGEs are obtained when room-temperature IL electrolytes or their analogues are confined within polymer hosts (see Figure 12). A large number of IGEs were reported in previous literature.[305-307] In particular, some polymerized ionic liquids (PILs)[308] with cationic chains such as pDDA-TFSI shown in Figure 12A have attracted considerable attention as electrolytes in electrochemical devices.[309,310] The fact that the anions are mobile is particularly interesting for their use as electrolytes, binders, or interface layers to modify graphite electrodes in DIBs. Adding ILs or liquid electrolytes can enhance ionic conductivity as well as make the PILs mechanically pliable so that they can be handled without damage during cell fabrication.[281,309] For instance, Kotronia et al.[281] demonstrated the synthesis of ternary ionogels using the IL, PIL, and KFSI salt and fabricated a compact MoS_2-graphite DIB, as shown in Figure 12B–D.[281]

A lot of progress has been made in recent years in the development of Al-DIBs based on IGEs. Mostly, polymers or monomers are blended with ILs obtained by reacting anhydrous $AlCl_3$ with imidazolium or other quaternary ammonium chlorides. For example, a GPE was prepared via free-radical polymerization of acrylamide monomer dissolved in a mixture of $AlCl_3$-EMICl IL and in dichloromethane solvent.[291] The GPE exhibited reversible aluminum deposition and stripping even after

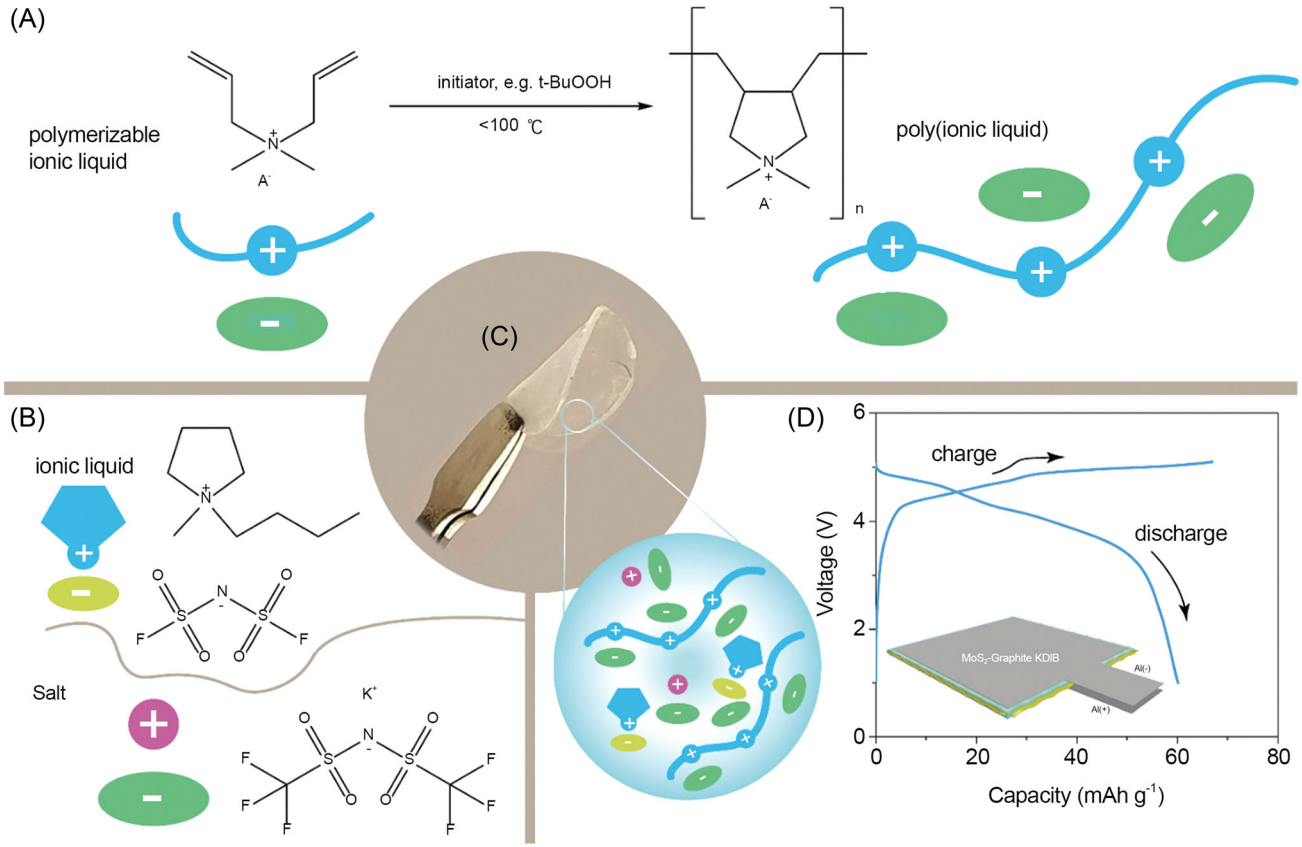

FIGURE 12 Preparation of ternary IGEs and their use in a dual-ion battery: (A) radical polymerization[304] of an ionic liquid to obtain poly(ionic liquid) material needed to prepare IGEs; the A^- can be any anion including Cl^- and TFSI, (B) structures of the pyrrolidinium-based ionic liquid with FSI anion, and the KTFSI salt, (C) a photo of the freestanding, flexible and transparent IGE is shown along with a schematic illustration of its composition, and (D) galvanostatic charge–discharge curves at 20 mA g^{-1} for a MoS_2-graphite pouch cell KDIB with both electrodes infused with a ternary IGE in a plain weave glass fiber fabric (40 μm). Reproduced under the Creative Commons License (CC-BY): Copyright 2021, John Wiley & Sons.[281] Inset is a schematic of the pouch cell.

exposure to air, which suggested that its sensitivity to moisture is lower when contained in a polymer matrix. A flexible quasi-solid-state Al-DIB was developed using a similar IGE as the separator and ion-conduction medium.[236] The pouch cell Al–graphite DIB was able to deliver a reversible ~120 mAh g^{-1} at 60 mA g^{-1} with ~90% CE and ~90% capacity retention after 100 cycles. A GPE was also obtained from EA as a monomer and IL as the electrolyte.[280] The EA in the IL was mixed with a cross-linking agent *N,N′*-methylene-bis-acrylamide in an appropriate ratio and in situ polymerized with AIBN initiator, resulting in crosslinked polymer chains in which the anions and cations of the IL could be stored. As far as DIBs are concerned, GPEs possess competitive advantages over liquid electrolytes in terms of cell design, safety, cycle life, and mechanical adaptability. The rate capabilities of some selected DIBs designed using lithium-, sodium-, potassium-, and aluminum-based GPEs are shown in Figure 13A. As shown in Figure 13B, GPEs can deliver comparable rate performance as liquid electrolytes used in DIBs, which confirms the efficiency and feasibility of the GPEs in practical DIBs.

3.4 | Advantages of GPEs

Regarding safety, a fire hazard is a critical aspect to considering during cell operation.[311] It has been demonstrated that infusing liquid electrolytes within a polymeric host considerably reduces the tendency to catch and sustain fire, demonstrating a desirable boost in safety. In particular, the incorporation of fluorinated solvents and salts further imparts self-extinguishing behavior to the GPEs. A clear illustration of this is shown in Figure 13C which illustrates that a highly crosslinked poly(diethyl allyl phosphate) with fluorinated solvents and $LiPF_6$ has a much shorter self-extinguishing time (SET) as compared to a standard electrolyte based on 1 M $LiPF_6$ in EC-EMC which can

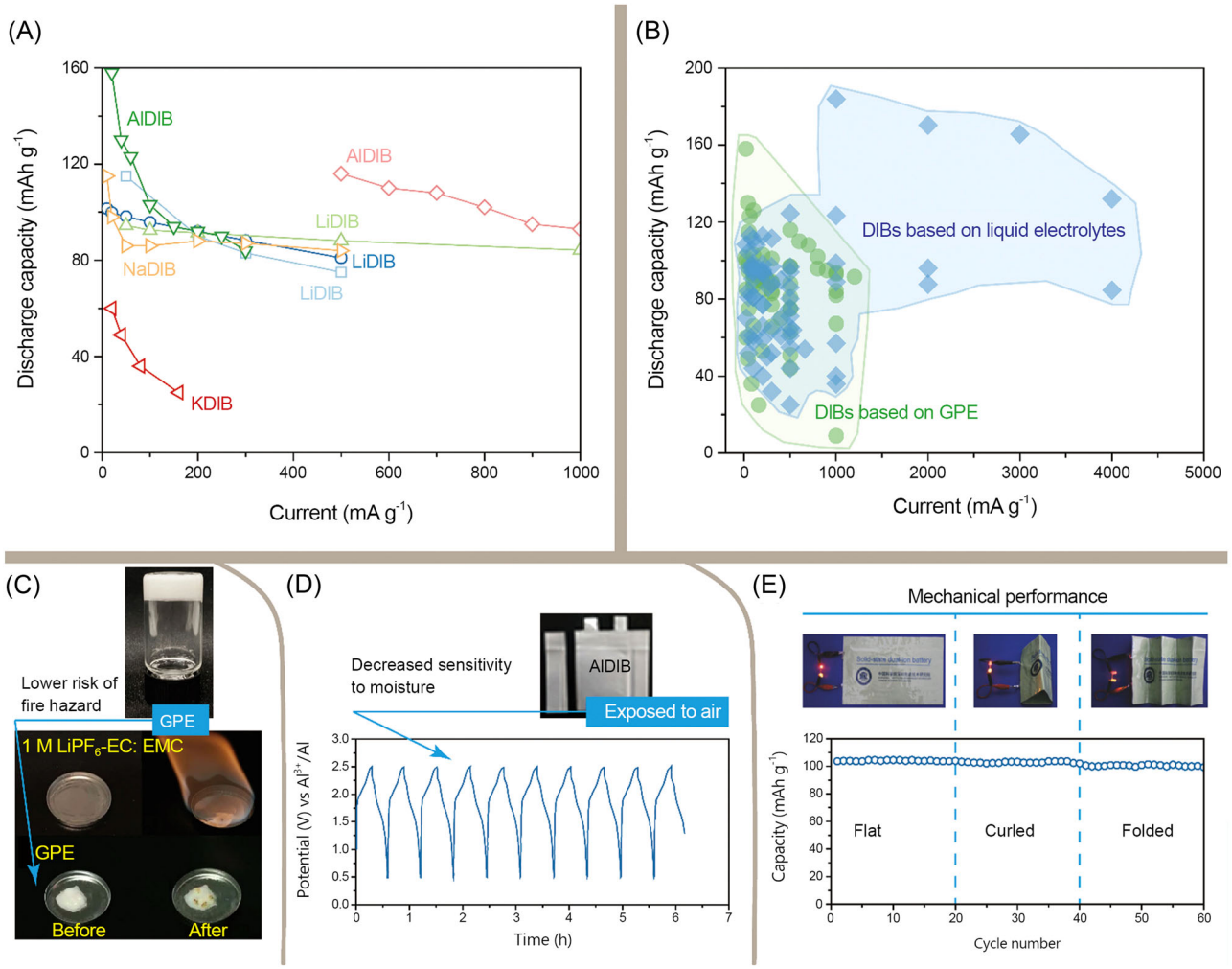

FIGURE 13 Performance of GPEs in DIBs with different cell chemistry: (A) rate capability of examples of DIBs using gelled-polymer and ionogel electrolytes, (B) comparing the performance of semi-solid-state DIBs with those based on liquid electrolytes, (C) flammability test comparing carbonate-based liquid electrolyte with a GPE, (D) galvanostatic cycling, at 200 mA g^{-1}, of an Al–graphite DIB demonstrating that the GPE is less prone to degradation in the presence of moisture as opposed to ionic liquid electrolytes normally employed in AlDIBs, and (E) a flexible and compact semi-solid-state Al–graphite is tested in its original and folded or bent states to assess its ability to withstand mechanical abuse, and its ability to perform in applications requiring flexibility. The plots in (A) are based on data from cited references.[217,236,255,260,278,279,281] Data used to prepare the plots in (B) are tabulated in Table S2 of the ESI. The photos in (C) were reproduced under the Creative Commons License (CC BY): Copyright 2021, Springer Nature.[255] The photo and galvanostatic data in (D) were reproduced with permission: Copyright 2021, Elsevier B.V.[280] The data and photos shown (E) were reproduced with permission: Copyright 2018, Wiley-VCH Verlag GmbH & Co KGaA.[282]

sustain fire even after removal of the torch (SET of 92 s/g).[255] Similar observation was reported for a GPE obtained by polymerizing EPETA (see Figure 11A) in the presence of 0.5 M $NaPF_6$ dissolved in a mixture of PC, EMC, FEC, and PS additive.[279] In addition, the presence of polymers in the electrolyte helps reduce electrolyte volatility and leakage out of the DIB cell in the event of mechanical damage, thus lowering the impact of moisture on some hydrophilic electrolytes such as $AlCl_3$-EMICl ILs.[236,280] In this regard, an Al-DIB pouch cell consisting of $AlCl_3$-EMICl IL within poly(ethyl acrylate) was intentionally opened while cycling.[280] As shown in Figure 13D, the cell kept on cycling with stable charge/discharge capacities with no visible electrolyte leakage. This is a significant attribute of GPEs given that EMICl-$AlCl_3$ ILs are prone to degradation by humidity and also aggravate the corrosion of cell components in the process. Furthermore, as briefly indicated above, the implementation of GPEs permits to manufacture thin and compact DIB cell designs which can potentially be deployed in applications that require mechanical flexibility, such as in wearable devices. In a typical experiment, a DIB pouch cell is tested under cyclic bending or folding multiple times to gauge how stable

the capacity is while simultaneously identifying any possible degradation in the mechanical properties of the cell.[236,280,282] For instance, an Al–graphite LiDIB cell based on a 4 M $LiPF_6$ in EMC (+2 wt% VC) confined within PVdF-HFP and PEO was tested while in its bent and folded states, and sustained stable capacity over 60 cycles, as shown in Figure 13E.[282] Likewise, other tests have established similar conclusions regarding the performance of quasi-solid-state DIBs. Nevertheless, it must be underlined that mechanical tests on pouch cells reflect the characteristics of not only the GPE but also the electrodes and the packaging material. The true mechanical properties and load-bearing capability of a GPE can be evaluated separately using dynamic mechanical thermal analysis, which is a powerful technique used to determine the stiffness and impact resistance of polymers and their composites. Another aspect of GPEs related to safety concerns their interfacial stability at both electrodes as well as the nature of decomposition products, which determine cell life and self-discharge characteristics. A variety of techniques have been used to gain insight into interfacial reactions and their products including electrochemical impedance spectroscopy, XPS, operando gas measurement, and mass spectrometry. In comparison to full-liquid electrolytes, GPEs exhibit a significant reduction in the amount of gasses evolved at high potentials in the course of anion intercalation and extraction processes (Figure 14A–C). The build-up of gas pressure in the pouch cells can be detrimental to the long-term performance of the cell and may even lead to dangerous eventualities. Thus, it is vital to ensure that the electrolytes or additives therein can effectively suppress or mitigate gassing during cycling. Such reactions can be monitored by tracking partial gas pressure in situ coupled with an online high-resolution mass spectrometer, which will help decide the cut-off potential at which gassing can be minimized. Increased evolution of hydrogen gas was detected in a porous PVdF-HFP membrane containing $LiPF_6$ in EMC and 3 wt% VC when the cut-off potential increased from 4.8 to 5 V.[260]

Apart from anion intercalation, GPEs designed for DIB use should conduct cations and be stable at the interface with the negative electrode. In the case of metal electrodes, they should enhance plating and stripping efficiency while preventing dendrite growth and penetration through the electrolyte. Reduction in the amount of solvent which is in contact with the alkali metal will help minimize decomposition reactions at the interface and usually results in lower overpotentials required for plating and stripping. Examples are shown in Figure 14D–F. The cyclic voltammograms in (D) show ternary ionogels consisting of KFSI and $Pyr_{14}FSI$ blended in a PDDA-TFSI polymer host[281] which displayed no sign of degradation when cycled up to 5 V versus K^+/K as well as allowing potassium plating and stripping cycles that were more efficient as compared to that in liquid electrolytes. Distinctive features of alkali metal plating and stripping through a GPE membrane will be manifest in the thickness and morphology of the deposits and the overpotentials required relative to that in liquid electrolytes.[255,279] As long as the polymer host and salt are stable, restricted access of the metal deposits to the solvent molecules prevents unwanted reactions and accumulation of resistive layer at the interface, as is commonly observed in liquid electrolytes. The absence of thick interface layers in GPEs thereby ensures better efficiency and lower overpotential for metal plating and stripping. In addition, it is likely that the mechanical stiffness of the polymer host, which most porous separators lack, or the tortuosity of the gel can act as a barrier to pieces detached from or dendrites growing from the metal deposits. The mechanical load applied by GPE may also limit the thickness of the metal deposit, leading to compact film as opposed to the porous, and thicker metal deposit obtained in the case of liquid electrolytes (see Figure 14G,H). Further enhancement of the interfacial contact between the negative electrode and the GPE can be achieved by adding fluorinated solvents and other salt additives which can generate stable interfacial layers.

Finally, some applications require operating batteries at less optimum temperatures, especially in places with very hot or very cold climates. In such cases, it is of paramount importance that the electrolytes are not only chemically stable at high temperatures, but they can also allow for sufficient ion conduction in spite of freezing conditions. In such a way, the DIBs should not be significantly hampered by high internal cell resistances when trying to deliver power. In general, GPEs have a higher tolerance to elevated temperatures as opposed to most liquid electrolytes in which the solvent molecules tend to evaporate, increasing the gas pressure in the cell and ultimately leading to cell rupture and even fire. Since the solvent and salt are dispersed in the polymer host, solvent release from GPEs is relatively hindered when the DIB cells are operated at high temperatures, and thus the impact of temperature is less adverse as compared to liquid electrolytes. As shown in Figure 14I, major differences between a GPE and liquid electrolytes used in Sn-graphite DIB were observed as the temperature increased to 70°C. The GPE still retained most of the capacity while the discharge capacity from the cell with a liquid electrolyte was negligible.[292] This might well have been due to electrolyte dry-up. At −20°C, the GPE could deliver a discharge capacity that was almost

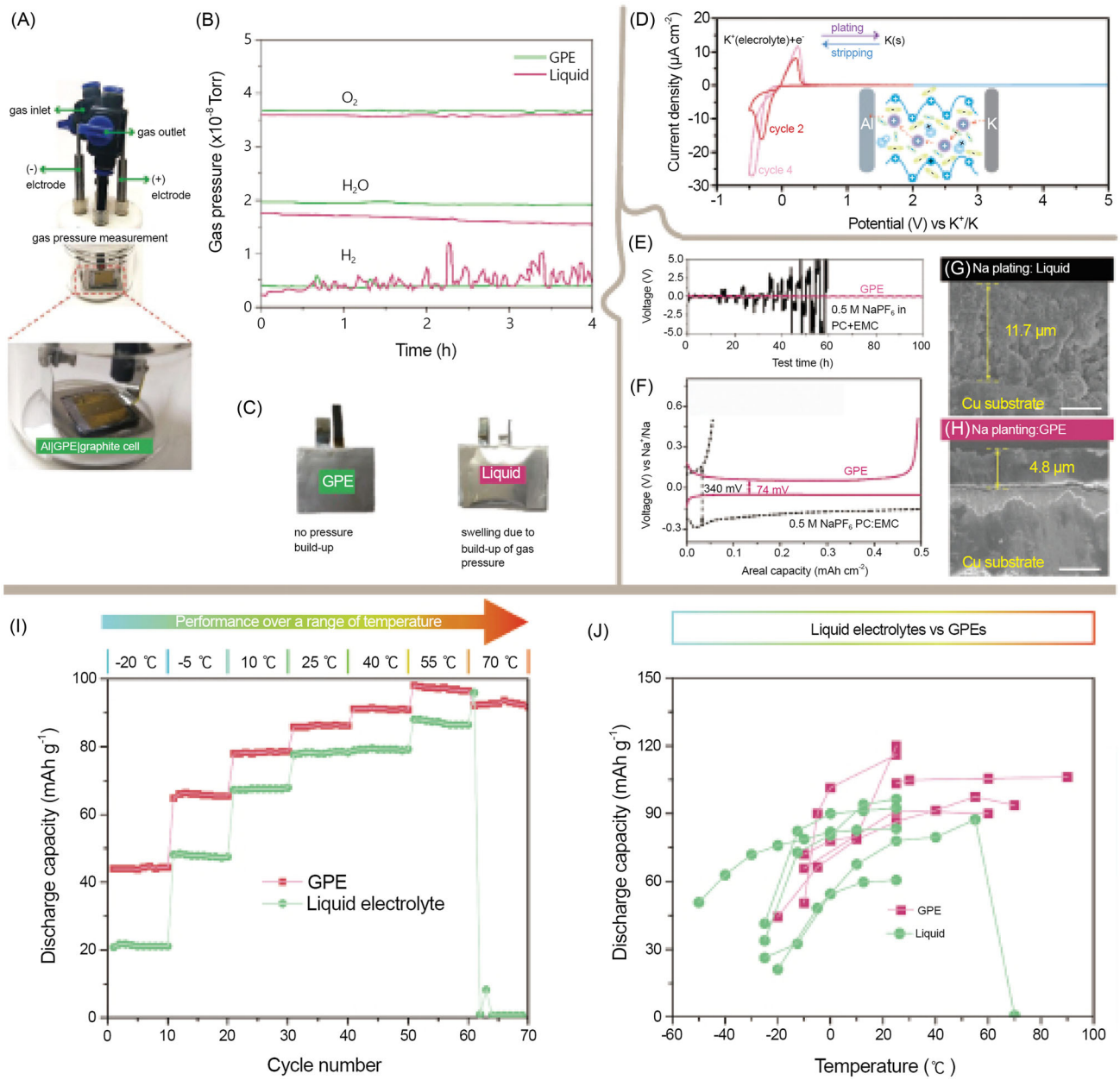

FIGURE 14 Gas pressure measurement and low-temperature performance of GPEs in DIBs with different cell chemistry: (A) a schematic of the set-up used to measure gas pressure developing during cycling of an Al|GPE|graphite DIB, (B) plots comparing partial pressures of some gasses generated in a GPE and a liquid electrolyte, and (C) pictures showing how gas build-up in pouch cells causes more swelling in a liquid electrolyte than a GPE. Reproduced with permission: Copyright 2018, Wiley-VCH Verlag GmbH & Co. KGaA.[236] (D) Cyclic voltammograms for cycles 1 and 2 of potassium metal plating and stripping in Al|IGE|K cells and anodic stability up to 5.0 V. Reproduced under the Creative Commons License (CC-BY): Copyright 2021, John Wiley & Sons.[281] (E) Chronopotentiograms showing that lower overpotentials are required to plate and strip Na metal through a GPE as opposed to a liquid electrolyte, (F) the voltage hysteresis between Na plating and stripping process is shown to be 74 mV for the GPE vis-à-vis 340 mV in the liquid electrolyte, (G) the SEM image shows the typical thickness of porous Na metal deposited out of the liquid electrolyte, and (H) in contrast to what is shown for the liquid electrolyte in (G) a much thinner (4.8 μm) and denser Na metal is plated on the negative electrode when a GPE is employed. Reproduced with permission: Copyright 2020, Elsevier Inc.[279] (I) Impact of cycling temperature on discharge capacities Sn–graphite DIB employing a liquid electrolyte (1 M $NaPF_6$ in EC-DMC-EMC 1:1:1 vol/vol) and a GPE (PVdF-HFP containing 5 wt% of Al_2O_3 nanoparticles and plasticized with 1 M $NaPF_6$ in EC-DMC-EMC 1:1:1 vol/vol) and cycled at 500 mA g^{-1}. Reproduced with permission: Copyright 2019, Wiley-VCH Verlag GmbH & Co. KGaA.[292] and (J) Comparisons of the temperature dependence of discharge capacities for DIBs based on various liquid electrolytes and GPEs.

twice of that obtained using conventional liquid electrolytes, which demonstrated that the Sn–graphite DIB based on GPE could outperform liquid electrolytes over a broad range of temperatures. The temperature dependence of discharge capacities for selected examples of GPEs and liquid electrolytes is shown in Figure 14J. The general trend is that as temperature increases, GPEs perform much better than liquid electrolytes, which, however, seems to excel as the temperature drops to below 0°C.

4 | SUMMARY AND FUTURE PROSPECTS FOR BETTER GPEs

As described above, the DIB concept is a promising alternative to current stationary battery systems which can ensure high power capability and cost benefits related to the avoidance of expensive transition metals, and it is potentially environment friendly. To date, various types of DIBs have been developed and extensively studied including those based on alkali (Li, Na, and K)- and Al-containing electrodes and electrolytes. Further development of DIBs for real-life applications will be facilitated by the innovative formulation of more efficient electrolytes.

In this review, we highlighted recent progress in the formulation, characterization, and application of various types of electrolytes investigated in DIBs, with an emphasis on GPEs. A summary of recent developments in molten inorganic salt electrolytes, ILs, HCEs, and aqueous electrolytes has also been provided, with a particular focus on their stability and compatibility with anion-intercalated graphite electrodes. It is anticipated that the knowledge gained from these electrolyte systems forms the basis for the development of GPEs which can enable quasi-solid-state DIBs. Moreover, strategies for improving the anodic stability of the electrolytes along with their compatibility with the negative and positive electrodes have been explored. Broadly speaking, the desired characteristics of electrolytes, summarized in Figure 15, include

- high oxidative stability in the range needed for reversible anion intercalation typically 3.0–5.2 V versus Li^+/Li,
- adequate salt concentration (>2 M depending on the type of salt) required to support ionic conductivity and energy storage in the graphite electrodes,
- capability to passivate the Al current collectors and ability to generate stable SEI and CEI layers,
- abundance and low cost of salts and solvents and

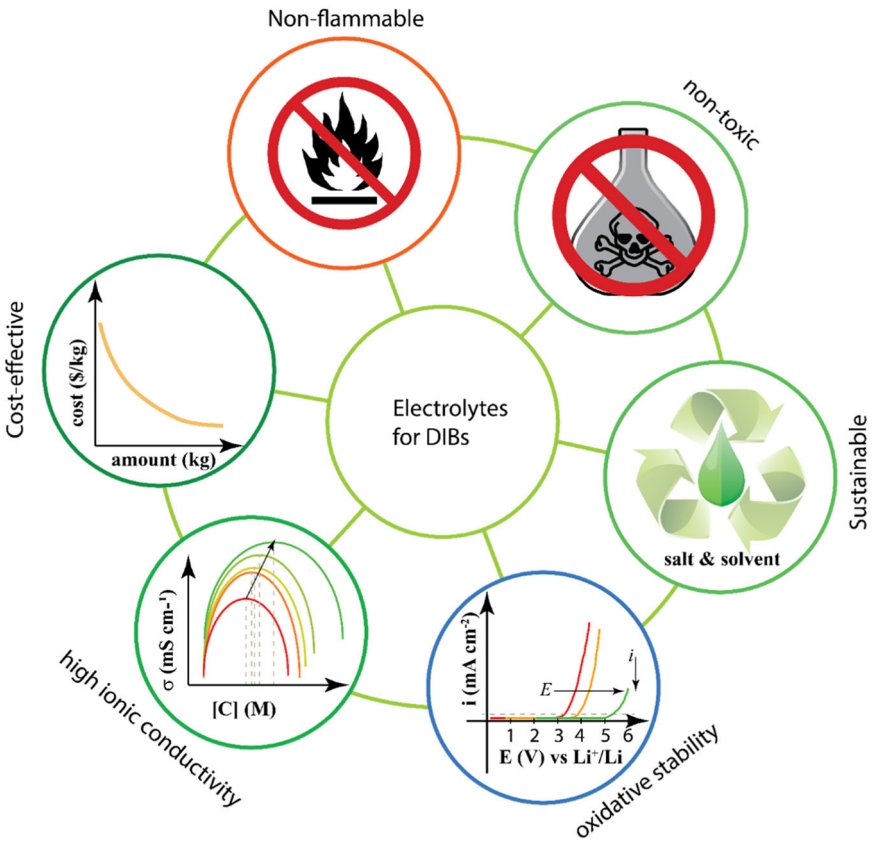

FIGURE 15 A schematic illustration of the fundamental requirements for electrolytes needed to produce sustainable and safe dual-ion batteries.

- environmental compatibility in which using green salts and solvents can ensure safety and sustainability.

Enabling DIBs will most certainly bring about additional benefits, apart from the high energy density promised by the graphite–graphite configuration. As compared to other high-voltage chemistries, such as graphite versus $LiCoO_2$ and even Si versus $LiNi_{0.8}Co_{0.1}Mn_{0.1}O_2$, all-graphite DIBs offer a way to take the scarce, expensive, or environmentally harmful materials completely out of the equation. This is particularly the case if salts of sodium, potassium, and multivalent metals such as aluminum, calcium, magnesium, or zinc can replace lithium in electrolytes and electrodes in the design of affordable DIBs. Of the elements currently used in DIBs, aluminum is the most abundant and one of the cheapest after graphite. Even though its reduction potential is lower than that of Li, it has a higher volumetric capacity. Besides, it should be pointed out that future research in DIBs must focus on the use of more sustainable electrolyte materials, such as chlorides and metal–chloride complexes in aqueous media.

Besides cost considerations, the elimination of transition metal oxides from the cathode ensures that a major source of oxygen is removed.[312-315] Reducing the amount of intrinsic oxygen in the cell is generally synonymous with better safety since oxygen is essential to sustaining fire in the event of a thermal runaway.[311] In this regard, concentrated electrolytes are intrinsically safer as compared to dilute electrolytes, due to the minimization of flammable solvents present in the mixture. The design of HCEs has been proven to decrease volatility and increase thermal stability which can depress flammability.[316,317] In addition, blending carbonates with nonflammable solvents (such as phosphates and water), which cannot be used in dilute electrolytes, allows for preparing HCEs with a lower risk of fire hazards.[72,189,200,231,318,319] Apart from this, it is worth pointing out the need for evaluation of the performance and safety of DIBs under abuse conditions. Industrially relevant lithium dual-ion cell prototypes have been evaluated at variable temperatures (ranging from −20 to 60°C) and under nail penetration tests.[195] More studies are needed in this regard to accelerate the realization of commercial DIBs.

Other important concerns facing DIB electrolytes are related to limited reversibility during the first cycle and poor capacity retention ascribed to electrolyte degradation and Al corrosion, and the excessive volume of electrolyte needed to boost energy density. Highly-concentrated carbonate electrolytes and ILs have found widespread use in both alkali- and aluminum-based DIBs, although the practical application of these electrolytes is still limited by poor CE (<90%) and quick self-discharge as opposed to state-of-the-art LIBs currently in use. Limited cycle life and low CE can be linked to the oxidative decomposition of electrolytes and Al dissolution during anion intercalation in the graphite electrode. These drawbacks underline the importance of more research to come up with more stable current collectors or novel electrode designs which do away with current collectors in parallel to electrolyte innovation. Furthermore, the impact of irreversible reactions occurring at the negative electrode can exacerbate capacity loss in the DIB cells. To mitigate performance degradation, various types of salt additives and cosolvents have been extensively studied. In particular, additives capable of forming stable SEI and CEI layers have been found to increase the CE to above 97%.

In addition to the type of salt used, anion intercalation capacity is also affected by the solvents used in the electrolyte. Some solvents like EC, GBL, SL, and some phosphates are reportedly associated with suppression of anion intercalation in graphite and thus should be used together with other less viscous carbonates like EMC, DMC, or carboxylate esters. Mixing various solvents such as carbonates, phosphates, sulfones, and esters can lead to HCEs with better oxidation stability, higher ionic conductivity, and decreased flammability and thus hold substantial promise in store for safe DIBs. Though ILs show better oxidation stability and nonflammability, most of them possess poor reductive stability or cause inefficient cation intercalation and are not compatible with graphite-negative electrodes. They also aggravate anodic Al dissolution by removing the native oxide protective layer, resulting in poor cycle life unless some additives like $LiBF_4$ or $LiPF_6$ are included. Perhaps, another downside of ILs is their cost which currently discourages large-scale application in commercial batteries. However, using ILs as components in GPEs along with solvent and salt additives might lead to a reduction in cost as well as an enhancement of the energy density and safety of DIBs.

Using various types of GPEs, recent works have demonstrated the design of quasi-solid-state DIBs which possess excellent flexibility, safety, and cycle life. Given the electrolytes provide ions needed for charge storage, it is usually necessary to make use of a critical amount of salt concentration sufficient to support ion conduction and to maximize intercalation capacity likewise. Thus, optimization of the electrolyte thickness and volume is essential to avoiding compromising the volumetric energy density. However, it is worth noting that the performance of GPEs may still be determined by the liquid phase while the polymeric host often merely serves as a 3D matrix and a physical separator, and thus the

addition of certain additives may be needed for performance enhancement.

In particular, GPEs have helped improve the performance of Al-based DIBs which normally employ acidic EMICl-$AlCl_3$ ILs that are corrosive and extremely sensitive to moisture. Ionogel GPEs used in different examples of quasi-solid-state Al-DIBs have resulted in a boost in cycle life, CE, energy density, lower moisture sensitivity, safety associated with reduced risk of electrolyte leakage, and less electrolyte degradation. Recent developments have also indicated that ILs can be replaced by much cheaper DES to design more affordable solid-state Al-DIBs suited for grid- and utility-scale applications. In brief, the multifunctional role of GPEs employed in DIBs can be manifested in their ability to provide the following advantages:

- high ionic conductivity over a broad temperature range
- thermal stability
- increased oxidative stability
- higher mechanical performance and load-bearing functionality
- flexiblility and formability that are amenable to applications in wearable electronics, or embedding within fabrics
- reduced flammability and thus improved safety
- dual functionality as separators and thus leading to compact cell designs with better energy and power densities

The major challenge is to find GPEs that satisfy the conflicting characteristics listed above, such as mechanical stability and electrical performance. A critical question in this regard is how well we can balance the desired mechanical performance with ionic conductivity. The presence of an excessive amount of inactive mechanical components will depreciate the ionic conductivity which eventually affects the electrochemical activity of the materials. Thus, it is important to incorporate multifunctional polymer electrolytes which possess bicontinuous microstructure with a polymer backbone needed for mechanical functionality and a porous medium capable of hosting sufficient electrolyte volume. By virtue of the design, bicontinuous GPEs are anticipated to deliver both mechanical and electrical performances which are effectively decoupled from each other. Such a design can be achieved in a class of block-copolymers that undergo spinodal decomposition during selective polymerization, or in response to quenching after thermal treatment or solvent evaporation. For instance, curing a mixture of epoxy resins and ILs in the presence of amines has been reported to generate a bicontinuous IL medium within a highly interconnected and porous epoxy matrix.[320,321] Depending on the IL content, such multifunctional electrolytes can deliver ionic conductivities on the order of 10^{-5}–10^{-3} S cm^{-1} near room temperature and while the associated Young's moduli vary between 150 and 800 MPa. Another approach involves integrating some structural components such as woven glass fiber fabrics within the polymer matrix which are sufficiently thin and, therefore, do not increase the thickness of the overall polymer electrolyte.[281] For example, PILs can be synthesized in situ directly within plain-weave glass fiber fabrics in the presence of IL or concentrated electrolytes to generate an IGE which doubles as an ion source and as a stiff and tough mechanical separator. If such a unique electrolyte design is to perform reasonably well, it is necessary to keep the fiber volume to a level that is only necessary to boost the mechanical performance of the IGEs. A blend of PIL[308] and IL can impart the IGE a high modulus and sufficient ionic conductivity. Especially, since ILs are safe to use, good solvents for salts, and good ion conductors, the polymeric component is just expected to transfer mechanical load. In addition, silica nanoparticles can be incorporated into PILs to generate hybrid IGEs which exhibit the desirable properties of the IL (with dissociated salt) and mechanical strength of the polymers and the inorganic nanofillers. This strategy opens up a novel opportunity in which the compositions of the blends can be varied to tune the electrical and mechanical properties of the IGEs.[307] Even though hybrid IGEs have been studied in different types of rechargeable batteries,[305,322] their use in DIBs is yet to be explored seriously, where they hold tangible promise to advance the design of safe and high-energy-density DIBs. Additionally, the ability to process IGEs from a solution allows for integration into complex electrode architectures. Another possibility is to create a bicontinuous polymer matrix with a mechanically stiff 3D network in which the IL component of the IGE can be confined. For example, silica nanofillers generated in situ via sol-gel synthesis can further enhance the structural properties of IGE by increasing the mechanical strength of the hybrid ionogels.[305,323] Another emerging strategy involves nanocomposite matrices in which the polymer or biopolymer network is cross-linked in situ using covalently bonded oxide nanofillers.[306] In these ternary systems, each component endows the GPEs with its unique properties without affecting the other performances: the IL provides thermal stability, plasticity, and ionic conduction, whereas the silica nanofillers covalently bonded to the polymer chains permit considerably improved mechanical strength without hampering ion transport. Apart from this, future studies can focus on the grafting or deposition of thin films of anion-conducting PILs on graphite to function as a stable CEI layer.

Similar challenges face the application of solvent-free SPEs in the design of fully solid-state DIBs. The SPEs must satisfy essential requirements, including electrochemical stability at the positive and negative electrodes, good interfacial bonding (adhesion to active materials), high ionic conductivity, high salt fraction, mechanical strength, and thermal stability. So far, the low ionic conductivity of SPEs constitutes an obstacle to their application in DIBs. At room temperature, the conductivities of SPEs are typically $<10^{-4}$ S cm^{-1} (see Figure 16), significantly lower than that liquid electrolytes (up to 10^{-2} S cm^{-1}) can offer. As for any electrolyte, the extent of salt dissociation and the relative mobilities of the ionic species are critical in SPEs.[325,326] The mobility of both anions and cations must be considered when selecting SPEs for a DIB application. In fact, the transference number should ideally be close to 0.5. Interestingly, this has been difficult to achieve for many SPEs. While the predominant polyethers which have strong Li-ion complexation usually show transference numbers around 0.1–0.2, polymers such as polycarbonates or polyesters possess less tendency to coordinate to cations and instead have transference numbers around 0.7 or higher.[276] Polymer blends or copolymers could thereby be an alternative to tailor these properties.

An SPE employed in a DIB should perform well mechanically, accommodating the stresses caused by cyclic volume changes[327] in the graphite electrode during anion uptake and release. Polymers with high elastic storage moduli can provide the mechanical strength required for such applications. However, the cumulative stress generated together in the polymer electrolyte, the active materials, and possibly an external load can still cause permanent deformation, resulting in delamination at the SPE-electrode interface. Another complication is the fact that the mechanical properties and ionic conductivity are coupled in classic SPEs, meaning that changing one property could affect the other (see Figure 16).[328-330] The segmental motion of the polymer chains in an SPE is essential for ion conduction; thus, polymers that are not mechanically stiff and have low T_g, are needed to enhance the ionic conductivity. The increased segmental motion of the polymer chains, however, results in a decrease in the stiffness of the SPE. On the other hand, extensive crosslinking in the SPEs may significantly reduce the mobility of the polymer chains, increasing mechanical stiffness, but sometimes at the expense of ion transport.[331-334] Apart from this, the mechanical stress developing in the SPE may also alter ionic conductivity if it causes a redistribution of the ions.[328] Therefore, it is crucial to devise a strategy that seeks to simultaneously optimize both ionic conductivity and mechanical stiffness.[332] One approach to decouple the two conflicting properties is the generation of multiphase SPEs consisting of a phase that conducts ions while the other phase, with high elastic modulus, imparts the desired mechanical performance.[335] Other solutions involve using block copolymers,[336] or incorporating inorganic nanofillers[337-344] which reinforce the stiffness of the SPEs while maintaining sufficient ionic conductivity.

Additionally, to be applied in a DIB, a polymer electrolyte must supply a sufficient amount of ions needed for energy storage and ionic conductivity; that is, the polymers must dissolve significant salt fractions. Otherwise, excessive depletion of ions from the electrolyte, when charging the DIB, will further diminish the ionic conductivity. Both the ionic conductivity and mechanical characteristics of the SPE are affected by the mole fraction of the salt

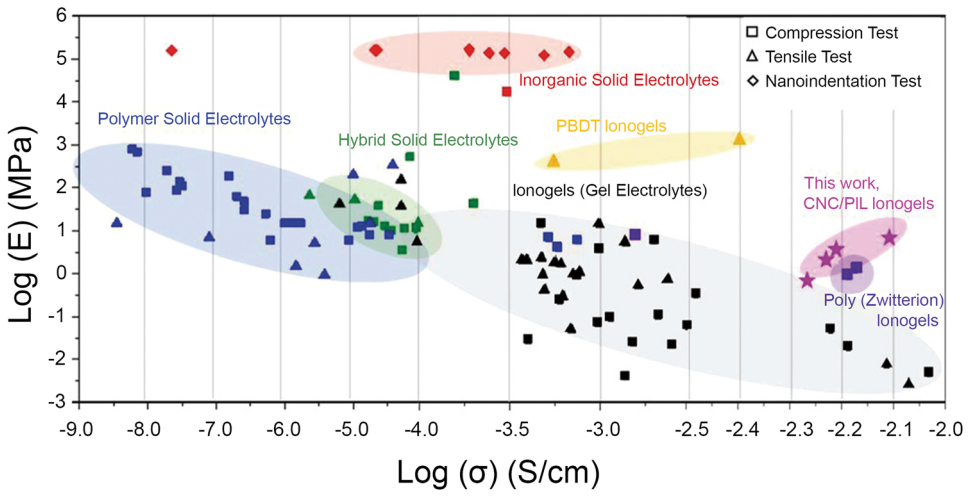

FIGURE 16 A logarithmic plot showing the relation between ionic conductivity (σ) and elastic modulus (E) for solid polymer electrolytes, ceramic electrolytes, and gel polymer electrolytes. Reproduced with permission: Copyright 2021, Wiley-VCH GmbH.[324]

dissolved in the solid polymer matrix.[328] Increasing the fraction of salts (e.g., $LiSO_3CF_3$, LiFSI, or LiTFSI) to >50 mol% generates polymer-in-salt electrolytes for which the segmental motion of the polymer is decoupled from the ionic conductivity of the SPE.[276,345-348] While the presence of excess salts can have a plasticizing effect and a lower T_g, they also lower the elastic modulus and thereby compromise the mechanical performance.[349]

Finally, as for any electrolyte, an SPE meant for use in a DIB must resist oxidation or consist of a component able to develop a stable interface. Unfortunately, similar to liquid salt-in-solvent electrolytes, a polymer that is stable both reductively and oxidatively is difficult to find.[350] Though PEO-based SPEs generally passivate both Li-metal and graphite electrodes well,[351] they are known to degrade at potentials beyond 4.0 V versus Li^+/Li,[352] which is too low to allow for anion intercalation. In principle, fluorinated polymers such as PVdF, and nitrile-containing should be able to extend the anodic stability of SPEs, as long as they can dissolve sufficiently high salt fraction.[343,353-358] Further improvement in the anodic stability of SPEs can be achieved using electrolyte additives and by surface coating of the graphite particles to generate stable CEI layers.[359-365] Solving these critical issues in SPEs will be a challenge worth pursuing.

ACKNOWLEDGMENTS

The authors acknowledge financial support from Batteries Sweden (Grant No. Vinnova-2019-00064), the Stand-Up for Energy consortium, the ISCF Faraday Challenge for the project on "Degradation of Battery Materials" (Grant No. EP/S003053/1, FIRG024), and the ERC (Grant No. 771777 FUN POLYSTORE).

CONFLICT OF INTEREST STATEMENT

The authors declare that there are no conflicts of interest.

ORCID

Habtom D. Asfaw https://orcid.org/0000-0001-5861-4281
Antonia Kotronia https://orcid.org/0000-0002-2272-4478
Nuria Garcia-Araez https://orcid.org/0000-0001-9095-2379
Kristina Edström https://orcid.org/0000-0003-4440-2952
Daniel Brandell https://orcid.org/0000-0002-8019-2801

REFERENCES

1. Placke T, Heckmann A, Schmuch R, Meister P, Beltrop K, Winter M. Perspective on performance, cost, and technical challenges for practical dual-ion batteries. *Joule*. 2018;2(12):2528-2550.
2. Wang M, Tang Y. A review on the features and progress of Dual-ion batteries. *Adv Energy Mater*. 2018;8(19):1703320.
3. Kravchyk KV, Kovalenko MV. Aluminum electrolytes for Al dual-ion batteries. *Commun Chem*. 2020;3(1):120.
4. Ji B, Zhang F, Song X, Tang Y. A novel potassium-ion-based dual-ion battery. *Adv Mater*. 2017;29(19):1700519.
5. Li J, Han C, Ou X, Tang Y. Concentrated electrolyte for high-performance Ca-ion battery based on organic anode and graphite cathode. *Angew Chem Int Ed*. 2022;61(14):e202116668.
6. Mu S, Liu Q, Kidkhunthod P, Zhou X, Wang W, Tang Y. Molecular grafting towards high-fraction active nanodots implanted in N-doped carbon for sodium dual-ion batteries. *Natl Sci Rev*. 2021;8(7):178.
7. Schafhaeutl C. On the compounds of carbon with silicon, iron, and other metals, which form the various galls of pig iron, steel, and wrought iron. *J Prakt Chem*. 1840;21(1):129-157.
8. Brodie BC XIII. On the atomic weight of graphite. *Philos Trans R Soc London*. 1859;149:249-259.
9. Kohlschütter V, Haenni P. About the knowledge of graphitic carbon and graphitic acid. *Z Anorg Allg Chem*. 1919;105(1):121-144.
10. Hassel O, Mark H. About the crystal structure of graphite. *Z Phys*. 1924;25(1):317-337.
11. Bernal JD, Bragg WL. The structure of graphite. *Proc R Soc A*. 1924;106(740):749-773.
12. Hofmann U, Frenzel A. Swelling of graphite and the formation of graphitic acid. *Ber Dtsch Chem Ges*. 1930;63(5):1248-1262.
13. Rüdorff W, Hofmann U. About graphite salts. *Z Anorg Allg Chem*. 1938;238(1):1-50.
14. Hummers WS, Offeman RE. Preparation of graphitic oxide. *J Am Chem Soc*. 1958;80(6):1339.
15. Thiele H. The processes involved in expanding graphite. *Z Anorg Allg Chem*. 1932;207(4):340-352.
16. Rüdorff W. Graphite intercalation compounds. In: Emeléus HJ, Sharpe AG, eds. *Advances in Inorganic Chemistry and Radiochemistry*. Academic Press; 1959:223-266.
17. Rüdorff W, Stumpp E, Spriessler W, Siecke FW. Reactions of graphite with metal chlorides. *Angew Chem Int Ed Engl*. 1963;2(2):67-73.
18. Stumpp E. The intercalation of metal chlorides and bromides into graphite. *Mater Sci Eng*. 1977;31:53-59.
19. Rüdorff W, Schulz H. On the incorporation of ferric chloride in the lattice of graphite. *Z Anorg Allg Chem*. 1940;245(2):121-156.
20. Inagaki M, Wang ZD. Synthesis of cupric chloride-graphite intercalation compounds by the molten salt method. *Synth Met*. 1987;20(1):1-8.
21. Rüdorff W, Zeller R. On aluminum chloride–graphite intercalation compounds. *Z Anorg Allg Chem*. 1955;279(3-4):182-193.
22. Dzurus ML, Hennig GR. Graphite Compounds1,2. *J Am Chem Soc*. 1957;79(5):1051-1054.
23. Hooley JG, Deitz VR. The intercalation of bromine in graphitized carbon fibers and its removal. *Carbon*. 1978;16(4):251-257.
24. Rüdorff W, Sils V, Zeller R. On the behavior of graphite towards iodine monochloride and chromyl chloride. *Z Anorg Allg Chem*. 1956;283(1-6):299-303.

25. Bartlett N, McQuillan B, Robertson AS. The synthesis of the first stage graphite salt C_8^+ AsF_6^- and its relationship to the first stage graphite/AsF_5 intercalate. *Mater Res Bull*. 1978; 13(12):1259-1264.
26. McCarron EM, Bartlett N. Composition and staging in the graphite–AsF_6 system and its relationship to graphite–AsF_5. *J Chem Soc Chem Commun*. 1980;(9):404-406.
27. Okino F, Bartlett N. Hexafluoroarsenates of graphite from its interaction with AsF_5' AsF_5+ F_2' and O_2AsF_6' and the structure of $C_{14}AsF_6$. *J Chem Soc Dalton Trans*. 1993;(14):2081-2090.
28. Okino F. Preparation and properties of graphite hexafluoroarsenates C_xAsF_6. *J Fluorine Chem*. 2000;105(2):239-248.
29. Bottomley MJ, Parry GS, Ubbelohde AR, Young DA. 1083. Electrochemical preparation of salts from well-oriented graphite. *J Chem Soc*. 1963:5674-5680.
30. Beck F, Junge H, Krohn H. Graphite intercalation compounds as positive electrodes in galvanic cells. *Electrochim Acta*. 1981;26(7):799-809.
31. Besenhard J, Fritz HP. Über die stufenweise Oxidation von Graphit in nichtwäßrigen, neutralen elektrolyten/on the stage-wise oxidation of graphite in nonaqueous, neutral electrolytes. *Z Naturforsch B*. 1972;27(11):1294-1298.
32. Deshpande SL, Bennion DN. Lithium dimethyl sulfite graphite cell. *J Electrochem Soc*. 1978;125(5):687-692.
33. Ohzuku T, Takehara Z, Yoshizawa S. A graphite compound as cathode for rechargeable nonaqueous lithium battery. *J Electrochem Soc*. 1978;46(8):438-441.
34. Matsuda Y, Morita M, Katsuma H. Charge–discharge characteristics of graphite as a positive electrode of lithium secondary cells. *J Electrochem Soc*. 1983;51(9):744-748.
35. Fouletier M, Armand M. Electrochemical method for characterization of graphite–aluminium chloride intercalation compounds. *Carbon*. 1979;17(5):427-429.
36. Gale RJ, Osteryoung RA. Electrochemical reduction of pyridinium ions in ionic aluminum chloride: alkylpyridinium halide ambient temperature liquids. *J Electrochem Soc*. 1980;127(10):2167-2172.
37. Carpio RA, King LA, Lindstrom RE, Nardi JC, Hussey CL. Density, electric conductivity, and viscosity of several *N*-alkylpyridinium halides and their mixtures with aluminum chloride. *J Electrochem Soc*. 1979;126(10):1644-1650.
38. Wilkes JS, Levisky JA, Wilson RA, Hussey CL. Dialkylimidazolium chloroaluminate melts: a new class of room-temperature ionic liquids for electrochemistry, spectroscopy and synthesis. *Inorg Chem*. 1982;21(3):1263-1264.
39. Gifford PR, Palmisano JB. An aluminum/chlorine rechargeable cell employing a room temperature molten salt electrolyte. *J Electrochem Soc*. 1988;135(3):650-654.
40. McCullough FP, Beale AF, inventors; Secondary electrical energy storage device and electrode there of patent application. US patent ZA849438B. 1989.
41. McCullough FP, Levine CA, Snelgrove RV, inventors; Secondary battery. US patent 4,830,938. 1989.
42. Maeda Y. Temperature change of graphite surface due to electrochemical intercalation of ClO_4^- ion. *Bull Chem Soc Japan*. 1989;62(11):3711-3713.
43. Maeda Y. Thermal behavior on graphite due to electrochemical intercalation. *J Electrochem Soc*. 1990;137(10): 3047-3052.
44. Carlin RT, De Long HC, Fuller J, Trulove PC. Dual intercalating molten electrolyte batteries. *J Electrochem Soc*. 1994;141(7):L73-L76.
45. Carlin RT, Fuller J, Kuhn WK, Lysaght MJ, Trulove PC. Electrochemistry of room-temperature chloroaluminate molten salts at graphitic and nongraphitic electrodes. *J Appl Electrochem*. 1996;26(11):1147-1160.
46. Santhanam R, Noel M. Electrochemical intercalation of ionic species of tetrabutylammonium perchlorate on graphite electrodes. A potential dual-intercalation battery system. *J Power Sources*. 1995;56(1):101-105.
47. Seel JA, Dahn JR. Electrochemical intercalation of PF_6 into graphite. *J Electrochem Soc*. 2000;147(3):892-898.
48. Dahn JR, Seel JA. Energy and capacity projections for practical dual-graphite cells. *J Electrochem Soc*. 2000;147(3):899-901.
49. Zhang X, Sukpirom N, Lerner MM. Graphite intercalation of bis(trifluoromethanesulfonyl) imide and other anions with perfluoroalkanesulfonyl substituents. *Mater Res Bull*. 1999; 34(3):363-372.
50. Yan W, Lerner MM. Electrochemical preparation of graphite bis(trifluoromethanesulfonyl) imide. *J Electrochem Soc*. 2001; 148(6):D83-D87.
51. Sutto TE, De Long HC, Trulove PC. Physical properties of substituted imidazolium based ionic liquids gel electrolytes. *Z Naturforsch A*. 2002;57(11):839-846.
52. Nishida T, Tashiro Y, Yamamoto M. Physical and electrochemical properties of 1-alkyl-3-methylimidazolium tetrafluoroborate for electrolyte. *J Fluorine Chem*. 2003;120(2): 135-141.
53. Garcia B, Lavallée S, Perron G, Michot C, Armand M. Room temperature molten salts as lithium battery electrolyte. *Electrochim Acta*. 2004;49(26):4583-4588.
54. Nakagawa H, Izuchi S, Kuwana K, Nukuda T, Aihara Y. Liquid and polymer gel electrolytes for lithium batteries composed of room-temperature molten salt doped by lithium salt. *J Electrochem Soc*. 2003;150(6):A695-A700.
55. Sugimoto T, Kikuta M, Ishiko E, Kono M, Ishikawa M. Ionic liquid electrolytes compatible with graphitized carbon negative without additive and their effects on interfacial properties. *J Power Sources*. 2008;183(1):436-440.
56. Ishikawa M, Sugimoto T, Kikuta M, Ishiko E, Kono M. Pure ionic liquid electrolytes compatible with a graphitized carbon negative electrode in rechargeable lithium-ion batteries. *J Power Sources*. 2006;162(1):658-662.
57. Paillard E, Zhou Q, Henderson WA, Appetecchi GB, Montanino M, Passerini S. Electrochemical and physicochemical properties of $PY_{14}FSI$-based electrolytes with LiFSI. *J Electrochem Soc*. 2009;156(11):A891-A895.
58. Placke T, Bieker P, Lux SF, et al. Dual-ion cells based on anion intercalation into graphite from ionic liquid-based electrolytes. *Z Phys Chem*. 2012;226(5-6):391-407.
59. Placke T, Fromm O, Lux SF, et al. Reversible intercalation of bis(trifluoromethanesulfonyl)imide anions from an ionic liquid electrolyte into graphite for high performance dual-ion cells. *J Electrochem Soc*. 2012;159(11):A1755-A1765.
60. Rothermel S, Meister P, Schmuelling G, et al. Dual-graphite cells based on the reversible intercalation of bis(trifluoromethanesulfonyl)imide anions from an ionic liquid electrolyte. *Energy Environ Sci*. 2014;7(10):3412-3423.

61. Fromm O, Meister P, Qi X, et al. Study of the electrochemical intercalation of different anions from non-aqueous electrolytes into a graphite-based cathode. *ECS Trans*. 2014;58(14):55-65.
62. Schmuelling G, Placke T, Kloepsch R, et al. X-ray diffraction studies of the electrochemical intercalation of bis(trifluoromethanesulfonyl)imide anions into graphite for dual-ion cells. *J Power Sources*. 2013;239:563-571.
63. Placke T, Schmuelling G, Kloepsch R, et al. In situ X-ray diffraction studies of cation and anion intercalation into graphitic carbons for electrochemical energy storage applications. *Z Anorg Allg Chem*. 2014;640(10):1996-2006.
64. Lin M-C, Gong M, Lu B, et al. An ultrafast rechargeable aluminium-ion battery. *Nature*. 2015;520(7547):324-328.
65. Zhang X, Tang Y, Zhang F, Lee C-S. A novel aluminum–graphite dual-ion battery. *Adv Energy Mater*. 2016;6(11):1502588.
66. Yang C, Chen J, Ji X, et al. Aqueous Li-ion battery enabled by halogen conversion–intercalation chemistry in graphite. *Nature*. 2019;569(7755):245-250.
67. Guo Q, Kim K-I, Li S, et al. Reversible insertion of I–Cl interhalogen in a graphite cathode for aqueous dual-ion batteries. *ACS Energy Lett*. 2021;6(2):459-467.
68. Fukutsuka T, Yamane F, Miyazaki K, Abe T. Electrochemical intercalation of bis(fluorosulfonyl)amide anion into graphite. *J Electrochem Soc*. 2015;163(3):A499-A503.
69. Ishihara T, Koga M, Matsumoto H, Yoshio M. Electrochemical intercalation of hexafluorophosphate anion into various carbons for cathode of dual-carbon rechargeable battery. *Electrochem Solid State Lett*. 2007;10(3):A74-A76.
70. Miyoshi S, Nagano H, Fukuda T, et al. Dual-carbon battery using high concentration LiPF 6 in dimethyl carbonate (DMC) electrolyte. *J Electrochem Soc*. 2016;163(7):A1206-A1213.
71. Read JA, Cresce AV, Ervin MH, Xu K. Dual-graphite chemistry enabled by a high voltage electrolyte. *Energy Environ Sci*. 2014;7(2):617-620.
72. Wrogemann JM, Künne S, Heckmann A, et al. Development of safe and sustainable dual-ion batteries through hybrid aqueous/nonaqueous electrolytes. *Adv Energy Mater*. 2020;10(8):1902709.
73. Kondo Y, Miyahara Y, Fukutsuka T, Miyazaki K, Abe T. Electrochemical intercalation of bis(fluorosulfonyl)amide anions into graphite from aqueous solutions. *Electrochem Commun*. 2019;100:26-29.
74. Kim K, Guo Q, Tang L, et al. Reversible insertion of Mg–Cl superhalides in graphite as a cathode for aqueous dual-ion batteries. *Angew Chem Int Ed*. 2020;59(45):19924-19928.
75. Guo Q, Kim K, Jiang H, et al. A high-potential anion-insertion carbon cathode for aqueous zinc dual-ion battery. *Adv Funct Mater*. 2020;30(38):2002825.
76. Li L, Zhang D, Deng J, et al. Review—progress of research on the preparation of graphene oxide via electrochemical approaches. *J Electrochem Soc*. 2020;167(15):155519.
77. Yu C-J, Ri U-S, Ri G-C, Kim J-S. Revealing the formation and electrochemical properties of bis(trifluoromethanesulfonyl) imide intercalated graphite with first-principles calculations. *Phys Chem Chem Phys*. 2018;20(20):14124-14132.
78. Zhang L, Wang H, Zhang X, Tang Y. A review of emerging dual-ion batteries: fundamentals and recent advances. *Adv Funct Mater*. 2021;31(20):2010958.
79. Hao J, Li X, Song X, Guo Z. Recent progress and perspectives on dual-ion batteries. *EnergyChem*. 2019;1(1):100004.
80. Kotronia A, Asfaw HD, Tai C-W, Hahlin M, Brandell D, Edström K. Nature of the cathode-electrolyte interface in highly concentrated electrolytes used in graphite dual-ion batteries. *ACS Appl Mater Interfaces*. 2021;13(3):3867-3880.
81. Wang Y, Zhang Y, Dong S, et al. An all-fluorinated electrolyte toward high voltage and long cycle performance dual-ion batteries. *Adv Energy Mater*. 2022;12(19):2103360.
82. Asfaw HD, Kotronia A. A polymeric cathode–electrolyte interface enhances the performance of MoS_2–graphite potassium dual-ion intercalation battery. *Cell Rep Phys Sci*. 2022;3(1):100693.
83. Song Y, Jiao S, Tu J, et al. A long-life rechargeable Al ion battery based on molten salts. *J Mater Chem A*. 2017;5(3):1282-1291.
84. Tu J, Wang J, Zhu H, Jiao S. The molten chlorides for aluminum–graphite rechargeable batteries. *J Alloys Compd*. 2020;821:153285.
85. Fukunaga A, Nohira T, Kozawa Y, et al. Intermediate-temperature ionic liquid NaFSA–KFSA and its application to sodium secondary batteries. *J Power Sources*. 2012;209:52-56.
86. Chen C-Y, Matsumoto K, Kubota K, Hagiwara R, Xu Q. An energy-dense solvent-free dual-ion battery. *Adv Funct Mater*. 2020;30(39):2003557.
87. Yamada Y, Chiang CH, Sodeyama K, Wang J, Tateyama Y, Yamada A. Corrosion prevention mechanism of aluminum metal in superconcentrated electrolytes. *ChemElectroChem*. 2015;2(11):1687-1694.
88. Kühnel R-S, Lübke M, Winter M, Passerini S, Balducci A. Suppression of aluminum current collector corrosion in ionic liquid containing electrolytes. *J Power Sources*. 2012;214:178-184.
89. Matsumoto K, Nishiwaki E, Hosokawa T, Tawa S, Nohira T, Hagiwara R. Thermal, physical, and electrochemical properties of $Li[N(SO_2F)_2]$-[1-ethyl-3-methylimidazolium] $[N(SO_2F)_2]$ ionic liquid electrolytes for Li secondary batteries operated at room and intermediate temperatures. *J Phys Chem C*. 2017;121(17):9209-9219.
90. Li Z, Li X, Zhang W. A high-performance graphite–graphite dual ion battery based on $AlCl_3$/NaCl molten salts. *J Power Sources*. 2020;475:228628.
91. Wang J, Tu J, Jiao H, Zhu H, Nanosheet-stacked flake graphite for high-performance Al storage in inorganic molten $AlCl_3$–NaCl salt. *Int J Miner Metall Mater*. 2020;27(12):1711-1722.
92. Matsumoto H, Sakaebe H, Tatsumi K, Kikuta M, Ishiko E, Kono M. Fast cycling of $Li/LiCoO_2$ cell with low-viscosity ionic liquids based on bis(fluorosulfonyl)imide $[FSI^-]$. *J Power Sources*. 2006;160(2):1308-1313.
93. Lewandowski A, Świderska-Mocek A. Ionic liquids as electrolytes for Li-ion batteries—an overview of electrochemical studies. *J Power Sources*. 2009;194(2):601-609.
94. Beltrop K, Meister P, Klein S, et al. Does size really matter? New insights into the intercalation behavior of anions into a

graphite-based positive electrode for dual-ion batteries. *Electrochim Acta*. 2016;209:44-55.
95. Wang W, Yang T, Li S, et al. 1-Ethyl-3-methylimidazolium tetrafluoroborate (EMI-BF_4) as an ionic liquid-type electrolyte additive to enhance the low-temperature performance of $LiNi_{0.5}Co_{0.2}Mn_{0.3}O_2$/graphite batteries. *Electrochim Acta*. 2019;317:146-154.
96. Hubble D, Brown DE, Zhao Y, et al. Liquid electrolyte development for low-temperature lithium-ion batteries. *Energy Environ Sci*. 2022;15(2):550-578.
97. Kunze M, Jeong S, Appetecchi GB, Schönhoff M, Winter M, Passerini S. Mixtures of ionic liquids for low temperature electrolytes. *Electrochim Acta*. 2012;82:69-74.
98. Lin R, Taberna P-L, Fantini S, et al. Capacitive energy storage from −50 to 100°C using an ionic liquid electrolyte. *J Phys Chem Lett*. 2011;2(19):2396-2401.
99. Tian J, Cui C, Xie Q, et al. EMIMBF_4–GBL binary electrolyte working at −70°C and 3.7 V for a high performance graphene-based capacitor. *J Mater Chem A*. 2018;6(8):3593-3601.
100. Sun Y, Liu B, Liu L, Yan X. Ions transport in electrochemical energy storage devices at low temperatures. *Adv Funct Mater*. 2022;32(15):2109568.
101. Xiang HF, Yin B, Wang H, et al. Improving electrochemical properties of room temperature ionic liquid (RTIL) based electrolyte for Li-ion batteries. *Electrochim Acta*. 2010;55(18):5204-5209.
102. Kühnel RS, Böckenfeld N, Passerini S, Winter M, Balducci A. Mixtures of ionic liquid and organic carbonate as electrolyte with improved safety and performance for rechargeable lithium batteries. *Electrochim Acta*. 2011;56(11):4092-4099.
103. Wu Y, Gong M, Lin M-C, et al. 3D graphitic foams derived from chloroaluminate anion intercalation for ultrafast aluminum-ion battery. *Adv Mater*. 2016;28(41):9218-9222.
104. Wang D-Y, Wei C-Y, Lin M-C, et al. Advanced rechargeable aluminium ion battery with a high-quality natural graphite cathode. *Nat Commun*. 2017;8:14283.
105. Zhu N, Zhang K, Wu F, Bai Y, Wu C. Ionic liquid-based electrolytes for aluminum/magnesium/sodium-ion batteries. *Energy Mater Adv*. 2021;2021:9204217.
106. Lai PK, Skyllas-Kazacos M. Aluminium deposition and dissolution in aluminium chloride—*n*-butylpyridinium chloride melts. *Electrochim Acta*. 1987;32(10):1443-1449.
107. Chao-Cheng Y. Electrodeposition of aluminum in molten $AlCl_3$-*n*-butylpyridinium chloride electrolyte. *Mater Chem Phys*. 1994;37(4):355-361.
108. Zhao Y, VanderNoot TJ. Electrodeposition of aluminium from nonaqueous organic electrolytic systems and room temperature molten salts. *Electrochim Acta*. 1997;42(1):3-13.
109. Jiang T, Chollier Brym MJ, Dubé G, Lasia A, Brisard GM. Electrodeposition of aluminium from ionic liquids: part I—electrodeposition and surface morphology of aluminium from aluminium chloride ($AlCl_3$)–1-ethyl-3-methylimidazolium chloride ([EMIm]Cl) ionic liquids. *Surf Coat Technol*. 2006;201(1-2):1-9.
110. Abbott AP, Harris RC, Hsieh Y-T, Ryder KS, Sun IW. Aluminium electrodeposition under ambient conditions. *Phys Chem Chem Phys*. 2014;16(28):14675-14681.
111. Muñoz-Torrero D, Palma J, Marcilla R, Ventosa E. A critical perspective on rechargeable Al-ion battery technology. *Dalton Trans*. 2019;48(27):9906-9911.
112. Kravchyk KV, Wang S, Piveteau L, Kovalenko MV. Efficient aluminum chloride–natural graphite battery. *Chem Mater*. 2017;29(10):4484-4492.
113. Kravchyk KV, Kovalenko MV. Rechargeable dual-ion batteries with graphite as a cathode: key challenges and opportunities. *Adv Energy Mater*. 2019;9(35):1901749.
114. Chen C-Y, Tsuda T, Kuwabata S, Hussey CL. Rechargeable aluminum batteries utilizing a chloroaluminate inorganic ionic liquid electrolyte. *Chem Commun*. 2018;54(33):4164-4167.
115. Yang C, Wang S, Zhang X, et al. Substituent effect of imidazolium ionic liquid: a potential strategy for high Coulombic efficiency al battery. *J Phys Chem C*. 2019;123(18):11522-11528.
116. Xu C, Li J, Chen H, Zhang J. Benzyltriethylammonium chloride electrolyte for high-performance Al-ion batteries. *ChemNanoMat*. 2019;5(11):1367-1372.
117. Lv Z, Han M, Sun J, et al. A high discharge voltage dual-ion rechargeable battery using pure ($DMPI^+$)($AlCl_4^-$) ionic liquid electrolyte. *J Power Sources*. 2019;418:233-240.
118. Kotobuki M, Lu L, Savilov SV, Aldoshin SM. Poly(vinylidene fluoride)-based Al ion conductive solid polymer electrolyte for Al battery. *J Electrochem Soc*. 2017;164(14):A3868-A3875.
119. Li C, Patra J, Li J, Rath PC, Lin M-H, Chang J-K. A novel moisture-insensitive and low-corrosivity ionic liquid electrolyte for rechargeable aluminum batteries. *Adv Funct Mater*. 2020;30(12):1909565.
120. Zhang E, Wang B, Wang J, et al. Rapidly synthesizing interconnected carbon nanocage by microwave toward high-performance aluminum batteries. *Chem Eng J*. 2020;389:124407.
121. Wang H, Gu S, Bai Y, Chen S, Wu F, Wu C. High-voltage and noncorrosive ionic liquid electrolyte used in rechargeable aluminum battery. *ACS Appl Mater Interfaces*. 2016;8(41):27444-27448.
122. Wang A, Yuan W, Fan J, Li L. A dual-graphite battery with pure 1-butyl-1-methylpyrrolidinium bis(trifluoromethylsulfonyl) imide as the electrolyte. *Energy Technol*. 2018;6(11):2172-2178.
123. Aladinli S, Bordet F, Ahlbrecht K, Tübke J, Holzapfel M. Anion intercalation into a graphite cathode from various sodium-based electrolyte mixtures for dual-ion battery applications. *Electrochim Acta*. 2017;231:468-478.
124. Meister P, Siozios V, Reiter J, et al. Dual-ion cells based on the electrochemical intercalation of asymmetric fluorosulfonyl-(trifluoromethanesulfonyl) imide anions into graphite. *Electrochim Acta*. 2014;130:625-633.
125. Meister P, Schmuelling G, Winter M, Placke T. New insights into the uptake/release of $FTFSI^-$ anions into graphite by means of in situ powder X-ray diffraction. *Electrochem Commun*. 2016;71:52-55.
126. Heckmann A, Meister P, Meyer HW, Rohrbach A, Winter M, Placke T. Synthesis of spherical graphite particles and their application as cathode material in dual-ion cells. *ECS Trans*. 2015;66(11):1-12.

127. Heckmann A, Meister P, Kuo L-Y, Winter M, Kaghazchi P, Placke T. A route towards understanding the kinetic processes of bis(trifluoromethanesulfonyl) imide anion intercalation into graphite for dual-ion batteries. *Electrochim Acta*. 2018;284:669-680.
128. Balabajew M, Reinhardt H, Bock N, et al. In-situ Raman study of the intercalation of bis(trifluoromethylsulfonyl)imid ions into graphite inside a dual-ion cell. *Electrochim Acta*. 2016;211:679-688.
129. Cho E, Mun J, Chae OB, et al. Corrosion/passivation of aluminum current collector in bis(fluorosulfonyl)imide-based ionic liquid for lithium-ion batteries. *Electrochem Commun*. 2012;22:1-3.
130. Kühnel R-S, Balducci A. Comparison of the anodic behavior of aluminum current collectors in imide-based ionic liquids and consequences on the stability of high voltage supercapacitors. *J Power Sources*. 2014;249:163-171.
131. Fan J, Zhang Z, Liu Y, Wang A, Li L, Yuan W. An excellent rechargeable $PP_{14}TFSI$ ionic liquid dual-ion battery. *Chem Commun*. 2017;53(51):6891-6894.
132. Li Z, Liu J, Li J, Kang F, Gao F. A novel graphite-based dual ion battery using $PP_{14}NTF_2$ ionic liquid for preparing graphene structure. *Carbon*. 2018;138:52-60.
133. Beltrop K, Qi X, Hering T, Röser S, Winter M, Placke T. Enabling bis(fluorosulfonyl)imide-based ionic liquid electrolytes for application in dual-ion batteries. *J Power Sources*. 2018;373:193-202.
134. Nádherná M, Reiter J, Moškon J, Dominko R. Lithium bis (fluorosulfonyl)imide–PYR_{14}TFSI ionic liquid electrolyte compatible with graphite. *J Power Sources*. 2011;196(18):7700-7706.
135. Meister P, Küpers V, Kolek M, et al. Enabling Mg-based ionic liquid electrolytes for hybrid dual-ion capacitors. *Batteries Supercaps*. 2021;4(3):504-512.
136. Shkrob IA, Marin TW, Zhu Y, Abraham DP. Why bis (fluorosulfonyl)imide is a "Magic Anion" for electrochemistry. *J Phys Chem C*. 2014;118(34):19661-19671.
137. Beltrop K, Beuker S, Heckmann A, Winter M, Placke T. Alternative electrochemical energy storage: potassium-based dual–graphite batteries. *Energy Environ Sci*. 2017;10(10): 2090-2094.
138. Angell M, Pan C-J, Rong Y, et al. High Coulombic efficiency aluminum-ion battery using an $AlCl_3$-urea ionic liquid analog electrolyte. *Proc Natl Acad Sci USA*. 2017;114(5):834-839.
139. Jiao H, Wang C, Tu J, Tian D, Jiao S. A rechargeable Al-ion battery: l/molten $AlCl_3$–urea/graphite. *Chem Commun*. 2017;53(15):2331-2334.
140. Angell M, Zhu G, Lin M-C, Rong Y, Dai H. Ionic liquid analogs of $AlCl_3$ with urea derivatives as electrolytes for aluminum batteries. *Adv Funct Mater*. 2020;30(4):1901928.
141. Li J, Tu J, Jiao H, Wang C, Jiao S. Ternary $AlCl_3$-urea-[EMIm]Cl ionic liquid electrolyte for rechargeable aluminum-ion batteries. *J Electrochem Soc*. 2017;164(13): A3093-A3100.
142. Wang C, Li J, Jiao H, Tu J, Jiao S. The electrochemical behavior of an aluminum alloy anode for rechargeable Al-ion batteries using an $AlCl_3$–urea liquid electrolyte. *RSC Adv*. 2017;7(51):32288-32293.
143. Ng KL, Malik M, Buch E, Glossmann T, Hintennach A, Azimi G. A low-cost rechargeable aluminum/natural graphite battery utilizing urea-based ionic liquid analog. *Electrochim Acta*. 2019;327:135031.
144. Canever N, Bertrand N, Nann T. Acetamide: a low-cost alternative to alkyl imidazolium chlorides for aluminium-ion batteries. *Chem Commun*. 2018;54(83):11725-11728.
145. Xu H, Bai T, Chen H, et al. Low-cost $AlCl_3/Et_3NHCl$ electrolyte for high-performance aluminum-ion battery. *Energy Stor Mater*. 2019;17:38-45.
146. Gan F, Chen K, Li N, Wang Y, Shuai Y, He X. Low cost ionic liquid electrolytes for rechargeable aluminum/graphite batteries. *Ionics*. 2019;25(9):4243-4249.
147. Tu J, Song W-L, Lei H, et al. Nonaqueous rechargeable aluminum batteries: progresses, challenges, and perspectives. *Chem Rev*. 2021;121(8):4903-4961.
148. Pasta M, Wessells CD, Huggins RA, Cui Y. A high-rate and long cycle life aqueous electrolyte battery for grid-scale energy storage. *Nat Commun*. 2012;3:1149.
149. Kim H, Hong J, Park K-Y, Kim H, Kim S-W, Kang K. Aqueous rechargeable Li and Na ion batteries. *Chem Rev*. 2014;114(23):11788-11827.
150. Luo J-Y, Cui W-J, He P, Xia Y-Y. Raising the cycling stability of aqueous lithium-ion batteries by eliminating oxygen in the electrolyte. *Nat Chem*. 2010;2(9):760-765.
151. Rodríguez-Pérez IA, Ji X. Anion hosting cathodes in dual-ion batteries. *ACS Energy Lett*. 2017;2(8):1762-1770.
152. Suo L, Borodin O, Gao T, et al. "Water-in-salt" electrolyte enables high-voltage aqueous lithium-ion chemistries. *Science*. 2015;350(6263):938-943.
153. Wang F, Borodin O, Ding MS, et al. Hybrid aqueous/non-aqueous electrolyte for safe and high-energy Li-ion. *Joule*. 2018;2(5):927-937.
154. Yang C, Chen J, Qing T, et al. 4.0 V Aqueous Li-ion batteries. *Joule*. 2017;1(1):122-132.
155. Yamada Y, Usui K, Sodeyama K, Ko S, Tateyama Y, Yamada A. Hydrate-melt electrolytes for high-energy-density aqueous batteries. *Nat Energy*. 2016;1(10): 16129.
156. Suo L, Oh D, Lin Y, et al. How solid-electrolyte interphase forms in aqueous electrolytes. *J Am Chem Soc*. 2017;139(51): 18670-18680.
157. Dong X, Yu H, Ma Y, et al. All-organic rechargeable battery with reversibility supported by "Water-in-Salt" electrolyte. *Chem Eur J*. 2017;23(11):2560-2565.
158. Rodríguez-Pérez IA, Zhang L, Leonard DP, Ji X. Aqueous anion insertion into a hydrocarbon cathode via a water-in-salt electrolyte. *Electrochem Commun*. 2019;109:106599.
159. Li H, Kurihara T, Yang D, Watanabe M, Ishihara T. A novel aqueous dual-ion battery using concentrated bisalt electrolyte. *Energy Stor Mater*. 2021;38:454-461.
160. Zhang H, Liu X, Qin B, Passerini S. Electrochemical intercalation of anions in graphite for high-voltage aqueous zinc battery. *J Power Sources*. 2020;449:227594.
161. Rodríguez-Pérez IA, Zhang L, Wrogemann JM, et al. Enabling natural graphite in high-voltage aqueous graphite||Zn metal dual-ion batteries. *Adv Energy Mater*. 2020; 10(41):2001256.
162. Wu X, Xu Y, Zhang C, et al. Reverse dual-ion battery via a $ZnCl_2$ water-in-salt electrolyte. *J Am Chem Soc*. 2019;141(15): 6338-6344.

163. Sandstrom SK, Chen X, Ji X. A review of halide charge carriers for rocking-chair and dual-ion batteries. *Carbon Energy*. 2021;3(4):627-653.
164. Yang J, Liu Y, Zhang Y, et al. Recent advances and future perspectives of rechargeable chloride-based batteries. *Nano Energy*. 2023;110:108364.
165. Xu J, Pollard TP, Yang C, et al. Lithium halide cathodes for Li metal batteries. *Joule*. 2023;7(1):83-94.
166. Chen H, Guo F, Liu Y, et al. A defect-free principle for advanced graphene cathode of aluminum-ion battery. *Adv Mater*. 2017;29(12):1605958.
167. Huang Y, Liang Z, Wang H. A dual-ion battery has two sides: the effect of ion-pairs. *Chem Commun*. 2020;56(69):10070-10073.
168. Huang Y, Fan H, Kamezaki H, Kang B, Yoshio M, Wang H. Facilitating tetrafluoroborate intercalation into graphite electrodes from ethylmethyl carbonate-based solutions. *ChemElectroChem*. 2019;6(11):2931-2936.
169. Wang Y, Wang H. Intercalation of tetrafluoroborate anions into graphite electrodes from mixed sulfones. *ACS Appl Energy Mater*. 2022;5(2):2366-2374.
170. Zhang L, Li J, Huang Y, Zhu D, Wang H. Synergetic effect of ethyl methyl carbonate and trimethyl phosphate on BF_4^- intercalation into a graphite electrode. *Langmuir*. 2019;35(11):3972-3979.
171. Gao J, Yoshio M, Qi L, Wang H. Solvation effect on intercalation behaviour of tetrafluoroborate into graphite electrode. *J Power Sources*. 2015;278:452-457.
172. Tian S, Qi L, Yoshio M, Wang H. Tetramethylammonium difluoro(oxalato)borate dissolved in ethylene/propylene carbonates as electrolytes for electrochemical capacitors. *J Power Sources*. 2014;256:404-409.
173. Tian S, Qi L, Wang H. Difluoro(oxalato)borate anion intercalation into graphite electrode from ethylene carbonate. *Solid State Ion*. 2016;291:42-46.
174. Wang Y, Wang S, Zhang Y, Lee P-K, Yu DYW. Unlocking the true capability of graphite-based dual-ion batteries with ethyl methyl carbonate electrolyte. *ACS Appl Energy Mater*. 2019;2(10):7512-7517.
175. Fan H, Gao J, Qi L, Wang H. Hexafluorophosphate anion intercalation into graphite electrode from sulfolane/ethylmethyl carbonate solutions. *Electrochim Acta*. 2016;189:9-15.
176. Bordet F, Ahlbrecht K, Tübke J, et al. Anion intercalation into graphite from a sodium-containing electrolyte. *Electrochim Acta*. 2015;174:1317-1323.
177. Xiang L, Ou X, Wang X, Zhou Z, Li X, Tang Y. Highly concentrated electrolyte towards enhanced energy density and cycling life of dual-ion battery. *Angew Chem Int Ed*. 2020;59(41):17924-17930.
178. Kravchyk KV, Bhauriyal P, Piveteau L, Guntlin CP, Pathak B, Kovalenko MV. High-energy-density dual-ion battery for stationary storage of electricity using concentrated potassium fluorosulfonylimide. *Nat Commun*. 2018;9:4469.
179. Santhanam R, Noel M. Effect of solvents on the intercalation/de-intercalation behaviour of monovalent ionic species from non-aqueous solvents on polypropylene-graphite composite electrode. *J Power Sources*. 1997;66(1-2):47-54.
180. Kawamura T, Tanaka T, Egashira M, Watanabe I, Okada S, Yamaki J. Methyl difluoroacetate inhibits corrosion of aluminum cathode current collector for lithium ion cells. *Electrochem Solid State Lett*. 2005;8(9):A459.
181. Tan H, Zhai D, Kang F, Zhang B. Synergistic PF_6^- and FSI^- intercalation enables stable graphite cathode for potassium-based dual ion battery. *Carbon*. 2021;178:363-370.
182. Jiang C, Fang Y, Zhang W, et al. A multi-ion strategy towards rechargeable sodium-ion full batteries with high working voltage and rate capability. *Angew Chem Int Ed*. 2018;57(50):16370-16374.
183. Lang J, Jiang C, Fang Y, Shi L, Miao S, Tang Y. Room-temperature rechargeable Ca-ion based hybrid batteries with high rate capability and long-term cycling life. *Adv Energy Mater*. 2019;9(29):1901099.
184. Qiao Y, Jiang K, Li X, et al. A hybrid electrolytes design for capacity-equivalent dual-graphite battery with superior long-term cycle life. *Adv Energy Mater*. 2018;8(24):1801120.
185. Wang F, Liu Z, Zhang P, et al. Dual-graphene rechargeable sodium battery. *Small*. 2017;13(47):1702449.
186. Ji B, Zhang F, Wu N, Tang Y. A dual-carbon battery based on potassium-ion electrolyte. *Adv Energy Mater*. 2017;7(20):1700920.
187. Yang K, Jia L, Liu X, et al. Revealing the anion intercalation behavior and surface evolution of graphite in dual-ion batteries via in situ AFM. *Nano Res*. 2020;13(2):412-418.
188. Ji B, Yao W, Tang Y. High-performance rechargeable zinc-based dual-ion batteries. *Sustain Energy Fuels*. 2020;4(1):101-107.
189. Zhang L, Huang Y, Fan H, Wang H. Flame-retardant electrolyte solution for dual-ion batteries. *ACS Appl Energy Mater*. 2019;2(2):1363-1370.
190. Yan T, Ding R, Ying D, et al. An intercalation pseudocapacitance-driven perovskite $NaNbO_3$ anode with superior kinetics and stability for advanced lithium-based dual-ion batteries. *J Mater Chem A*. 2019;7(40):22884-22888.
191. Ying D, Ding R, Huang Y, et al. Conversion/alloying pseudocapacitance-dominated perovskite $KZnF_3$ anode for advanced lithium-based dual-ion batteries. *Chem Eur J*. 2020;26(13):2798-2802.
192. Li C, Xue J, Huang A, et al. Poly(*N*-vinylcarbazole) as an advanced organic cathode for potassium-ion-based dual-ion battery. *Electrochim Acta*. 2019;297:850-855.
193. Logan ER, Tonita EM, Gering KL, et al. A study of the transport properties of ethylene carbonate-free Li electrolytes. *J Electrochem Soc*. 2018;165(3):A705-A716.
194. Wang M, Jiang C, Zhang S, Song X, Tang Y, Cheng H-M. Reversible calcium alloying enables a practical room-temperature rechargeable calcium-ion battery with a high discharge voltage. *Nat Chem*. 2018;10(6):667-672.
195. Liu Q, Chen S, Yu X, et al. Low cost and superior safety industrial grade lithium dual-ion batteries with a second life. *Energy Technol*. 2018;6(10):1994-2000.
196. Zhang M, Shoaib M, Fei H, et al. Hierarchically porous N-doped carbon fibers as a free-standing anode for high-capacity potassium-based dual-ion battery. *Adv Energy Mater*. 2019;9(37):1901663.
197. Wang X, Wang S, Shen K, He S, Hou X, Chen F. Phosphorus-doped porous hollow carbon nanorods for high-performance sodium-based dual-ion batteries. *J Mater Chem A*. 2020;8(7):4007-4016.

198. Li W-H, Liang H-J, Hou X-K, et al. Feasible engineering of cathode electrolyte interphase enables the profoundly improved electrochemical properties in dual-ion battery. *J Energy Chem*. 2020;50:416-423.
199. Yu A, Pan Q, Zhang M, Xie D, Tang Y. Fast rate and long life potassium-ion based dual-ion battery through 3D porous organic negative electrode. *Adv Funct Mater*. 2020;30(24):2001440.
200. Ou X, Li J, Tong X, Zhang G, Tang Y. Highly concentrated and nonflammable electrolyte for high energy density K-based dual-ion battery. *ACS Appl Energy Mater*. 2020; 3(10):10202-10208.
201. Wang Y, Zhang L, Zhang F, Ding X, Shin K, Tang Y. High-performance Zn-graphite battery based on $LiPF_6$ single-salt electrolyte with high working voltage and long cycling life. *J Energy Chem*. 2021;58:602-609.
202. Zhu D, Fan H, Wang H. PF_6^- intercalation into graphite electrode from propylene carbonate. *ACS Appl Energy Mater*. 2021;4(3):2181-2189.
203. Wu S, Zhang F, Tang Y. A novel calcium-ion battery based on dual-carbon configuration with high working voltage and long cycling life. *Adv Sci*. 2018;5(8):1701082.
204. Fan H, Qi L, Yoshio M, Wang H. Hexafluorophosphate intercalation into graphite electrode from ethylene carbonate/ethylmethyl carbonate. *Solid State Ion*. 2017;304:107-112.
205. Zhao S, Huang Y, Wang Y, Zhu D, Zhang L, Wang H. Intercalation behavior of tetrafluoroborate anion in a graphite electrode from mixed cyclic carbonates. *ACS Appl Energy Mater*. 2021;4(1):737-744.
206. Gao J, Tian S, Qi L, Wang H. Intercalation manners of perchlorate anion into graphite electrode from organic solutions. *Electrochim Acta*. 2015;176:22-27.
207. Gao J, Tian S, Qi L, Yoshio M, Wang H. Hexafluorophosphate intercalation into graphite electrode from gamma-butyrolactone solutions in activated carbon/graphite capacitors. *J Power Sources*. 2015;297:121-126.
208. Wang H, Yoshio M. Suppression of PF_6^- intercalation into graphite by small amounts of ethylene carbonate in activated carbon/graphite capacitors. *Chem Commun*. 2010;46(9): 1544-1546.
209. Rohatgi A. *Webplotdigitizer: Version 4.4*. WebPlotDigitizer; 2020.
210. Fan H, Qi L, Wang H. Intercalation behavior of hexafluorophosphate into graphite electrode from propylene/ethylmethyl carbonates. *J Electrochem Soc*. 2017;164(9):A2262-A2267.
211. Wang B, Wang Y, Huang Y, Zhang L, Ma S, Wang H. Hexafluorophosphate intercalation into the graphite electrode from mixed cyclic carbonates. *ACS Appl Energy Mater*. 2021;4(5):5316-5325.
212. Zhu D, Huang Y, Zhang L, Fan H, Wang H. PF_6^- intercalation into graphite electrode from gamma-butyrolactone/ethyl methyl carbonate. *J Electrochem Soc*. 2020;167(7):070513.
213. Xi X-T, Li W-H, Hou B-H, Yang Y, Gu Z-Y, Wu X-L. Dendrite-free lithium anode enables the lithium//graphite dual-ion battery with much improved cyclic stability. *ACS Appl Energy Mater*. 2019;2(1):201-206.
214. Xi X-T, Feng X, Nie X-J, et al. Dendrite-free deposition on lithium anode toward long-life and high-stable Li//graphite dual-ion battery. *Chem Commun*. 2019;55(58):8406-8409.
215. Heckmann A, Thienenkamp J, Beltrop K, Winter M, Brunklaus G, Placke T. Towards high-performance dual-graphite batteries using highly concentrated organic electrolytes. *Electrochim Acta*. 2018;260:514-525.
216. Holoubek J, Yin Y, Li M, et al. Exploiting mechanistic solvation kinetics for dual-graphite batteries with high power output at extremely low temperature. *Angew Chem Int Ed*. 2019;58(52):18892-18897.
217. Han X, Zhang H, Liu T, et al. An interfacially self-reinforced polymer electrolyte enables long-cycle 5.35 V dual-ion batteries. *J Mater Chem A*. 2020;8(3):1451-1456.
218. Xu K, Angell CA. Sulfone-based electrolytes for lithium-ion batteries. *J Electrochem Soc*. 2002;149(7):A920-A926.
219. Su C-C, He M, Redfern PC, Curtiss LA, Shkrob IA, Zhang Z. Oxidatively stable fluorinated sulfone electrolytes for high voltage high energy lithium-ion batteries. *Energy Environ Sci*. 2017;10(4):900-904.
220. Ren X, Chen S, Lee H, et al. Localized high-concentration sulfone electrolytes for high-efficiency lithium-metal. *Chem*. 2018;4(8):1877-1892.
221. Tong X, Ou X, Wu N, Wang H, Li J, Tang Y. High oxidation potential ≈6.0 V of concentrated electrolyte toward high-performance dual-ion battery. *Adv Energy Mater*. 2021; 11(25):2100151.
222. Wang Y, Huang Y, Wang H. Tetrafluoroborate anion intercalation into graphite electrode from sulfolane. *Chem Lett*. 2021;50(5):996-998.
223. Wang Y, Li J, Huang Y, Wang H. Anion storage behavior of graphite electrodes in $LiBF_4$/sulfone/ethyl methyl carbonate solutions. *Langmuir*. 2019;35(46):14804-14811.
224. Chiba K, Ueda T, Yamaguchi Y, Oki Y, Saiki F, Naoi K. Electrolyte systems for high withstand voltage and durability II. Alkylated cyclic carbonates for electric double-layer capacitors. *J Electrochem Soc*. 2011;158(12):A1320-A1327.
225. Han P, Han X, Yao J, et al. Mesocarbon microbead based dual-carbon batteries towards low cost energy storage devices. *J Power Sources*. 2018;393:145-151.
226. Liu T, Han X, Zhang Z, et al. A high concentration electrolyte enables superior cycleability and rate capability for high voltage dual graphite battery. *J Power Sources*. 2019;437:226942.
227. Wang X, Yasukawa E, Kasuya S. Nonflammable trimethyl phosphate solvent-containing electrolytes for lithium-ion batteries: I. Fundamental properties. *J Electrochem Soc*. 2001;148(10):A1058-A1065.
228. Xu K, Ding MS, Zhang S, Allen JL, Jow TR. An attempt to formulate nonflammable lithium ion electrolytes with alkyl phosphates and phosphazenes. *J Electrochem Soc*. 2002; 149(5):A622-A625.
229. Zhang L, Wang H. Anion intercalation into a graphite electrode from trimethyl phosphate. *ACS Appl Mater Interfaces*. 2020;12(42):47647-47654.
230. Zhang L, Wang Y, Wu Z, Wang H. Combining experiments and theoretical calculations to investigate the intercalation behavior of bis(trifluoromethanesulfonimide) anion into graphite electrodes from alkyl phosphates. *ACS Appl Mater Interfaces*. 2021;13(29):34197-34201.
231. Jiang X, Liu X, Zeng Z, et al. A nonflammable Na^+-based dual-carbon battery with low-cost, high voltage, and long cycle life. *Adv Energy Mater*. 2018;8(36):1802176.

232. Smart MC, Ratnakumar BV, Chin KB, Whitcanack LD. Lithium-ion electrolytes containing ester cosolvents for improved low temperature performance. *J Electrochem Soc*. 2010;157(12):A1361-A1374.
233. Fan H, Qi L, Wang H. Hexafluorophosphate anion intercalation into graphite electrode from methyl propionate. *Solid State Ion*. 2017;300:169-174.
234. Zhang L, Fan H, Wang H. Methyl acetate-based solutions for dual-ion batteries. *Electrochim Acta*. 2020;342:135992.
235. Zhang L, Wang H. Performance of graphite positive electrodes in $LiPF_6$–methyl acetate/trimethyl phosphate solutions. *J Electrochem Soc*. 2020;167(10):100506.
236. Yu Z, Jiao S, Li S, et al. Flexible stable solid-state Al-ion batteries. *Adv Funct Mater*. 2019;29(1):1806799.
237. Kotronia A, Asfaw HD, Edström K. Evaluating electrolyte additives in dual-ion batteries: overcoming common pitfalls. *Electrochim Acta*. 2023;459:142517.
238. Wang Y, Zhang Y, Duan Q, Lee P-K, Wang S, Yu DYW. Engineering cathode-electrolyte interface of graphite to enable ultra long-cycle and high-power dual-ion batteries. *J Power Sources*. 2020;471:228466.
239. Edström K, Gustafsson T, Thomas JO. The cathode–electrolyte interface in the li-ion battery. *Electrochim Acta*. 2004;50(2-3):397-403.
240. Kotronia A, van Ekeren WWA, Desta Asfaw H, Edström K. Impact of binders on self-discharge in graphite dual-ion batteries. *Electrochem Commun*. 2022;107424.
241. Wu L-N, Shen S-Y, Hong Y-H, et al. Novel MnO–graphite dual-ion battery and new insights into its reaction mechanism during initial cycle by operando techniques. *ACS Appl Mater Interfaces*. 2019;11(13):12570-12577.
242. Wang S, Tu J, Xiao J, Zhu J, Jiao S. 3D skeleton nanostructured Ni_3S_2/Ni foam@RGO composite anode for high-performance dual-ion battery. *J Energy Chem*. 2019;28:144-150.
243. Qin P, Wang M, Li N, Zhu H, Ding X, Tang Y. Bubble-sheet-like interface design with an ultrastable solid electrolyte layer for high-performance dual-ion batteries. *Adv Mater*. 2017;29(17):1606805.
244. Han X, Xu G, Zhang Z, et al. An in situ interface reinforcement strategy achieving long cycle performance of dual-ion batteries. *Adv Energy Mater*. 2019;9(16):1804022.
245. Ohzuku T, Ueda A, Yamamoto N. Zero-strain insertion material of $Li[Li_{1/3}Ti_{5/3}]O_4$ for rechargeable lithium cells. *J Electrochem Soc*. 1995;142(5):1431-1435.
246. He Y-B, Li B, Liu M, et al. Gassing in $Li_4Ti_5O_{12}$-based batteries and its remedy. *Sci Rep*. 2012;2(1):913.
247. Wu L-N, Peng J, Sun Y-K, et al. High-energy density Li metal dual-ion battery with a lithium nitrate-modified carbonate-based electrolyte. *ACS Appl Mater Interfaces*. 2019;11(20):18504-18510.
248. Xing L, Zheng X, Schroeder M, et al. Deciphering the ethylene carbonate–propylene carbonate mystery in Li-ion batteries. *Acc Chem Res*. 2018;51(2):282-289.
249. Zheng T, Xiong J, Zhu B, et al. From −20°C to 150°C: a lithium secondary battery with a wide temperature window obtained via manipulated competitive decomposition in electrolyte solution. *J Mater Chem A*. 2021;9(14):9307-9318.
250. Wang S, Jiao S, Tian D, et al. A novel ultrafast rechargeable multi-ions battery. *Adv Mater*. 2017;29(16):1606349.
251. Song C, Li Y, Li H, et al. A novel flexible fiber-shaped dual-ion battery with high energy density based on omni-directional porous Al wire anode. *Nano Energy*. 2019;60:285-293.
252. Heidrich B, Heckmann A, Beltrop K, Winter M, Placke T. Unravelling charge/discharge and capacity fading mechanisms in dual-graphite battery cells using an electron inventory model. *Energy Storage Mater*. 2019;21:414-426.
253. Tong X, Zhang F, Ji B, Sheng M, Tang Y. Carbon-coated porous aluminum foil anode for high-rate, long-term cycling stability, and high energy density dual-ion batteries. *Adv Mater*. 2016;28(45):9979-9985.
254. Li C, Yang H, Xie J, Wang K, Li J, Zhang Q. Ferrocene-based mixed-valence metal–organic framework as an efficient and stable cathode for lithium-ion-based dual-ion battery. *ACS Appl Mater Interfaces*. 2020;12(29):32719-32725.
255. Wu J, Wang X, Liu Q, et al. A synergistic exploitation to produce high-voltage quasi-solid-state lithium metal batteries. *Nat Commun*. 2021;12:5746.
256. Rowden B, Garcia-Araez N. A review of gas evolution in lithium ion batteries. *Energy Rep*. 2020;6:10-18.
257. Ryall N, Garcia-Araez N. Highly sensitive operando pressure measurements of Li-ion battery materials with a simply modified swagelok cell. *J Electrochem Soc*. 2020;167(11):110511.
258. Nozu R, Suzuki E, Kimura O, Onagi N, Ishihara T. Dual-ion battery using graphitic carbon and $Li_4Ti_5O_{12}$: suppression of gas formation and increased cyclability. *Electrochim Acta*. 2020;332:135238.
259. Nozu R, Suzuki E, Kimura O, Onagi N, Ishihara T. Tetraethylammonium tetrafluoroborate additives for suppressed gas formation and increased cycle stability of dual-ion battery. *Electrochim Acta*. 2020;337:135711.
260. Wang S, Xiao X, Fu C, Tu J, Tan Y, Jiao S. Room temperature solid state dual-ion batteries based on gel electrolytes. *J Mater Chem A*. 2018;6(10):4313-4323.
261. Krause LJ, Lamanna W, Summerfield J, et al. Corrosion of aluminum at high voltages in non-aqueous electrolytes containing perfluoroalkylsulfonyl imides; new lithium salts for lithium-ion cells. *J Power Sources*. 1997;68(2):320-325.
262. Morita M, Shibata T, Yoshimoto N, Ishikawa M. Anodic behavior of aluminum in organic solutions with different electrolytic salts for lithium ion batteries. *Electrochim Acta*. 2002;47(17):2787-2793.
263. Matsumoto K, Inoue K, Nakahara K, Yuge R, Noguchi T, Utsugi K. Suppression of aluminum corrosion by using high concentration LiTFSI electrolyte. *J Power Sources*. 2013;231:234-238.
264. McOwen DW, Seo DM, Borodin O, Vatamanu J, Boyle PD, Henderson WA. Concentrated electrolytes: decrypting electrolyte properties and reassessing Al corrosion mechanisms. *Energy Environ Sci*. 2014;7(1):416-426.
265. Wang J, Yamada Y, Sodeyama K, Chiang CH, Tateyama Y, Yamada A. Superconcentrated electrolytes for a high-voltage lithium-ion battery. *Nat Commun*. 2016;7:12032.
266. Kühnel RS, Reber D, Remhof A, Figi R, Bleiner D, Battaglia C. "Water-in-salt" electrolytes enable the use of

cost-effective aluminum current collectors for aqueous high-voltage batteries. *Chem Commun*. 2016;52(68):10435-10438.
267. Heckmann A, Krott M, Streipert B, Uhlenbruck S, Winter M, Placke T. Suppression of aluminum current collector dissolution by protective ceramic coatings for better high-voltage battery performance. *ChemPhysChem*. 2017;18(1):156-163.
268. Wang S, Kravchyk KV, Filippin AN, et al. Aluminum chloride-graphite batteries with flexible current collectors prepared from earth-abundant elements. *Adv Sci*. 2018;5(4):1700712.
269. Zhou D, Shanmukaraj D, Tkacheva A, Armand M, Wang G. Polymer electrolytes for lithium-based batteries: advances and prospects. *Chem*. 2019;5(9):2326-2352.
270. Song JY, Wang YY, Wan CC. Review of gel-type polymer electrolytes for lithium-ion batteries. *J Power Sources*. 1999;77(2):183-197.
271. Feuillade G, Perche P. Ion-conductive macromolecular gels and membranes for solid lithium cells. *J Appl Electrochem*. 1975;5(1):63-69.
272. Osada I, de Vries H, Scrosati B, Passerini S. Ionic-liquid-based polymer electrolytes for battery applications. *Angew Chem Int Ed*. 2016;55(2):500-513.
273. Meyer WH. Polymer electrolytes for lithium-ion batteries. *Adv Mater*. 1998;10(6):439-448.
274. Armand M. Polymers with ionic conductivity. *Adv Mater*. 1990;2(6-7):278-286.
275. Berthier C, Gorecki W, Minier M, Armand MB, Chabagno JM, Rigaud P. Microscopic investigation of ionic conductivity in alkali metal salts-poly(ethylene oxide) adducts. *Solid State Ion*. 1983;11(1):91-95.
276. Mindemark J, Lacey MJ, Bowden T, Brandell D. Beyond PEO—alternative host materials for Li^+-conducting solid polymer electrolytes. *Prog Polym Sci*. 2018;81:114-143.
277. Pal P, Ghosh A. Robust succinonitrile plastic crystal-based ionogel for all-solid-state Li-ion and dual-ion batteries. *ACS Appl Energy Mater*. 2020;3(5):4295-4304.
278. Yu Z, Jiao S, Tu J, et al. Gel electrolytes with a wide potential window for high-rate Al-ion batteries. *J Mater Chem A*. 2019;7(35):20348-20356.
279. Xu X, Lin K, Zhou D, et al. Quasi-solid-state dual-ion sodium metal batteries for low-cost energy storage. *Chem*. 2020;6(4):902-918.
280. Kim I, Jang S, Lee KH, Tak Y, Lee G. In situ polymerized solid electrolytes for superior safety and stability of flexible solid-state Al-ion batteries. *Energy Storage Mater*. 2021;40:229-238.
281. Kotronia A, Edström K, Brandell D, Asfaw HD. Ternary ionogel electrolytes enable quasi-solid-state potassium dual-ion intercalation batteries. *Adv Energy Sustain Res*. 2022;3(1):2100122.
282. Chen G, Zhang F, Zhou Z, Li J, Tang Y. A flexible dual-ion battery based on PVDF-HFP-modified gel polymer electrolyte with excellent cycling performance and superior rate capability. *Adv Energy Mater*. 2018;8(25):1801219.
283. Liu Z, Wang X, Liu Z, et al. Low-cost gel polymer electrolyte for high-performance aluminum-ion batteries. *ACS Appl Mater Interfaces*. 2021;13(24):28164-28170.
284. Zhai S, Wang N, Tan X, et al. Interface-engineered dendrite-free anode and ultraconductive cathode for durable and high-rate fiber Zn dual-ion microbattery. *Adv Funct Mater*. 2021;31(13):2008894.
285. Lv Z, Zhou S, Huang H, et al. A flexible $[(DMPI^+)(AlCl_4^-)]$/PVDF-HFP polymer gel electrolyte and its electrochemical performance for dual-graphite batteries. *Mater Chem Phys*. 2022;289:126468.
286. Elia GA, Acevedo CI, Kazemi R, Fantini S, Lin R, Hahn R. A gel polymer electrolyte for aluminum batteries. *Energy Technol*. 2021;9(8):2100208.
287. Costa CM, Gomez Ribelles JL, Lanceros-Méndez S, Appetecchi GB, Scrosati B. Poly(vinylidene fluoride)-based, co-polymer separator electrolyte membranes for lithium-ion battery systems. *J Power Sources*. 2014;245:779-786.
288. Sun H, Fu X, Xie S, Jiang Y, Peng H. Electrochemical capacitors with high output voltages that mimic electric eels. *Adv Mater*. 2016;28(10):2070-2076.
289. Qiao J, Fu J, Lin R, Ma J, Liu J. Alkaline solid polymer electrolyte membranes based on structurally modified PVA/PVP with improved alkali stability. *Polymer*. 2010;51(21):4850-4859.
290. Lu W, Henry K, Turchi C, Pellegrino J. Incorporating ionic liquid electrolytes into polymer gels for solid-state ultracapacitors. *J Electrochem Soc*. 2008;155(5):A361-A367.
291. Sun X-G, Fang Y, Jiang X, Yoshii K, Tsuda T, Dai S. Polymer gel electrolytes for application in aluminum deposition and rechargeable aluminum ion batteries. *Chem Commun*. 2016;52(2):292-295.
292. Xie D, Zhang M, Wu Y, Xiang L, Tang Y. A flexible dual-ion battery based on sodium-ion quasi-solid-state electrolyte with long cycling life. *Adv Funct Mater*. 2020;30(5):1906770.
293. Croce F, Appetecchi GB, Persi L, Scrosati B. Nanocomposite polymer electrolytes for lithium batteries. *Nature*. 1998;394(6692):456-458.
294. Cheng X, Pan J, Zhao Y, Liao M, Peng H. Gel polymer electrolytes for electrochemical energy storage. *Adv Energy Mater*. 2018;8(7):1702184.
295. Zhang Y, Zhao Y, Cheng X, et al. Realizing both high energy and high power densities by twisting three carbon-nanotube-based hybrid fibers. *Angew Chem Int Ed*. 2015;54(38):11177-11182.
296. Weng W, Sun Q, Zhang Y, et al. A gum-like lithium-ion battery based on a novel arched structure. *Adv Mater*. 2015;27(8):1363-1369.
297. Lu Q, He Y-B, Yu Q, et al. Dendrite-free, high-rate, long-life lithium metal batteries with a 3D cross-linked network polymer electrolyte. *Adv Mater*. 2017;29(13):1604460.
298. Quartarone E, Mustarelli P. Electrolytes for solid-state lithium rechargeable batteries: recent advances and perspectives. *Chem Soc Rev*. 2011;40(5):2525-2540.
299. Ferrara C, Dall'Asta V, Berbenni V, Quartarone E, Mustarelli P. Physicochemical characterization of $AlCl_3$-1-ethyl-3-methylimidazolium chloride ionic liquid electrolytes for aluminum rechargeable batteries. *J Phys Chem C*. 2017;121(48):26607-26614.
300. Lee KH, Zhang S, Lodge TP, Frisbie CD. Electrical impedance of spin-coatable ion gel films. *J Phys Chem B*. 2011;115(13):3315-3321.

301. Tokuda H, Hayamizu K, Ishii K, Susan MABH, Watanabe M. Physicochemical properties and structures of room temperature ionic liquids. 1. Variation of anionic species. *J Phys Chem B*. 2004;108(42):16593-16600.
302. Sung H, Wang Y, Wan C. Preparation and characterization of poly(vinyl chloride-co-vinyl acetate)-based gel electrolytes for Li-ion batteries. *J Electrochem Soc*. 1998;145(4):1207-1211.
303. Mohamed NS, Arof AK. Investigation of electrical and electrochemical properties of PVDF-based polymer electrolytes. *J Power Sources*. 2004;132(1-2):229-234.
304. Wandrey C, Hernández-Barajas J, Hunkeler D. Diallyldimethylammonium chloride and its polymers. In: Capek I, Hernfández-Barajas J, Hunkeler D, Reddinger JL, Reynolds JR, Wandrey C, eds. *Radical Polymerisation Polyelectrolytes*. Berlin, Heidelberg: Springer; 1999: 123-183.
305. Chen N, Zhang H, Li L, Chen R, Guo S. Ionogel electrolytes for high-performance lithium batteries: a review. *Adv Energy Mater*. 2018;8(12):1702675.
306. Li X, Li S, Zhang Z, Huang J, Yang L, Hirano S. High-performance polymeric ionic liquid–silica hybrid ionogel electrolytes for lithium metal batteries. *J Mater Chem A*. 2016;4(36):13822-13829.
307. Guyomard-Lack A, Abusleme J, Soudan P, Lestriez B, Guyomard D, Bideau JL. Hybrid silica–polymer ionogel solid electrolyte with tunable properties. *Adv Energy Mater*. 2014;4(8):1301570.
308. Yuan J, Mecerreyes D, Antonietti M. Poly(ionic liquid)s: an update. *Prog Polym Sci*. 2013;38(7):1009-1036.
309. Pont A-L, Marcilla R, De Meatza I, Grande H, Mecerreyes D. Pyrrolidinium-based polymeric ionic liquids as mechanically and electrochemically stable polymer electrolytes. *J Power Sources*. 2009;188(2):558-563.
310. Appetecchi GB, Kim GT, Montanino M, et al. Ternary polymer electrolytes containing pyrrolidinium-based polymeric ionic liquids for lithium batteries. *J Power Sources*. 2010;195(11):3668-3675.
311. Zhao Y, Xue K, Tan T, Yu DYW. Thermal stability of graphite electrode as cathode for dual-ion batteries. *ChemSusChem*. 2023;16(4):e202201221.
312. Wandt J, Freiberg ATS, Ogrodnik A, Gasteiger HA. Singlet oxygen evolution from layered transition metal oxide cathode materials and its implications for lithium-ion batteries. *Mater Today*. 2018;21(8):825-833.
313. Jung R, Metzger M, Maglia F, Stinner C, Gasteiger HA. Chemical versus electrochemical electrolyte oxidation on NMC111, NMC622, NMC811, LNMO, and conductive carbon. *J Phys Chem Lett*. 2017;8(19):4820-4825.
314. Imhof R, Novák P. Oxidative electrolyte solvent degradation in lithium-ion batteries: an in situ differential electrochemical mass spectrometry investigation. *J Electrochem Soc*. 1999;146(5):1702-1706.
315. Zhu Y, Wang Z, Bian H, et al. Critical conditions for the thermal runaway propagation of lithium-ion batteries in air and argon environments. *J Therm Anal Calorim*. 2022;147 (23):13699-13710.
316. Wang J, Yamada Y, Sodeyama K, et al. Fire-extinguishing organic electrolytes for safe batteries. *Nat Energy*. 2018;3(1): 22-29.
317. Wang Z, Zhang F, Sun Y, et al. Intrinsically nonflammable ionic liquid-based localized highly concentrated electrolytes enable high-performance Li-metal batteries. *Adv Energy Mater*. 2021;11(17):2003752.
318. Zhang L, Wang H. Dual-graphite batteries with flame-retardant electrolyte solutions. *ChemElectroChem*. 2019; 6(17):4637-4644.
319. Zhu J, Xu Y, Fu Y, et al. Hybrid aqueous/nonaqueous water-in-bisalt electrolyte enables safe dual ion batteries. *Small*. 2020;16(17):1905838.
320. Matsumoto K, Endo T. Confinement of ionic liquid by networked polymers based on multifunctional epoxy resins. *Macromolecules*. 2008;41(19):6981-6986.
321. Shirshova N, Bismarck A, Carreyette S, et al. Structural supercapacitor electrolytes based on bicontinuous ionic liquid–epoxy resin systems. *J Mater Chem A*. 2013;1(48): 15300-15309.
322. Le Bideau J, Viau L, Vioux A. Ionogels, ionic liquid based hybrid materials. *Chem Soc Rev*. 2011;40(2):907-925.
323. Gayet F, Viau L, Leroux F, et al. Unique combination of mechanical strength, thermal stability, and high ion conduction in PMMA−silica nanocomposites containing high loadings of ionic liquid. *Chem Mater*. 2009;21(23):5575-5577.
324. Lee H, Erwin A, Buxton ML, et al. Shape persistent, highly conductive ionogels from ionic liquids reinforced with cellulose nanocrystal network. *Adv Funct Mater*. 2021;31 (38):2103083.
325. Gorecki W, Jeannin M, Belorizky E, Roux C, Armand M. Physical properties of solid polymer electrolyte PEO(LiTFSI) complexes. *J Phys Condens Matter*. 1995;7(34):6823-6832.
326. Stolz L, Hochstädt S, Röser S, Hansen MR, Winter M, Kasnatscheew J. Single-ion versus dual-ion conducting electrolytes: the relevance of concentration polarization in solid-state batteries. *ACS Appl Mater Interfaces*. 2022;14(9): 11559-11566.
327. Huesker J, Froböse L, Kwade A, Winter M, Placke T. In situ dilatometric study of the binder influence on the electrochemical intercalation of bis(trifluoromethanesulfonyl) imide anions into graphite. *Electrochim Acta*. 2017;257: 423-435.
328. Grazioli D, Verners O, Zadin V, Brandell D, Simone A. Electrochemical-mechanical modeling of solid polymer electrolytes: impact of mechanical stresses on Li-ion battery performance. *Electrochim Acta*. 2019;296:1122-1141.
329. Snyder JF, Carter RH, Wetzel ED. Electrochemical and mechanical behavior in mechanically robust solid polymer electrolytes for use in multifunctional structural batteries. *Chem Mater*. 2007;19(15):3793-3801.
330. Greenhalgh E, Ankersen J, Asp L, et al. Mechanical, electrical and microstructural characterisation of multifunctional structural power composites. *J Compos Mater*. 2014;49(15):1823-1834.
331. Asp LE. Multifunctional composite materials for energy storage in structural load paths. *Plast Rubber Compos*. 2013;42(4):144-149.
332. Snyder JF, Wetzel ED, Watson CM. Improving multifunctional behavior in structural electrolytes through copolymerization of structure- and conductivity-promoting monomers. *Polymer*. 2009;50(20):4906-4916.

333. Willgert M, Kjell MH, Jacques E, Behm M, Lindbergh G, Johansson M. Photoinduced free radical polymerization of thermoset lithium battery electrolytes. *Eur Polym J*. 2011;47(12):2372-2378.
334. Johansson IL, Brandell D, Mindemark J. Mechanically stable UV-crosslinked polyester-polycarbonate solid polymer electrolyte for high-temperature batteries. *Batteries Supercaps*. 2020;3(6):527-533.
335. Glynos E, Papoutsakis L, Pan W, et al. Nanostructured polymer particles as additives for high conductivity, high modulus solid polymer electrolytes. *Macromolecules*. 2017;50(12):4699-4706.
336. Bergfelt A, Hernández G, Mogensen R, et al. Mechanically robust yet highly conductive diblock copolymer solid polymer electrolyte for ambient temperature battery applications. *ACS Appl Polym Mater*. 2020;2(2):939-948.
337. Young W-S, Kuan W-F, Epps III TH. Block copolymer electrolytes for rechargeable lithium batteries. *J Polym Sci Part B Polym Phys*. 2014;52(1):1-16.
338. Singh M, Odusanya O, Wilmes GM, et al. Effect of molecular weight on the mechanical and electrical properties of block copolymer electrolytes. *Macromolecules*. 2007;40(13):4578-4585.
339. Manuel Stephan A. Review on gel polymer electrolytes for lithium batteries. *Eur Polym J*. 2006;42(1):21-42.
340. Young W-S, Epps III TH. Ionic conductivities of block copolymer electrolytes with various conducting pathways: sample preparation and processing considerations. *Macromolecules*. 2012;45(11):4689-4697.
341. Srivastava S, Schaefer JL, Yang Z, Tu Z, Archer LA. 25th Anniversary article: polymer–particle composites: phase stability and applications in electrochemical energy storage. *Adv Mater*. 2014;26(2):201-234.
342. Manuel Stephan A, Nahm KS. Review on composite polymer electrolytes for lithium batteries. *Polymer*. 2006;47(16):5952-5964.
343. Zhang P, Yang LC, Li LL, Ding ML, Wu YP, Holze R. Enhanced electrochemical and mechanical properties of P(VDF-HFP)-based composite polymer electrolytes with SiO_2 nanowires. *J Membr Sci*. 2011;379(1-2):80-85.
344. Klongkan S, Pumchusak J. Effects of nano alumina and plasticizers on morphology, ionic conductivity, thermal and mechanical properties of PEO-$LiCF_3SO_3$ solid polymer electrolyte. *Electrochim Acta*. 2015;161:171-176.
345. Angell CA, Liu C, Sanchez E. Rubbery solid electrolytes with dominant cationic transport and high ambient conductivity. *Nature*. 1993;362(6416):137-139.
346. Tong B, Song Z, Wu H, et al. Ion transport and structural design of lithium-ion conductive solid polymer electrolytes: a perspective. *Mater Futures*. 2022;1(4):042103.
347. Yoon H-K, Chung W-S, Jo N-J. Study on ionic transport mechanism and interactions between salt and polymer chain in PAN based solid polymer electrolytes containing $LiCF_3SO_3$. *Electrochim Acta*. 2004;50(2-3):289-293.
348. Wang X, Chen F, Girard GMA, et al. Poly(ionic liquid)s-in-salt electrolytes with Co-coordination-assisted lithium-ion transport for safe batteries. *Joule*. 2019;3(11):2687-2702.
349. Okumura T, Nishimura S. Lithium ion conductive properties of aliphatic polycarbonate. *Solid State Ion*. 2014;267:68-73.
350. Hernández G, Johansson IL, Mathew A, Sångeland C, Brandell D, Mindemark J. Going beyond sweep voltammetry: alternative approaches in search of the elusive electrochemical stability of polymer electrolytes. *J Electrochem Soc*. 2021;168(10):100523.
351. Xu C, Sun B, Gustafsson T, Edström K, Brandell D, Hahlin M. Interface layer formation in solid polymer electrolyte lithium batteries: an XPS study. *J Mater Chem A*. 2014;2(20):7256-7264.
352. Homann G, Stolz L, Nair J, Laskovic IC, Winter M, Kasnatscheew J. Poly(ethylene oxide)-based electrolyte for solid-state-lithium-batteries with high voltage positive electrodes: evaluating the role of electrolyte oxidation in rapid cell failure. *Sci Rep*. 2020;10(1):4390.
353. Zhou Q, Ma J, Dong S, Li X, Cui G. Intermolecular chemistry in solid polymer electrolytes for high-energy-density lithium batteries. *Adv Mater*. 2019;31(50):1902029.
354. Chen R, Liu F, Chen Y, et al. An investigation of functionalized electrolyte using succinonitrile additive for high voltage lithium-ion batteries. *J Power Sources*. 2016;306:70-77.
355. Alarco P-J, Abu-Lebdeh Y, Abouimrane A, Armand M. The plastic-crystalline phase of succinonitrile as a universal matrix for solid-state ionic conductors. *Nat Mater*. 2004;3(7):476-481.
356. Ha H-J, Kwon YH, Kim JY, Lee S-Y. A self-standing, UV-cured polymer networks-reinforced plastic crystal composite electrolyte for a lithium-ion battery. *Electrochim Acta*. 2011;57:40-45.
357. Hu P, Chai J, Duan Y, Liu Z, Cui G, Chen L. Progress in nitrile-based polymer electrolytes for high performance lithium batteries. *J Mater Chem A*. 2016;4(26):10070-10083.
358. Wang P, Chai J, Zhang Z, et al. An intricately designed poly(vinylene carbonate-acrylonitrile) copolymer electrolyte enables 5 V lithium batteries. *J Mater Chem A*. 2019;7(10):5295-5304.
359. Seki S, Kobayashi Y, Miyashiro H, Mita Y, Iwahori T. Fabrication of high-voltage, high-capacity all-solid-state lithium polymer secondary batteries by application of the polymer electrolyte/inorganic electrolyte composite concept. *Chem Mater*. 2005;17(8):2041-2045.
360. Zhao C-Z, Zhao Q, Liu X, et al. Rechargeable lithium metal batteries with an In-built Solid-state polymer electrolyte and a high voltage/loading Ni-rich layered cathode. *Adv Mater*. 2020;32(12):1905629.
361. Chen H, Zheng M, Qian S, et al. Functional additives for solid polymer electrolytes in flexible and high-energy-density solid-state lithium-ion batteries. *Carbon Energy*. 2021;3(6):929-956.
362. Fan LZ, Hu YS, Bhattacharyya AJ, Maier J. Succinonitrile as a versatile additive for polymer electrolytes. *Adv Funct Mater*. 2007;17(15):2800-2807.
363. Kobayashi Y, Seki S, Yamanaka A, Miyashiro H, Mita Y, Iwahori T. Development of high-voltage and high-capacity all-solid-state lithium secondary batteries. *J Power Sources*. 2005;146(1-2):719-722.
364. Miyashiro H, Kobayashi Y, Seki S, et al. Fabrication of all-solid-state lithium polymer secondary batteries using Al_2O_3-coated $LiCoO_2$. *Chem Mater*. 2005;17(23):5603-5605.

365. Johansson IL, Sångeland C, Uemiya T, et al. Improving the electrochemical stability of a polyester–polycarbonate solid polymer electrolyte by zwitterionic additives. *ACS Appl Energy Mater*. 2022;5(8):10002-10012.

AUTHOR BIOGRAPHIES

Dr. Habtom D. Asfaw is currently a researcher in the Department of Chemistry at Uppsala University working on the synthesis and processing of carbon materials for application in lithium-, sodium- and potassium-ion batteries, and dual-ion intercalation batteries. In particular, his research aims at materials synthesis, electrolyte formulation, and interface characterization in an effort to enhance the efficiency and life of dual-ion batteries. Prior to his current post, Habtom had postdoctoral research stints at Empa-ETH in Switzerland and Imperial College London in the United Kingdom. He earned his PhD degree from Uppsala University in 2017, and a joint MSc degree in 2012 from Université Paul Sabatier, Université Jules Verne, and Warsaw University of Technology.

Professor Daniel Brandell received his PhD degree in 2005 at Uppsala University, Sweden, on a thesis comprising Molecular Dynamics studies of polymer electrolytes. After postdoctoral studies in Estonia and the USA, he returned to Uppsala. In 2016, he was appointed Professor of Materials Chemistry. Since 2020, he coordinates the research center "Batteries Sweden." In his research, he combines computational chemistry spanning density functional theory calculations, molecular dynamic simulations, and finite element method electrochemical modeling with experimental activities, with a clear focus on Li-ion batteries and other "next-generation" battery chemistries such as Na-ion batteries, solid-state systems, Li–sulfur, organic batteries, and so forth, and has published more than 200 papers in the field. He holds several research grants, including an ERC consolidator grant from 2017 on polymer electrolytes, has many collaboration projects with the industry, and is involved in designing educational activities in the battery technology area.

SUPPORTING INFORMATION

Additional supporting information can be found online in the Supporting Information section at the end of this article.

How to cite this article: Asfaw HD, Kotronia A, Garcia-Araez N, Edström K, Brandell D. Charting the course to solid-state dual-ion batteries. *Carbon Energy*. 2023;e425. doi:10.1002/cey2.425